Katja Urpalainen

Development of a fractional multi-wavelength pulse oximetry algorithm

School of Electrical Engineering

Thesis submitted for examination for the degree of Master of Science in Technology.

Espoo 17.10.2011

Thesis supervisor:

Prof. Raimo Sepponen

Thesis instructor:

D.Sc. (Tech.) Matti Huiku

Aalto University
School of Electrical
Engineering

AALTO UNIVERSITY
SCHOOL OF ELECTRICAL ENGINEERING

ABSTRACT OF THE
MASTER'S THESIS

Author: Katja Urpalainen

Title: Development of a fractional multi-wavelength pulse oximetry algorithm

Date: 17.10.2011 Language: English Number of pages:6+74

Department of Electronics

Professorship: Applied electronics Code: S-66

Supervisor: Prof. Raimo Sepponen

Instructor: D.Sc. (Tech.) Matti Huiku

Adequate oxygen supply is vital for living tissues and cells. Today, oxygen saturation measurement by pulse oximetry is a mandatory physiological parameter in patient monitoring. It tells about the oxygen supply to tissues. In the presence of elevated fractions of dyshemoglobins, pulse oximeters cannot measure oxygen saturation of blood reliably. Accurate and instant diagnosis of dyshemoglobinemia, carbon monoxide poisoning, and acquired methemoglobinemia is difficult due to nonspecific symptoms. Thus, in acute care blood samples must be taken for ensuring adequate tissue oxygenation.

This thesis is a part of a project that aims to develop a novel, multi-wavelength pulse oximeter that would provide a noninvasive and continuous total hemoglobin and dyshemoglobin measurement. A prototype device that expanded the conventional two wavelength system to eight wavelengths has been used to collect development data from volunteer subjects for the algorithm development.

In this thesis the quality of the plethymosgraphic signals is compared to a commercial pulse oximeter. Autocorrelation is used to evaluate the extra plethymosgraphic signals. A fractional hemoglobin algorithm measuring oxyhemoglobin, carboxyhemoglobin, methemoglobin, and reduced hemoglobin fractions is developed. The Beer-Lambert theory of non-scattering media is used to solve analyte fractions after the *in vivo* measured signal are transformed to the corresponding non-scatter signals using regression modeling. The algorithm is evaluated against clinically relevant accuracy requirements, and validated using k-fold cross-validation.

The quality of the plethymosgraphic data turned out to be inadequate for the fractional measurement of hemoglobins. Although the algorithm did not meet the requirements, positive signs were seen, especially with methemoglobin measurement performance. An improved prototype and more development data are needed to prove the feasibility of the fractional hemoglobin algorithm.

Keywords: Beer-Lambert transformation, carboxyhemoglobin, continuous, methemoglobin, multi-wavelength, non-invasive, plethymosgraphic signal, pulse oximetry, regression modeling

AALTO-YLIOPISTO
SÄHKÖTEKNIIKAN KORKEAKOULU

DIPLOMITYÖN
TIIVISTELMÄ

Tekijä: Katja Urpalainen

Työn nimi: Fraktionaalisen moniaallonpituuspulssioksimetrian algoritmikehitys

Päivämäärä: 17.10.2011 Kieli: Englanti Sivumäärä:6+74

Elektroniikan laitos

Professuuri: Sovellettu elektroniikka Koodi: S-66

Valvoja: Prof. Raimo Sepponen

Ohjaaja: TkT Matti Huiku

Riittävä hapensaanti on elintärkeää kudosten ja solujen toiminnalle. Pulssioksimetria mittaa veren happisaturaatiota, joka kertoo osaltaan kudosten hapensaannista. Se on nykyään yksi pakollisista potilasmonitoroinnin mittauksista. Korkeat dyshemoglobiinipitoisuudet vääristävät pulssioksimetrian arviota veren happisaturaatiosta. Yleisimpien dyshemoglobiinien, karboksi- ja methemoglobiinin, kohonneiden pitoisuuksien luotettava diagnoosi on vaikeaa ilman verinäytteitä, koska niiden aiheuttamat oireet ovat epäspesifejä.

Tämä diplomityö on osa projektia, jonka tarkoituksena on kehittää moniaallonpituuspulssioksimetri, joka mittaa dyshemoglobiiniosuudet ja kokonaishemoglobiinipitoisuuden ihoa vaurioittamatta. Projektin ensimmäinen prototyyppilaitteisto mittaa kahdeksaa plethymosgrafista signaalia normaalin kahden aallonpituuden sijaan. Laitteistolla kerättiin vapaaehtoisilta koehenkilöiltä tutkimusaineistoa, joka kattaa laajan karboksi- ja methemoglobiinipitoisuusalueen.

Plethymosgrafisen tutkimusaineiston laatua analysoitiin vertaamalla sitä perinteiseen pulssioksimetriaan. Lisättyjen kanavien laadun tutkimiseen käytettiin autokorrelaatiota. Tämän jälkeen kehitettiin fraktionaalinen hemoglobiinialgoritmi, joka laskee oksi-, karboksi-, met- ja deoksihemoglobiiniosuudet. Työssä käytettiin regressiomallinnusta muuntamaan mitatut *in vivo* signaalit vastaamaan siroamattomia Beerin ja Lambertin signaaleita, jolloin pitoisuudet voidaan ratkaista lineaarisesta yhtälöryhmästä. Algoritmin suorituskykyä verrattiin kliinisiin tarkkuusvaatimuksiin ja algoritmi validoitiin käyttämällä k-kertaista ristiinvalidointia. Kerätyn tutkimusaineiston laatu osoittautui riittämättömäksi fraktionaaliseen mittaukseen. Vaikkei algoritmi täyttänyt kliinisiä vaaatimuksia, lupaavia merkkejä erityisesti methemoglobiinin osalta oli havaittavissa. Uusi parannettu prototyyppi pitää kehittää ja lisää tutkimusaineistoa pitää kerätä, jotta algoritmin suorituskyky voidaan osoittaa riittäväksi.

Avainsanat: Beer-Lambert–muunnos, fraktionaalinen, karboksihemoglobiini, methemoglobiini, moniaallonpituus, noninvasiivinen, pulssioksimetria, plethymosgrafinen signaali, regressiomallinnus

Preface

This Master's thesis has been supported by GE Healthcare Finland Oy. This thesis is a part of a hemoglobin research project that is also part of the FinnWell program of the Finnish Funding Agency for Technology and Innovation (TEKES). I want to thank the company and Engineering Manager Tapani Niklander for providing me this great opportunity to work in this project.

I want to express my gratitude to the whole team, researchers Victor Ostroverkov and Milos Todorovic from the headquarters for GE Global Research, and researcher Antti Tolonen from VTT Technical Research Center of Finland, for the support and spirit during the work. Special thanks to the project leader and my instructor Matti Huiku. His comments and ideas encouraged and challenged me to complete and finalize the thesis. I want also to thank my fellow employees from the nice working atmosphere.

Finally, I would like to thank my family and friends, for the support and care given during my studies.

Otaniemi, 17.10.2011

Katja Urpalainen

Contents

Symbols and abbreviations

Symbols

A	absorbance
dA	normalized differential absorbance
c	concentration
ε	extinction coefficient
I	intensity
l	path-length
λ	wavelength
p	partial pressure
t	time
T	temperature, transmission

Abbreviations

CO	Carbon monoxide, cardiac output
CO_2	Carbon dioxide
CTR	Current transfer ratio
DC	Direct current
fCTR	Functional current transfer ratio
FFT	Fast Fourier Transform
FLT	Functional light transmission
FrOx	Fractional pulse oximetry
Hb	Hemoglobin
HbCO	Carboxyhemoglobin
HbMet	Methemoglobin
HbO_2	Oxyhemoglobin, oxygenated hemoglobin
HbX	hemoglobin fraction
LB	Beer-Lambert
LED	Light Emitting Diode
MSE	Mean square error
O_2	Oxygen
PCA	Principal component analysis
PPG	photoplethymosgraphic signal
R	ratio-of-ratios
RHb	Reduced hemoglobin, deoxygenated hemoglobin
RSD, SD	(relative) standard deviation
SBIC	Schwarz Bayesian Information Criteria
SaO_2	Arterial oxygen saturation of blood
SpO_2	Oxygen saturation measured by pulse oximetry
tHb	total hemoglobin concentration

1 Introduction

Adequate oxygen supply is vital for living tissues and cells. In the absence of oxygen supply cells will die and irreversible cell damage may occur in a few minutes. Low blood oxygenation is extremely difficult to diagnose. Thus, continuous monitoring of oxygen delivery is needed in healthcare. Today, oxygen saturation measurement by pulse oximetry is a mandatory physiological parameter in patient monitoring. It is a spectrophotometric measurement, plethymosgraphic signals of the pulsating blood that gives an estimation of oxygen saturation of arterial blood. It was invented in 1975 by Takuo Aoyagi and commercialized in 1981 by the Biox company.

Pulse oximetry has its limitations. Conventional pulse oximeters are incapable to measure oxygen delivery capacity of blood in the presence of dyshemoglobins (carboxyhemoglobin or methemoglobin), or at low total hemoglobin concentration. Carbon monoxide poisoning and methemoglobinemia often remain undetected before dangerous levels, because of the common nature of the symptoms such as headache, dizziness, and weakness. Carbon monoxide poisoning is a major cause of death by poisoning in industrialized countries. Methemoglobinemia is more common than thought and has been shown to cause morbidity and mortality. Anemia, low total hemoglobin concentration, is the most common disorder in the blood.

Current laboratory methods to measure dyshemoglobinemia and total hemoglobin concentration are invasive, time consuming, and discontinuous. Development of novel multi-wavelength oximeters that would provide reliable noninvasive and continuous total hemoglobin and dyshemoglobin measurement, is driven by these limitations. Diagnosis of anemia, carbon monoxide poisoning, or acquired methemoglobinemia with the non-invasive and continuous multi-wavelength oximeters would improve patient safety and lower the cost of care. In 2005, one of the leading pulse oximeter manufacturers, Masimo Corporation, released a noninvasive and continuous pulse oximeter for fractional hemoglobin measurement. In 2008, they expanded it to measure total hemoglobin. Controversial results of the accuracy of the devices have been reported.

This thesis is a part of project that aims for a non-invasive and continuous total hemoglobin and dyshemoglobin measurement. The project started in 2008 with the development of a prototype device. The conventional oximetry technology was extended from two to eight wavelengths. Development data was collected in 2009 and 2010 from volunteer subjects to cover different dyshemoglobin levels and changing saturation range. The scope of this thesis is to analyze the plethymosgraphic data acquired with the prototype, and to develop a robust and simple fractional pulse oximetry (FrOx) algorithm that can reliably measure oxyhemoglobin, carboxyhemoglobin, methemoglobin, and reduced hemoglobin fractions.

Literature review of the theory of tissue oxygenation, pulse oximetry, and current multi-wavelength solutions is conducted in chapter two. Chapter three reviews the prototype development and clinical data collection phases of the project, and then methods used in the data-analysis and algorithm development are explained. In chapters four and five, the results are presented and discussed.

2 Background

Oxygen transport is vital for living organs, as oxygen is continuously needed for metabolic reactions that release energy from nutrient molecules. Cells will die in absence of oxygen supply. To understand how oxygen reaches cells, this chapter first reviews how oxygen is transported to tissues through circulatory and respiratory systems. Then pulse oximetry as a common tool for blood oxygen saturation measurement is reviewed. At the end a new approach to blood oxygenation measurement, multi-wavelength pulse oximetry, is described.

2.1 Tissue oxygenation

Tissue oxygenation can be described as a multiple staged process where respiratory and cardiovascular systems cooperate to supply oxygen (O_2) and eliminate carbon dioxide (CO_2) in the body. In tissue oxygenation process presented in Figure 1, respiratory system takes care of the gas exchange in the body (respiration) while pulmonary and systemic circulation of cardiovascular system take care of oxygen and carbon dioxide transportation in the blood.

Following sections explain in more detail how oxygen and carbon dioxide are exchanged and transported in the body. Then hypoxia, tissue oxygenation deficiency, is reviewed.

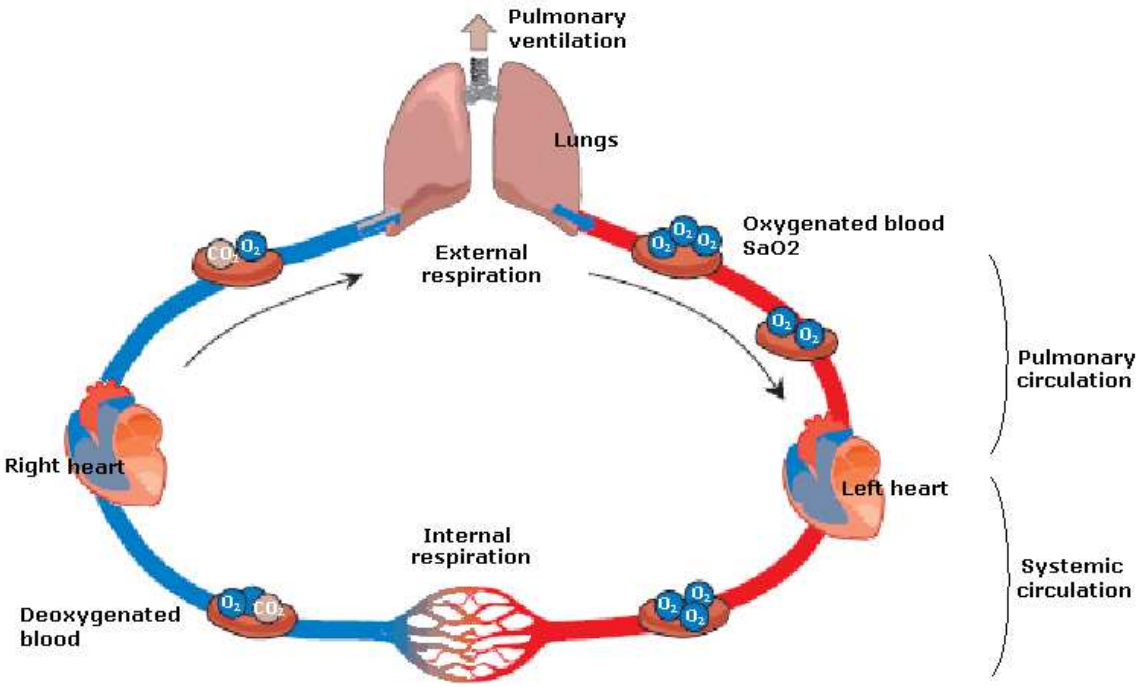

Figure 1: Process of tissue oxygenation

2.1.1 Exchange of oxygen and carbon dioxide

In tissue oxygenation process (Fig. 1), pulmonary ventilation (breathing) moves the ambient air in and out of the alveoli of the lungs through a series of cavities and tubes of the respiratory system. Air flows between the atmosphere and the lungs because of alternating pressure differences created by respiratory muscles. The rate of ventilation is controlled by respiratory neurons which get feedback from many mechanical and chemical receptors. For example rate of ventilation accelerates during exercise due to increased carbon dioxide concentration in the blood. [1, 2]

The deoxygenated blood enters pulmonary circulation from the right heart. External (pulmonary) respiration takes care of the diffusion of oxygen and carbon dioxide between the alveoli and blood in pulmonary capillaries. Gases dissolve, diffuse, and react according to their partial pressure, P, that is defined as the pressure which the gas would have if it were the only gas present in the volume. Difference in partial pressures between two regions initiates diffusion, the flow of gas molecules from a region of higher partial pressure to a region of lower partial pressure. While the inspired air in the alveoli has higher partial pressure of oxygen than in pulmonary capillary, oxygen diffuses through alveolar-capillary membrane to the deoxygenated blood until equilibrium of partial pressures is reached. At the same time carbon dioxide diffuses to the opposite direction to reach the equilibrium. The rate of gas exchange depends on the partial pressure difference, surface area, diffusion distance and the solubility and molecular weight of the gases. [1]

After external respiration pulmonary circulation transports oxygenated blood to the left heart from where it is pumped to the systemic circulation that covers all body tissues. As the oxygen rich blood reaches systemic capillaries internal (tissue) respiration takes care of the gas exchange between systemic capillaries and tissue cells through interstitial fluid. Internal respiration does not occur before systemic capillaries even if oxygenated blood passes oxygen depleted tissues because diffusion distance is too big in bigger arteries [2]. As systemic tissue cells have about 5 mmHg lower partial pressure of oxygen than oxygenated blood, oxygen diffuses into the surrounding tissue. After internal respiration deoxygenated blood returns to the right heart from where it is pumped to the pulmonary circulation and a new loop begins. [1]

Oxygen dissociation curve shown in Figure 2 presents the oxygen saturation level of hemoglobin as a function of partial pressure of oxygen (P_{O_2}) or in other words, the affinity of oxygen to hemoglobin. The shape of the curve has physiological advantages. The flat upper part means that despite relatively high changes in P_{O_2} in external respiration the saturation level will be high. Normally P_{O_2} of oxygenated blood in systemic arteries is about 100 mmHg. The steep lower part means that large amounts of oxygen can be released without a large drop in capillary P_{O_2} during internal respiration. P_{O_2} of deoxygenated blood in systemic veins is about 40 mmHg. During exercise or higher metabolic activity the partial pressure can decrease to about 20 mmHg. [2, 3]

Many external factors either move the dissociation curve to the left (higher affinity) where oxygen is more tightly bind to hemoglobin or to the right (lower affinity)

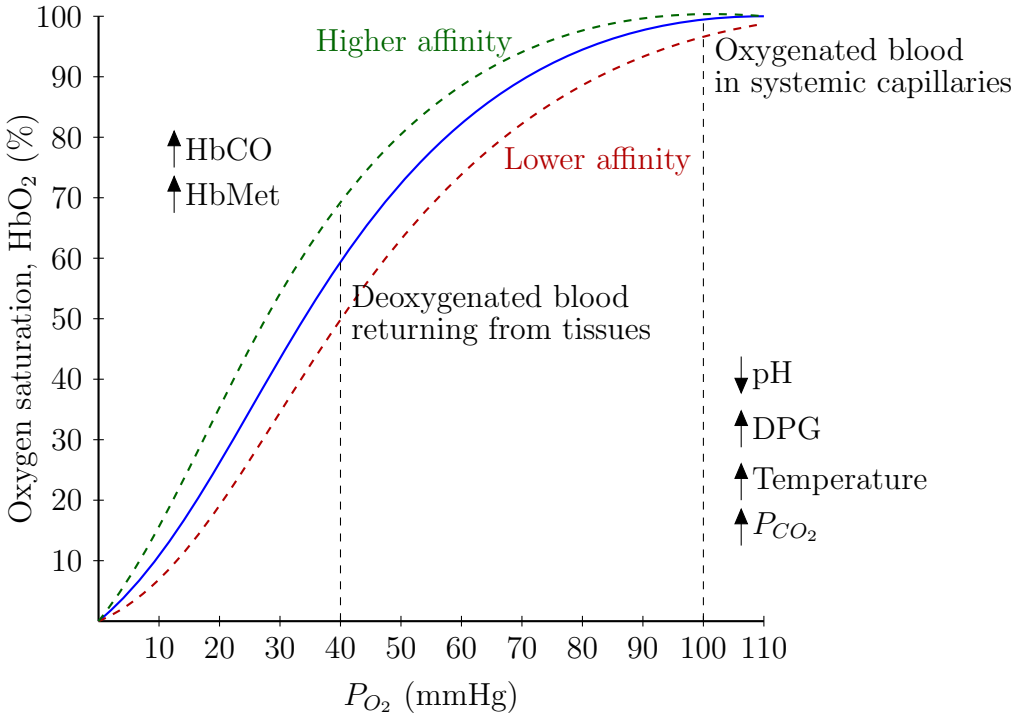

Figure 2: Oxygen hemoglobin dissociation curve. Red dotted line describes the situation where oxygen affinity is decreased and the green dotted line when the oxygen affinity is increased. The typical partial pressures of deoxygenated and oxygenated blood are marked with dotted vertical lines.

where oxygen is released more easily. These changes are illustrated in Figure 2 with green and red dotted lines. Increasing acidity (decreasing pH) moves the curve to the right because increased amount of hydrogen ions alters the structure of the hemoglobin molecule and its oxygen-carrying capacity decreases. Same effect occurs when partial pressure of carbon dioxide increases and more hydrogen ions are available in the blood. In addition, increasing temperature and 2,3-bisphosphoglycerate (DPG) concentration, break down product of glycolysis, help unloading of oxygen from hemoglobin and the curve moves to the right. Increase in concentrations of dyshemoglobins moves the curve to the left. [1, 3]

2.1.2 Transport of oxygen and carbon dioxide in the blood

Oxygen and carbon dioxide are transported in the blood with different ways. Oxygen is transported either in dissolved state or in chemical combination with hemoglobin in the red blood cells. Only about 1.5 percent of oxygen is dissolved in blood plasma and the rest is bound to the hemoglobin molecule.

Figure 3 presents the structure of the hemoglobin molecule. The quaternary structure of hemoglobin consists of globin, a protein composed of two alpha and two beta polypeptide chains and four nonprotein pigments called hemes. A heme contains an iron atom that is normally in the ferrous (Fe^{2+}) oxidation state to

support oxygen binding. The change in the shape of the quaternary structure with level of oxygenation alters the optical absorption spectrum. [1, 3]

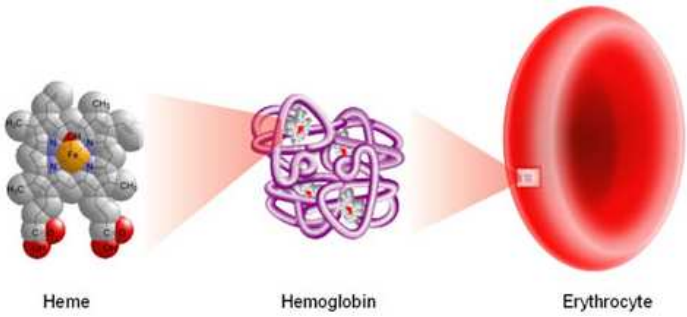

Figure 3: Iron-containing heme, hemoglobin molecule and red blood cell [4].

Oxygen and hemoglobin combine in an easily reversible reaction written in Equation 1 to form oxyhemoglobin (HbO_2). After first oxygen molecule binds to heme of the hemoglobin molecule it is easier for other oxygen molecules to bind to the other hemes. This is true also for the reverse reaction. [3]

$$\underset{\text{Reduced hemoglobin}}{\text{RHb}} + \underset{\text{Oxygen}}{O_2} \longleftrightarrow \underset{\text{Oxyhemoglobin}}{HbO_2} \tag{1}$$

Hemoglobin has some competitive binding of other compounds than oxygen including carbon monoxide, cyanide, sulfur monoxide, nitrogen dioxide and sulfide. All of these bind to the iron in the heme inhibiting oxygen-binding. Also change in the oxidation to ferric (Fe^{3+}) state converts hemoglobin into methemoglobin (HbMet), which cannot bind oxygen. [1]

Carbon dioxide is transported in the blood in three ways: about seven percent is dissolved in blood plasma, 23 percent is combined with globin forming products called carbamino compounds, and the rest as bicarbonate ions within red blood cells. [1]

2.1.3 Hypoxia

Hypoxia, cellular oxygen deficiency, occurs when oxygen demand in tissues exceeds oxygen delivery. Tissue oxygen delivery is defined as described in Equation 2. Cardiac output (CO) is the amount of blood flow in the cardiovascular system, total hemoglobin concentration (tHb) is a measure of oxygen carrying capacity of the blood and arterial oxygen saturation (SaO_2) is the relative amount of oxygenated hemoglobin.

$$\underset{\text{Oxygen delivery}}{\text{DO2 (g/min)}} = \underset{\text{cardiac output}}{\text{CO (L/min)}} \cdot \underset{\text{hemoglobin concentration}}{\text{tHb (g/L)}} \cdot \underset{\text{oxygen saturation}}{\text{SaO2 (\%)}} \tag{2}$$

Possible symptoms of hypoxia include severe headaches, cyanosis (a bluish discoloration of the skin and mucous membranes), nausea, hyperventilation, fatigue,

seizures, coma, and death. The symptoms vary depending on the severity of the hypoxia. Prolonged gradually developing hypoxia is difficult to recognize. Extreme hypoxia, anoxia, is complete deprivation of oxygen supply to the tissues. In presence of anoxia, especially some organs with high metabolic rate may suffer irreversible damages. For example cerebral cortex survives for less than one minute, heart for five minutes, liver and kidney for ten minutes and skeletal muscles for two hours. [2,3,5]

Hypoxia is classified in four groups based on the cause: hypoxic, anemic, ischemic or histotoxic hypoxia. In hypoxic hypoxia,oxygen concentration of arterial blood is low due to low partial pressure of oxygen in arterial blood caused by respiratory disease or low fraction of inspired oxygen. In anemic hypoxia, the amount of functional hemoglobin is reduced for example because of elevated dyshemoglobin or anemia. In ischemic hypoxia, blood flow is very low affecting the rate of oxygen delivery. In histotoxic hypoxia, some toxic agent prevents tissues to use oxygen even in otherwise sufficient supplies of oxygen.

Hypoxemia is defined as low oxygen saturation in blood and does not necessarily cause hypoxia if the demand of oxygen does not exceed oxygen delivery. In this section, causes of hypoxemia, carboxyhemoglobinemia, methemoglobinemia and anemia are further reviewed. [1, 2]

Carboxyhemoglobinemia

Carbon monoxide (CO) poisoning or carboxyhemoglobinemia is a leading cause of death by poisoning in developed countries. CO is colorless, odorless and poisonous gas that binds to hemoglobin forming carboxyhemoglobin (HbCO). Carbon monoxide's affinity to bind to hemoglobin is 200–250 times greater than oxygen's. Carbon monoxide decreases the oxygen carrying capacity of hemoglobin and increasing concentration of HbCO decreases the oxygen release from hemoglobin to tissues. CO poisoning is caused by inhalation of carbon monoxide, tobacco smoking, fumes, faulty heating systems, automobiles, charcoal burners and fires. Nonsmokers have normal carboxyhemoglobin levels from one to three percent whereas smokers may have level up to fifteen percent. [6]

Symptoms of carboxyhemoglobinemia are similar with conditions such as flu, viral infections, migraine and food poisoning. Common nature of symptoms can be seen from Table 1 which lists the acute symptoms reported by patients after carbon monoxide exposure. Only weak correlation has been shown between the HbCO level and the severity of the symptoms. Skin decoloration to cherry pink is seldom seen in living patients although it is the classical feature of CO poisoning [7]. Delayed symptoms can occur after many days or even months after poisoning. These include myocardial injury and development of neurophysiological syndrome with symptoms such as behavioral changes, parkinsonism and dementia. Because CO poisoning can result in long-term morbidity even if treated, prevention, diagnosis and treatment are extremely important. CO exposure for more than one hour may increase morbidity. Especially very young and old people are at greater risk. [6, 8, 9]

Yearly about 2800 people die unintentionally for CO poisoning in the United States from which non-fire related deaths account for approximately 500 [8, 10].

Table 1: Symptoms reported by patients after exposure to carbon dioxide.

Symptom	Percentage of patients
Headache	91
Dizziness	77
Weakness	53
Nausea	47
Confusion	43
Shortness of breath	40
Visual changes	25

Hampson and Weaver estimated that there are approximately 50 000 emergency department visit for CO poisoning corresponding to a prevalence of 1 to 10 000 in a population in the United States every year. The count was significantly higher than previous estimations (10 000 to 15 000). [11] In Great Britain the death rate was 250 but there is a concern that figures are greater [9].

When diagnosis of carboxyhemoglobinemia is established the patient needs to be removed from the source and then treated with high flow of normobaric or hyperbaric oxygen (HBO) as soon as possible. In HBO, patients are exposed to high partial pressure of oxygen. Carbon monoxide has half-life of four to six hours in room air, 40 to 80 minutes in normobaric 100 % oxygen and 15 to 30 minutes in HBO. Some contradictory results of the benefit of HBO have been reported and the treatment includes risks. [6, 7, 9]

Methemoglobinemia

Methemoglobin is formed when ferrous iron (Fe^{2+}) is oxidized to ferric state (Fe^{3+}) which is unable to carry oxygen. Normal methemoglobin level in the blood is from zero to two percent. Several endogenous reduction systems exist to maintain hemoglobin in ferrous state. During methemoglobinemia oxygen carrying capacity is reduced for two reasons: maximum oxygen carrying capacity is lowered and any oxygen that is carried by a deoxidized hemoglobin subunit is held on to more tightly and poorly released to tissues. Also ferric iron has greater affinity for monovalent anions (CN^-, F^- and Cl^-) compared to uncharged binding compounds (CO_2, CO and O_2). [12]

Some common drugs including dapsone and local anesthetic agents such as benzocaine and lidocaine, a variety of nitrogen containing chemicals, dyes, fertilizers and industrial products cause methemoglobinemia. Some of these oxidize hemoglobin directly and some by reducing oxygen to free radical O_2^-. Methemoglobinemia is also induced if protective reduction systems are inhibited. Genetic defects in red blood cell metabolism or hemoglobin structure also cause methemoglobinemia. [12, 13]

Diagnosing methemoglobinemia is extremely difficult. It is asymptomatic up to concentrations of $10 - 15$ % and even with higher concentrations symptoms are similar with general disorders like cold, flu and viral infections. With higher than 10 % concentration color of blood may turn to chocolate brown. Table 2 shows the symptoms and signs associated with different methemoglobin levels. [3, 14] Rapid changes may induce severe symptoms with when lifelong methemoglobinemia can be asymptomatic with same levels [13]. Few studies show that clinical factors such as sepsis, anemia, hospitalization are associated to acquired methemoglobinemia [15–17].

Table 2: Symptoms and signs of methemoglobinemia

%MetHb	Symptoms or signs
0–15	asymptomatic
15–20	chocolate brown blood, clinical cyanosis
20–45	dyspnoe; fatigue, dizziness, lethargy, headache, syncope
45–55	decreasing level of consciousness
55–70	come, convulsions, cardiovascular failure, cardiac arrhytmias
> 70	death

In 2004, Ash-Bernal *et al.* published retrospective analysis that proved that acquired methemoglobinemia (> 2 %) is more common than thought. They collected CO-oximetry data for 28 months and found that 414 (19 %) of 2167 patients had elevated methemoglobin levels. During the study acquired methemoglobinemia let to one death and three near-deaths. In this study, dapsone was the most common etiology of acquired methemoglobinemia. [15]

Moore *et al.* [18] reported that in cases where benzocaine products were used, 67 % of cases involved either definite or probable acquired methemoglobinemia. In addition, Guay [19] summarized all episodes of local anesthetic-related methemoglobinemias found from literature. Based on the study they concluded that benzocaine should not be used anymore and use of prilocaine should be avoided with under 6-year old children, pregnant women or with patients taking other oxidizing drugs.

The treatment of methemoglobinemia should include both symptomatic and specific therapy. Symptomatic treatment ensures oxygen supply and maximizes the oxygen carrying capacity of hemoglobin. Most common specific treatment is infusion of methylene blue. Also ascorbic acids are given for some patients. In all cases, aggressiveness and type of treatment needs to be determined case by case keeping symptoms and other conditions in mind. [13, 14, 19]

Anemia

Anemia is the most common disorder in the blood. In anemia, the oxygen-carrying capacity of blood is reduced because of reduced number of red blood cells or decreased amount of hemoglobin in the blood. Iron-deficiency, impaired red blood cell

production, increased red blood cell destruction, blood loss and fluid overload are common causes of anemia. [1]

Medically anemia is defined as hemoglobin concentration (tHb) under 120 g/L for females and under 130 g/L for males. Generally anemia is thought to be a minor medical condition although healthcare professionals have stated that it affects negatively to mortality and morbidity. Worldwide it is estimated that over two billion people are affected by anemia. [20]

Symptoms of anemia include weakness, fatigue, poor concentration, coldness and skin paleness. In addition, it is associated with other diseases such as cancer, HIV and rheumatoid arthritis. WHO has stated that anemia is the largest global illness adversely affecting mortality and worker capacity. Especially in developing countries these effects of anemia are amplified. [1, 20, 21]

Treatment of anemia depends on the severity or the cause. Iron-deficiency anemia is easy treat with iron supplements. Medicines that stimulate red blood cell production can be used with chronic anemia. Acute anemia or cases with ongoing blood loss can be treated with blood transfusion. [1]

2.2 Pulse oximetry

Pulse oximetry is a relatively recent essential tool in current practice of medicine both in care of anaesthesia and critical care that measures blood oxygenation. Current two wavelength pulse oximetry is based on two principles: distinction of arterial blood pulsation from the other tissue components, and different absorption spectra of oxyhemoglobin (HbO_2) and reduced hemoglobin (RHb) over wavelengths.

Conventional pulse oximeters show plethymosgraphic signal and SpO_2 value that is defined as arterial oxygen saturation measured by pulse oximetry. Plethymosgraphic signal presented in Figure 4 is the transmission signal of alternating arterial blood component that is normalized with constant component reflecting the absorption of static arterial blood component, venous blood and other tissues such as skin, pigmentation and bones. The transmission of light decreases during systole and increases during diastole. [3]

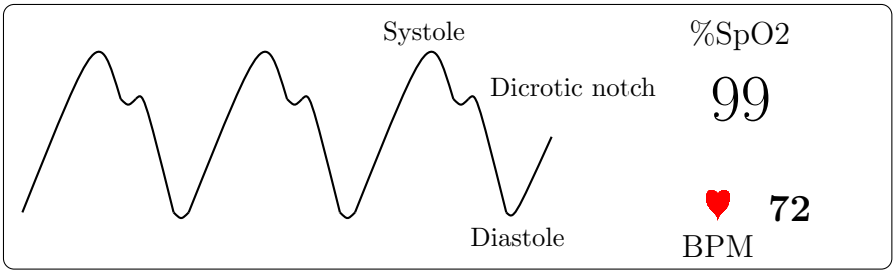

Figure 4: A typical view of pulse oximeter screen. In addition to SpO_2 value, plethymosgraphic signal and pulse rate are shown.

Plethymosgraphic signal is normally used to recognize unreliable SpO_2 measurement but it can also be used in detecting and diagnosing cardiac arrhythmias,

measuring vascular distensibility and determination of systolic blood pressure. Standardization and quantification of the plethymosgraph needs still to be clarified before the clinical potential of plethymosgraphic signal is revealed. In addition to SpO_2 measurement and plethymosgraph modern pulse oximeters provide some other information, such as pulse rate (PR), perfusion index (PI), a measure of relative strength of perfusion, and pleth variability index (PVI), a measure of fluid responsiveness. [3, 22, 23]

This section describes how blood oxygenation can be measured by pulse oximetry. First the basis of oximetry, Beer-Lambert law, is explained, then the theory of pulse oximetry and calibration methods are described. At the end accuracy and limitations of pulse oximetry are reviewed.

2.2.1 Beer-Lambert law in oximetry

The measurement principle of oximetry is based on Beer-Lambert law presented in Figure 5 that describes light attenuation through a sample of homogenous non-scattering media.

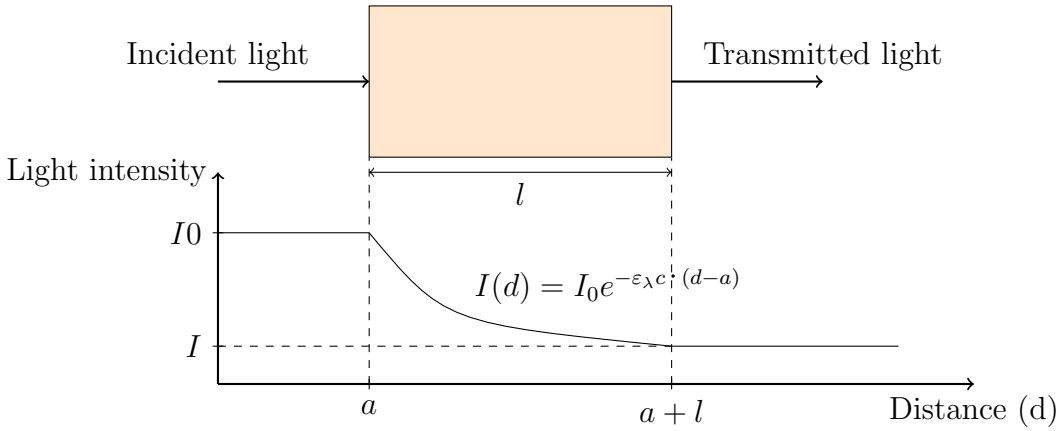

Figure 5: Beer-Lambert law

Mathematically law is expressed as

$$I = I_0 e^{-\varepsilon_\lambda c l}, \tag{3}$$

where I is the transmitted intensity of the light, I_0 is the incident intensity, ε_λ is the extinction coefficient or absorptivity of the absorbent at wavelength λ, c is the concentration of the absorbent, and l the optical path-length of the sample. Beer-Lambert law is valid when there is one unknown substance in clear, non-turbid solution and constant path-length. In addition, there should be no chemical reactions or reactions between absorbent and solvent.

In case where the sample consists of layers of absorbents as presented in Figure 6, the total intensity of transmitted light presented in Equation 4 is a linear superposition of intensities of each absorbent

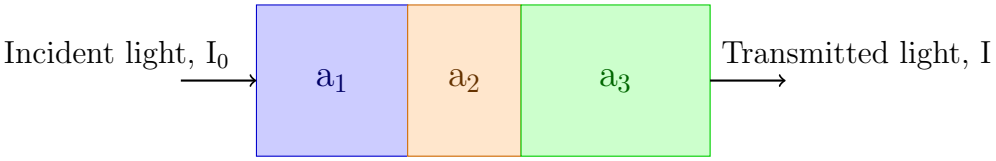

Figure 6: Layers of absorbents in a sample in Beer-Lambert situation.

$$I = I_0 e^{\sum -\varepsilon_{\lambda,a} c_a l_a} = I_0 e^{-A}, \tag{4}$$

where a represents an absorbent or analyte. [2,3]

Oximetry is based on the change in the absorption of electromagnetic energy (color) of hemoglobin molecule when its chemical binding is altered. Oxyhemoglobin, reduced hemoglobin, carboxyhemoglobin and methemoglobin have their own characteristic colors that can be described with extinction coefficients. The extinction coefficients of four most common hemoglobin species are presented in Figure 7 in the wavelength range from 570 to 1000 nm the visible light end of the spectrum into the near infrared. Figure shows that HbCO is not absorbing almost at all at long wavelength and has quite similar absorption with oxyhemoglobin with short wavelengths. Methemoglobin absorbs heavily around 640 nm and wavelengths above 840 nm. Wavelengths most commonly used in pulse oximetry 660 nm (red) and 940 nm (infrared) are marked with vertical lines. Their selection is based on large difference in absorptions of HbO2 and RHb, manageable tissue absorption and flatness of spectrum. [2,3]

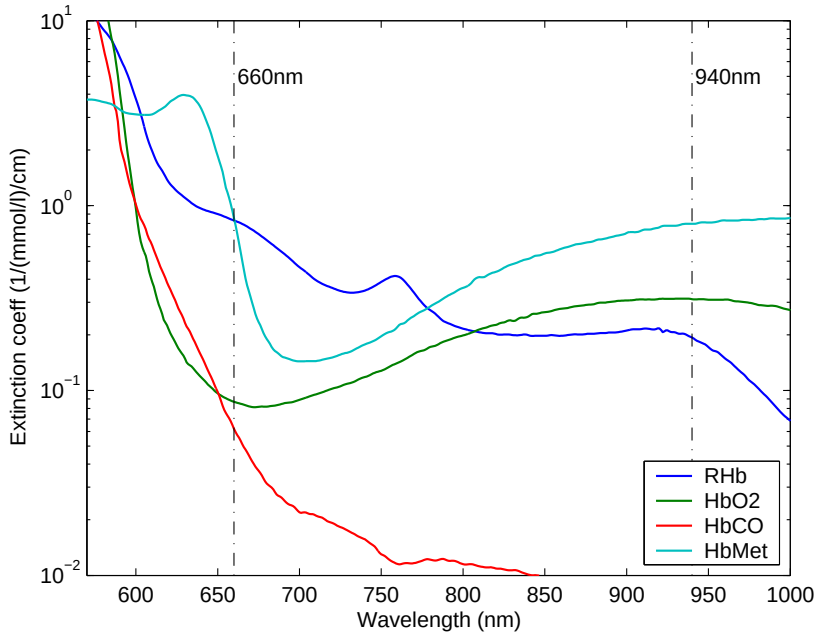

Figure 7: Extinction coefficients of hemoglobin species in the range from 570 to 1000 nm.

2.2.2 Theory of pulse oximetry

Absorbance (A) at wavelength λ is defined as the negative natural logarithm of the fraction of light that passes through a sample called transmission T. Combined with Equation 4 the absorbance can be written in form

$$A_\lambda = -ln(T) = -ln\left(\frac{I}{I_0}\right) = \sum_a \varepsilon_{\lambda,a} \cdot c_a \cdot l_a, \tag{5}$$

where a represents all tissue components such as arterial blood, venous blood, skin and bones in the sample.

Figure 8 presents the how the photoplethymosgraphic (PPG) signal is formed. The lower part presents the tissue layers in a sample and upper part shows the transmission signal. DC component of transmission signal is defined as the transmission without blood volume pulsation. DC component varies only slowly due to respiration, sympathetic nervous system activity, thermoregulation and changes in total hemoglobin concentration. In pulse oximeters, the time-dependent arterial pulsation of transmission signal, also called AC component, is separated from the total transmission signal. The strength of the AC component is only about one to two percent of the total transmission. It is the time-derivative of the total absorbance where the only time-dependent signal is the path length, l_{art}, through arterial blood. Differential absorption (dA_λ) is presented in equation

$$dA_\lambda = \frac{d(A_\lambda)}{dt} \cdot \Delta t = \frac{dl_{art}}{dt} \cdot \sum \varepsilon_{\lambda,art} \cdot c_{art} \cdot \Delta t. \tag{6}$$

On the other hand differential absorption can be assessed through transmitted intensity (Eq. 5) through the arterial blood component as written in equation

$$dA_\lambda = \frac{d\left(-ln\left(\frac{I(t)}{I_0}\right)\right)}{dt} \cdot \Delta t = \frac{I'(t)}{I(t)} \cdot \Delta t \cong \frac{AC_\lambda}{DC_\lambda} = \frac{I_{max} - I_{min}}{I_{max}}. \tag{7}$$

During one pulse differential absorption can be approximated with the DC component (DC_λ) and AC component (AC_λ) intensities, that can be calculated from the minimum transmission after systolic rise, I_{min}, and diastolic maximum transmission of light, I_{max}.

Current conventional two wavelength pulse oximeters use light-emitting diodes (LEDs) of wavelengths 660 nm (red light) and 940 nm (near-infrared light) and semiconductor photodetector to obtain plethymosgraphic signal from an extremity such as finger or earlobe. Ratio of two differential absorptions with different wavelengths, ratio-of-ratios (R), is calculated to obtain SpO_2. Based on theory, R can be presented with equation

$$R = \frac{dA_{red}}{dA_{ired}} = \frac{(\varepsilon_{HbO_2,red} \cdot c_{HbO2} + \varepsilon_{RHb,red} \cdot c_{RHb}) \cdot \Delta l}{(\varepsilon_{HbO_2,ired} \cdot c_{HbO2} + \varepsilon_{RHb,ired} \cdot c_{RHb}) \cdot \Delta l}. \tag{8}$$

When the thickness of the heartbeat-added arterial layer, Δl, is estimated to be equal for both wavelengths, assumption, $tHb \cdot SpO_2 \approx c_{HbO2}$, is made, and a

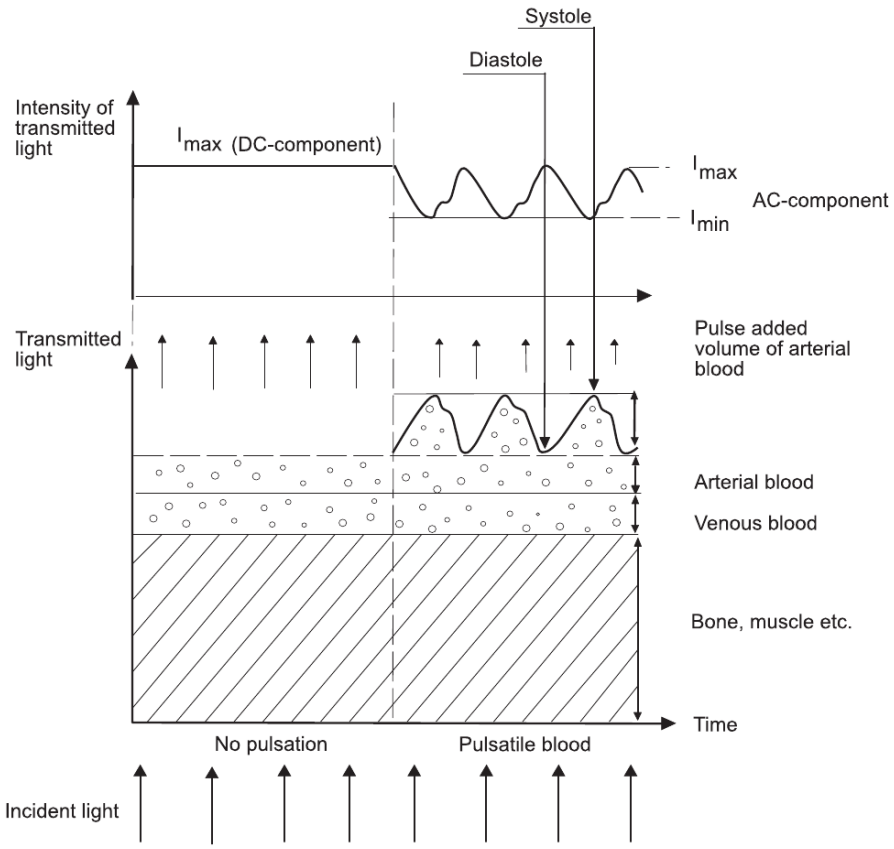

Figure 8: Light transmission during plethymosgraphic measurement.

constraint of two hemoglobin species, $c_{RHb} + c_{HbO2} = tHb$, is included, the equation can be rewritten in form

$$R = \frac{\varepsilon_{HbO_2,red} \cdot SpO_2 + \varepsilon_{RHb,red} \cdot (1 - SpO_2)}{\varepsilon_{HbO_2,ired} \cdot SpO_2 + \varepsilon_{RHb,ired} \cdot (1 - SpO_2)}, \tag{9}$$

which can be solved for SpO_2 as presented in equation

$$SpO_2 = -\frac{\varepsilon_{RHb,red} - R \cdot \varepsilon_{RHb,ired}}{(\varepsilon_{HbO_2,red} - \varepsilon_{RHb,red}) - R \cdot (\varepsilon_{HbO_2,ired} - \varepsilon_{RHb,ired})}. \tag{10}$$

Theory presented above is based on the Beer-Lambert assumptions that in reality are not valid in *in vivo* tissues. Other substances are present in blood and the incident light is partially scattered, refracted and reflected. The detected light at the photodetector consists of photons that travel different routes. Some of the photons travel through the tissue without migrating from the line that emitter and detector form and some scatter farther from the line and still reach the detector at the other end. When the absorption increases the detected light tends to come more from the shorter paths. Because of this path lengths vary with different wavelengths. Because of these deviations from the Beer-Lambert law conventional pulse oximeters are empirically calibrated to give better estimation of oxygen saturation. [2, 24]

2.2.3 Calibration

Pulse oximeters are calibrated to compensate deviations from Beer-Lambert law. They can be calibrated either against functional or fractional oxygen saturation of arterial blood. [3, 25] Functional saturation is defined as shown in equation:

$$\text{Functional } SaO_2 = \frac{c_{HbO_2}}{c_{HbO_2} + c_{RHb}} \times 100\%. \tag{11}$$

Using this definition oxygen saturation can reach 100 % even in the presense of other ligands such as HbCO. Many manufacturers use functional calibration in their devices. Dyshemoglobins, carboxyhemoglobin and methemoglobin, are included in the definition of fractional saturation presented in equation:

$$\text{Fractional } SaO_2 = \frac{c_{HbO_2}}{c_{HbO_2} + c_{RHb} + c_{HbCO} + c_{HbMet}} \times 100\%. \tag{12}$$

Calibration procedure of pulse oximeters is presented in Figure 10. Test subjects are volunteers that range in age, gender and skin tone. For example U.S. Food and Drug Administration (FDA) requires that at least 30 % of volunteers need to have dark skin pigmentation. Calibration of pulse oximeters assumes normal dyshemoglobin level that is ensured with pre-screening blood test before data collection. Normal methemoglobin level is about 0.4 % and carboxyhemoglobin level of $1 - 3$ %.

In test subject preparation, arterial cannula is set for drawing arterial blood samples. Blood circulation of fingers is checked after cannulation. Measurement sensors are attached to the extremities of the test subject. Before data collection starts 100 % saturation level is ensured by letting the subject breath an oxygen/air mix. [2, 26]

During data collection oxygen content of the blood is reduced incrementally by letting the subject breath gas mixtures with low oxygen content. Blood samples are taken at each level when the pulse oximeter shows stable reading and they are analyzed with CO-oximeters. Samples are collected at least over saturation range from 70 % to 100 %. With *in vivo* calibration method only saturation levels down to 60 % can be reached due to ethical issues. Values below 60 % can be achieved through *in vitro* calibration using blood. [2, 27]

In calibration curve of pulse oximeters either functional or fractional saturation is plotted against measured ratio-of-ratios. A best fit curve is fitted to the collected data using regression methods. The data is stored in form of look-up table of calibration equation in the pulse oximeter. An example of a calibration plot is shown in Figure 9. [2]

Pulse oximeter performance against requirements of authorities needs to be verified before they can reach the market. For example FDA recommends the use of standard ISO 9919 that was recently revised with ISO 80601-2-61 *Medical electrical equipment – Part 2-61: Particular requirements for basic safety and essential performance of pulse oximeter equipment.* It requires that manufacturers need to report the calibration range, reference, accuracy, methods of calibration and range of displayed saturation level. In addition, FDA recommends that at least 200 data points

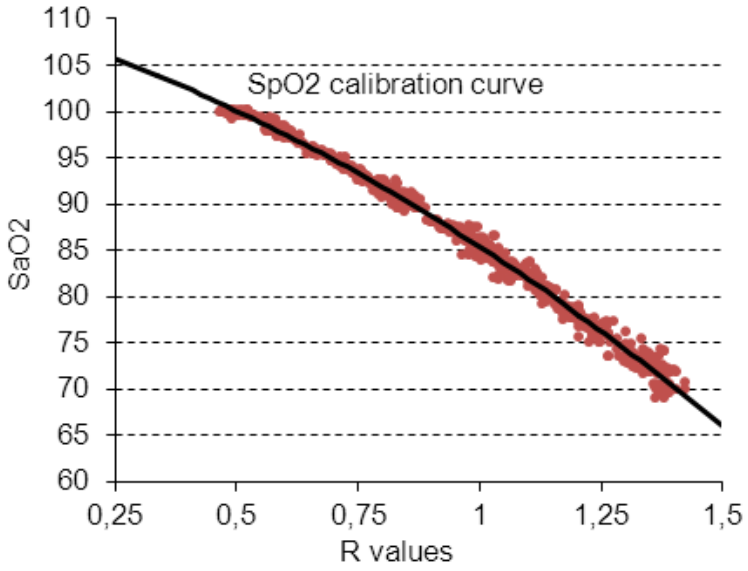

Figure 9: An example of a calibration data set and a best fit calibration curve.

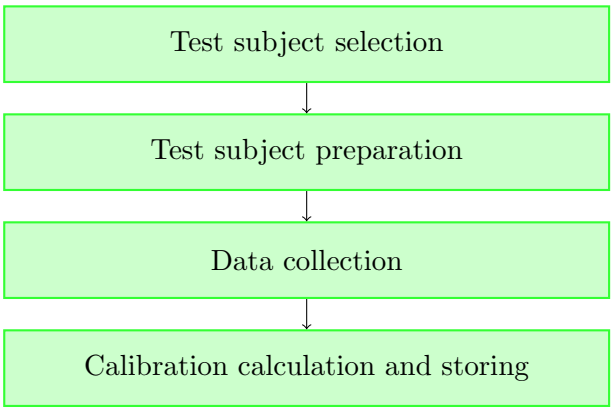

Figure 10: Calibration procedure of pulse oximeters.

equally spaced over a saturation range of 70 to 100 % are collected and accuracy (A_{RMS}) is at least $3 - 3.5$ %. [2, 26, 27]

In calibration process, blood samples are analyzed with CO-oximeters. CO-oximetry or hemoximetry is the 'gold standard' of blood oxygenation measurements. CO-oximetry is invasive and non-continuous measurement designed to measure total hemoglobin and hemoglobin species. In CO-oximeters small samples of blood are hemolyzed to reduce the amount of scattering and passed into to a cuvette with known path-length. Commercially available devices use at least four wavelengths to be able to measure all four relevant forms of hemoglobin. Wavelengths are selected normally from the range under 700 nm. [2, 3]

All errors in CO-oximetry readings are carried into the pulse oximeters in the calibration phase. Any scattering substances left in the cuvette such as lipids or cell fragments produce an error in the reading. The CO-oximetry accuracy of fractional

oxygen saturation is about $0-1$ % with high saturation (≥ 97 %) and error increases with lower saturation levels. Methemoglobin accuracy was estimated to be about $0-1$ % and carboxyhemoglobin $0-4$ %. [27, 28]

In addition to inconvenience of the CO-oximetry measurement due to invasive blood samples, other disadvantages are discontinuity and the cost of the measurement. Hampson *et al.* [29] reported that fewer than half-of acute care hospitals had the capability to measure dyshemoglobin. Others have to send the samples to an another hospital. Anyway CO-oximetry is one of the most accurate methods for measuring all four species of hemoglobin and it is used as the standard against which other methods are compared. [2, 3]

2.2.4 Accuracy and limitations of pulse oximetry

Several factors affect the accuracy of pulse oximetry reading. In pulse oximetry, SpO_2 values are compared to CO-oximetry results. Commonly reported parameters are bias, precision and accuracy root mean square (A_{RMS}). Bias is defined as the mean of differences between pulse oximeter value and CO-oximeter value as presented in equation

$$\text{bias} = \frac{\sum_i^N (SpO2_i - SaO2_{COox,i})}{N} = \overline{x}, \tag{13}$$

where $SaO2_{COox,i}$ is the CO-oximeter value, $SpO2_i$ is the saturation measured by pulse oximetry and N is the number of measurements in a specified oxygen saturation range. Positive bias means that pulse oximeter overestimates the actual saturation. Precision is the standard deviation of the data cloud around the best fit line as presented in equation

$$precision = \sqrt{\frac{\sum_i^N (SpO2_i - SpO2_{mean,i})^2}{N-1}}, \tag{14}$$

where $SpO2_{mean,i}$ is the value of the best fit curve. Precision tells how big the data cloud is, not how far from the correct value the values are. Accuracy root mean square (A_{RMS}) is the root mean square error of the pulse oximeter value and CO-oximeter value. A_{RMS} is the value that is required by regulatory agencies when overall quality of the device is evaluated. [2, 27] It is calculated with equation,

$$A_{RMS} = \sqrt{\frac{\sum_i^N (SpO2_i - SaO2_{COox,i})^2}{N}}. \tag{15}$$

In healthy volunteers, oximeters have been reported to have less than two percent bias and less than three percent precision when SaO_2 is above 90 %. The accuracy differs between manufacturers mainly due to different signal processing techniques. Accuracy deteriorates when SaO_2 decreases. [30, 31]

Various limitations of pulse oximetry affect its accuracy. They arise from different sources and can be divided in two categories, technical and physiological limita-

tions. Some of them can be avoided with pulse oximeter design or signal processing techniques. Table 3 lists the most common limitations of pulse oximetry. [2, 3]

Table 3: Limitations of pulse oximetry

Technical	Physiological
Ambient light	Dyshemoglobins
Optical shunt	Other absorbents
Motion artifacts	Low perfusion
Calibration	Venous pulsations
Malpositioning of the sensor	Pigmentation

As pulse oximeters only have two wavelengths, they can measure only two substances. Other substances (false absorbers) in the blood or on the tissue such as HbCO or HbMet interfere spectrally with pulse oximetry. The effects of HbCO and HbMet on pulse oximetry are presented in Figure 11. In presence of elevated HbCO, pulse oximeters overestimate SaO_2 values approximately with the percentage of HbCO in the blood [32, 33]. With elevating methemoglobin level, SpO_2 reading initially decreases but not as steeply as SaO_2. With HbMet level at $30 - 35$ % % SpO_2 level stabilizes to a level of $82 - 86$ % because HbMet adds to both signals when ratio-of-ratios drives towards unity. [34]

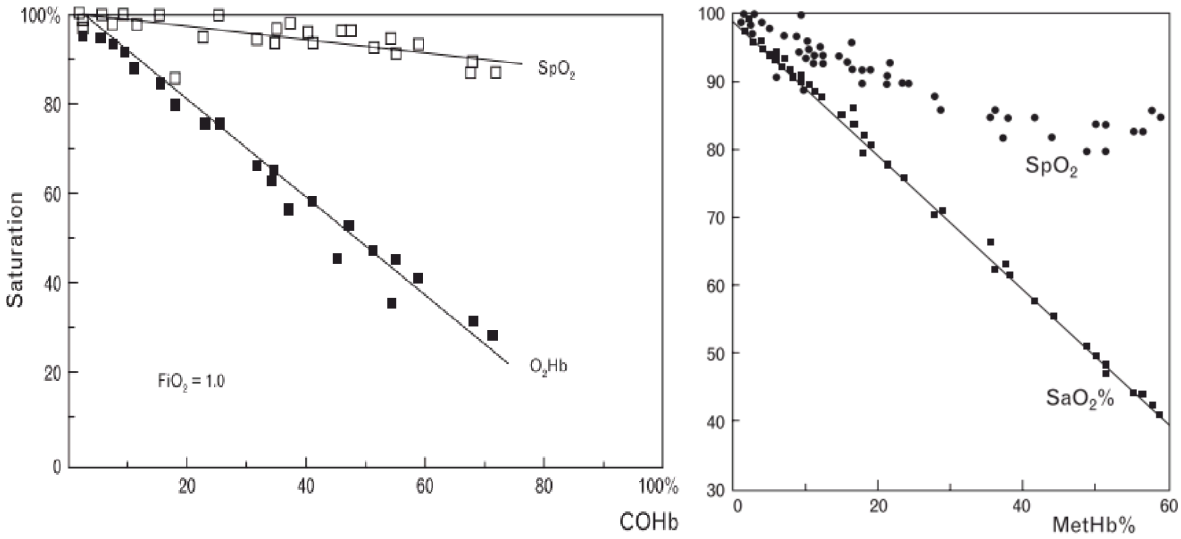

Figure 11: The effects of carboxyhemoglobin [32] and methemoglobin [34] on pulse oximetry readings. Black squares represent SaO_2 (O_2Hb) values and unfilled squares on the left and black circles on the right represent SpO_2 values.

Reynolds *et al.* [35] calculated the effects of elevated dyshemoglobin levels theoretically and compared them to *in vitro* test results. They noticed that the theoretical relationships based on a pure absorbing solution are not easily applicable to a clinical situation but give a good approximation of the effects.

Intravenous dyes such as methylene blue, indocyanine green and indigo carmine can be a reason for falsely low SpO_2 readings. For example methylene blue has very high absorbance at 660 nm. In contrary, hyperbilirubinemia does not affect the accuracy, even though it might cause artifactual high HbCO and HbMet levels measured by CO-oximetry. Other possible sources of errors are black, green and blue nail polishes. Fetal hemoglobin and sickling red blood cells have been reported not to have significant effects on pulse oximetry. Controversy reports have been reported from the effect of anemia, some of them claim that underestimation of SaO_2 occurs at low hemoglobin concentrations and some that anemia has no effect on SpO_2. [3, 30]

Triscupid incompetence with regurgitation, arteriovenous dissociation, right heart block and right atrial myxoma might cause pulsation in large venules and veins where oxygen saturation is lower than in arteries. This induces an error to the signal because in presence of both venous and arterial pulsations pulse oximeter cannot distinguish the arterial pulsation. [3]

Low peripheral blood perfusion caused by hypothermia, low cardiac output, vasoconstriction or hypotension reduces the pulsatile volume of blood in the tissue which reduces the signal strength and quality. This makes it difficult for a pulse oximeter to distinguish the signal from the background noise. [2, 36]

Ambient light from sources such as fluorescent light, surgical lamps, fiberoptic instruments and sunlight causes an additional DC signal that interferes with the optical measurement. Measurement cycle of pulse oximeters is designed to reduce the effect of ambient light. It consist of three periods, one for each wavelength transmission and one for ambient light measurement. Proper design and placement of the sensor also reduce the effects of ambient light. Despite the efforts the noise from the ambient light still remains in the measured signal. Also light from the LEDs will cause an error if it reaches the detector without passing through pulsatile arterial bed (optical shunting). [2, 30]

Transient motion is a significant source of error and cause of false alarms. Even tiny movements add artifacts to the plethymosgraphic signal because the AC component is only 1-2 % of the total transmission. Some of the motion artifacts such as shivering, seizure activity, repetitive cough or exercise can be removed by signal processing methods or visually observing plethymosgraphic signal but artifacts in the cardiac frequency range are difficult to distinguish. [2, 30]

Calibration assumptions and methods cause also errors in the measurement. Calibration is usually done for saturation range $70 - 100$ %. Pulse oximeters have been shown to be inaccurate when oxygen saturation is less than 75 %. Subject variability and use of human adult hemoglobin are also sources of error. [3]

Other possible sources of errors in pulse oximetry are skin pigmentation and sensor type [37], magnetic resonance imaging, improper probe position, supplementary oxygen, or various medical conditions. [2, 3, 30]

2.3 Multi-wavelength pulse oximetry

Conventionally total hemoglobin concentration and dyshemoglobin fractions are measured with CO-oximetry. CO-oximeter availability in hospitals is poor [29] and cost effective and non-invasive user friendly tool for measuring total hemoglobin and true fractional hemoglobin values is needed.

Fractional multi-wavelength pulse oximetry would increase the accuracy of arterial oxygen saturation measurement and detect carboxyhemoglobinemia and methemoglobinemia. Specially in a busy emergency department (EDs) or pre-hospital or emergency medical services (EMS) area, a device that would identify unexpected CO poisoning might lead to early detection and treatment of the condition [38–41]. Ash-Bernal *et al* [15] recommended frequent CO-oximeter tests to detect and treat methemoglobinemia.

The total hemoglobin (tHb) blood test is one of the most ordered laboratory test in acute and outpatient settings. In United States, tHb measurement is performed over 400 million times per year [42]. Non-invasive and continuous hemoglobin or hematocrit (proportion of blood volume that is occupied by red blood cells) measurement would provide immediate information of patient's red blood cell concentration. In particular, the benefits would be in area of blood transfusions and general fluid management. One possible application would be increasing patient safety and comfort in all care areas where tHb measurements are needed. For example common blood sample test for detecting anemia could be replaced with non-invasive tHb measurement. [20]

This section reviews the theory and calibration methods of multi-wavelength oximetry. At the end current solutions in multi-wavelength oximetry are reviewed

2.3.1 Theory of multi-wavelength pulse oximetry

The Beer-Lambert theory for pulse oximetry presented in previous section 2.2.2 can be generalized to apply for a multi-wavelength system. For a system of n wavelengths and m analytes Equation 6 can be expressed with the following matrix notation,

$$\begin{bmatrix} dA^{LB}_{\lambda 1} \\ \vdots \\ dA^{LB}_{\lambda n} \end{bmatrix} = \begin{bmatrix} \Delta l_{\lambda 1} \cdots 0 \\ \vdots \ddots \vdots \\ 0 \cdots \Delta l_{\lambda n} \end{bmatrix} \begin{bmatrix} \varepsilon_{\lambda 1, HbX_1} \cdots \varepsilon_{\lambda 1, HbX_m} \\ \vdots \ddots \vdots \\ \varepsilon_{\lambda n, HbX_1} \cdots \varepsilon_{\lambda n, HbX_m} \end{bmatrix} \cdot \begin{bmatrix} HbX_1 \\ \vdots \\ HbX_m \end{bmatrix} \cdot c(Hb), \qquad (16)$$

where dA^{LB}_{λ} is the differential absorption within the Beer-Lambert model, $\varepsilon_{\lambda,HbX}$ is the millimolar extinction coefficient, HbX are hemoglobin fractions, Δl_{λ} is the optical path-length for wavelength λ and $c(Hb)$ is the hemoglobin concentration. In Beer-Lambert model, path-length is independent of the wavelength. This linear equation can be solved only if m is equal or greater than n, which means that at least four wavelengths are needed to solve four hemoglobin species.

2.3.2 Calibration of multi-wavelength pulse oximeter

No widely accepted calibration method for multi-wavelength pulse oximetry have been published. Few methods have been presented in patents but none of these have been commercialized.

Jarman [43] presented a direct calibration method for calculating hemoglobin fractions. She expanded the conventional method to four wavelengths and applied a direct model for all hemoglobin species in the blood as presented in equation

$$HbX = \frac{a_1 * dA_1 + a_2 * dA_2 + a_3 * dA_3 + a_4 * dA_4}{b_1 * dA_1 + b_2 * dA_2 + b_3 * dA_3 + b_4 * dA_4}, \tag{17}$$

where dA_λ is the differential absorption signal, a_i and b_i are calibration coefficients experimentally determined over a large population average. In 1999, she modified the calibration process to include two stages, where methemoglobin fraction was first determined with one set of calibration coefficients and a second calibration round was used to solve oxyhemoglobin, reduced hemoglobin and carboxyhemoglobin fractions. [44]

Aoyagi *et al.* [45] presented a different approach for the calibration. Instead of Beer-Lambert model they applied Schuster's theory of radiation through a foggy atmosphere to the multi-wavelength system. They added a wavelength neutral scattering plate in front of the light source to change the direction of the incident light. In addition, they included the effect of tissue and venous blood in their equations. Although in the patent [46] regarding the same approach they claim to solve for all hemoglobin species the latter publication [45] only refers to improvements in conventional pulse oximetry.

Huiku *et al.* [47] suggested that the above methods include several erroneous assumptions. Direct modeling of hemoglobin species is not possible because a system of equations presented in Equation 16 is not linear in real tissues. *In-vivo* extinction coefficients used in the equations are functions of the concentrations themselves, which means that constant calibration coefficients cannot be found. In their proposal, they transform the *in vivo* measured ratio-of-ratios, $R_{in-vivo}$, first to the corresponding Beer-Lambert ratios, R_{LB}, as presented in equation

$$R_{LB} = f_{\lambda 1,\lambda 2}(\Sigma_a, \Sigma_s) R_{in-vivo}, \tag{18}$$

where the transformation, f, depends on the total tissue scattering (Σ_s) and absorption (Σ_a) at wavelengths $\lambda 1$ and $\lambda 2$ but not anymore on the hemoglobin fractions. The absorption dependence refers to the total absorption in the whole tissue. Then information of the analyte composition is not needed as photons do not care what kind of absorption center they encounter in the tissues. The path-lengths in Equation 16 vary in the tissues. The transformation is based on path-length multipliers (PLMs), which tell how much the path-lengths change as a function of tissue absorption and scattering. [48] A tissue model is generated using three tissue layers (epidermis, bloodless dermis and blood) and the normal values for tissue parameters reported in the literature. PLMs and tissue model coefficients are found using the tissue model that reproduces the calibration for a two wavelength standard

oximetry. The calibration for other wavelengths can be found using the tissue model and calibration data collectionis not needed.

On the left side of Figure 12, path-length multiplier (PLM) represents the transformation as a function of tissue parameters that are incorporated in the quantity Σ_a/Σ_s. When the absorption increases only the photons that travel the shortest route through the tissue can reach the detector and the PLM is near one. As absorption decreases also photons that travel longer routes can reach the detector. When photons scatter a lot they rarely reach the detector and the PLM is near one as only photons that do not scatter reach the detector. The transformation curve for standard pulse oximetry derived with the tissue model is presented on the right side of the Figure 12. [47]

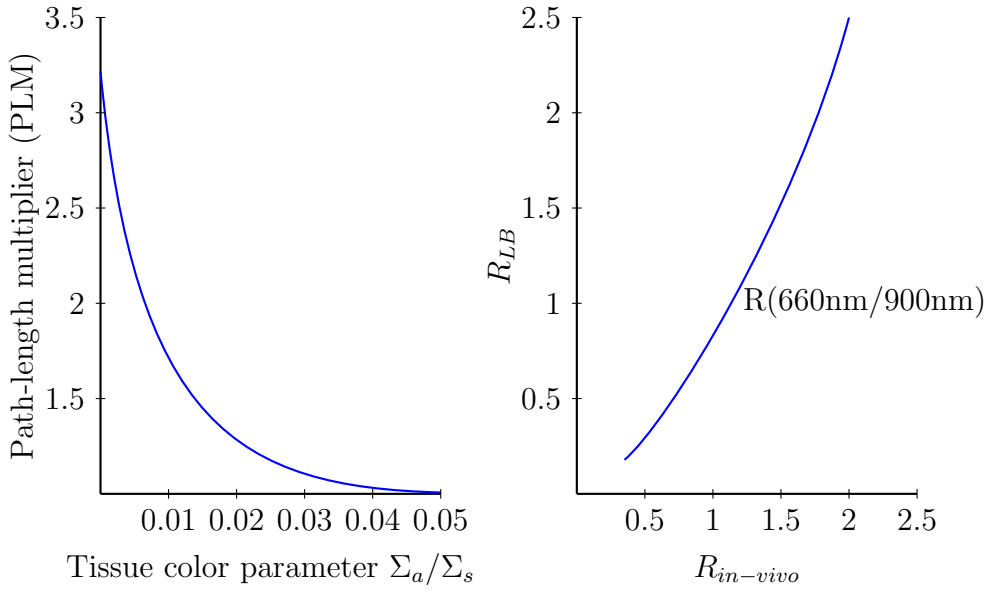

Figure 12: On the left: Path-length multiplier (PLM) as a function of tissue optical character parameter Σ_a/Σ_s of the transformation model obtained from the calibration data of conventional pulse oximetry. On the right: transformation model for the standard pulse oximetry. [47]

2.3.3 A commercial multi-wavelength pulse oximeter

In 2005, Masimo Corporation released a commercial device Rad-57 Pulse CO-Oximeter for noninvasive and continuous fractional hemoglobin measurement. Accuracy of methemoglobin measurement (SpMet®) is specified to ± 1 % for a range from 1 to 15 % and for carboxyhemoglobin measurement (SpCO®) to ± 3 % for a range from 1 to 40 % [49]. There has been controversy reports on the accuracy and usefulness of this device to detect carboxyhemoglobinemia [38–41, 50–56]. Table 4 lists the authors, year, settings and the results of the studies reporting SpCO bias and precision. Generally the results are a bit worse than the specifications. In some studies a significant bias is present and in some precision is poor.

Table 4: Accuracy of SpCO measurement

Authors	Year	Setting	Bias (%)	Precision (%)
Mottram et al. [50]	2005	Respiratory department	2	1.8
Barker et al [51]	2006	Laboratory	-1.2	2.2
Layne et al. [52]	2006	pulmonary lab	-0.65	1.8
Layne et al. [52]	2006	ED	-0.54	4.34
Coulange et al. [38]	2008	ED	-1.5	2.5
Suner et al. [40]	2008	ED	-4.2	
Kot et al. [53]	2008	Hyperbaric center	0.5	4.3
Piatkowski et al. [54]	2009	burn center	3.2	2.4
Touger et al. [55]	2010	ED	1.4	6.6
Roth et al. [56]	2011	ED	2.99	3.27

Only three studies are conducted on the methemoglobin accuracy. Results are presented in Table 5. In the study by Feiner *et al.* in 2009 methemoglobin accuracy was unacceptable. Also SpO_2 readings were underestimated as methemoglobin level increased. [57] A more recent article from Feiner *et al.* [58] reports acceptable accuracy for HbMet over saturation range of $74 - 100$ % and HbMet range of $0 - 14$ %. In the latter study, a new probe was used and software was modified by Masimo to improve the performance.

Table 5: Accuracy of SpMet measurement

Authors	Year	Setting	Bias (%)	Precision (%)	A_{RMS} (%)
Barker et al. [51]	2006	Laboratory	-0.17	0.59	N/A
Feiner et al. [57]	2009	Laboratory	7.7	13.0	15.1
Feiner et al. [58]	2010	Laboratory	0.16	0.83	0.84

Because hemoglobin is the strongest absorber in the blood, spectrophotometric methods have been investigated to measure tHb. Inter-patient variations, concentrations of other chromophores such as melanin and various flavins, the presence of dyshemoglobins and changes in the optical path-length have been the main challenges in spectrophotometric methods. [20] At the end of 2008 Masimo Corporation introduced Pulse CO-Oximetry^{TM} for noninvasive, immediate and continuous hemoglobin measurement (SpHb) using multi-wavelength spectrophotometric method. Macknet *et al.* [42] compared SpHb values to invasive CO-oximetry results from twenty healthy subjects undergoing hemodilution. They reported a bias of -0.15 g/dL and precision of 0.92 g/dL from 165 samples, which fulfills the accuracy specification of the manufacturer (1 g/dL).

Based on the studies reported above usefulness of the Masimo technology is not obvious and more clinical evidence from different settings are needed before the measurements will be widely accepted for clinical use.

3 Materials and methods

This thesis is a part of project that aims to develop a multi-wavelength pulse oximeter that measures fractional hemoglobins and total hemoglobin. The project has been ongoing since 2008. Figure 13 presents the main tasks of the project consisting of goal setting, prototype development, data collection, data analysis, and fractional pulse oximetry (FrOx) algorithm development. Future work includes prototype enhancements and the development of total hemoglobin (tHb) algorithm based on the knowledge achieved during the project. The part that this thesis is about, data analysis and algorithm development, is marked with an orange box.

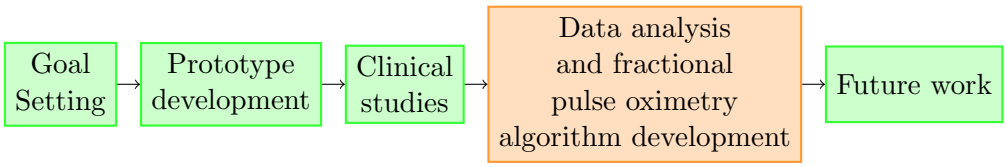

Figure 13: Hemoglobin project

This section first reviews the previous steps of this project, goal setting, prototype development, and data collection. After this methods used in data analysis and algorithm development are discussed in more detail.

3.1 Goal setting

The goal of the project is to develop a multi-wavelength oximeter that measures fractional hemoglobins and total hemoglobin with a single device. Clinically relevant accuracy for the measurement algorithm for hemoglobin species and total hemoglobin was determined through interviews with clinicians and a literature analysis. Literature analysis of this thesis further confirmed the requirements for algorithm accuracy. [15, 20, 26, 40, 55, 56, 58] Requirements are presented in Table 6 for different saturation levels. Requirements are presented as percentage points away from the true value. Other requirements for the algorithm are robustness and simplicity.

Table 6: Clinically relevant accuracy requirements for fractional hemoglobin and tHb measurements.

SaO_2 (range)	SpO_2 (40 – 100 %)	HbO_2 (40 – 100 %)	HbCO (0 – 80 %)	HbMet (0 – 80 %)	tHb (30 – 200 g/L)
100 – 90 %	± 2 %	± 2 %	± 3 %	± 1 %	± 10 g/L
90 – 70 %	± 2 %	± 2 %	± 5 %	± 2 %	unspecified
70 – 40 %	unspecified	unspecified	unspecified	unspecified	unspecified

The literature review shows that a screening tool for recognizing elevated dyshemoglobin levels would be useful. Dyshemoglobin thresholds that are relevant for clinical diagnosis of dyshemoglobinemia are set to 2 % with elevated HbMet and to 6 % with elevated HbCO.

3.2 Prototype development

During 2008 a multi-wavelength data collection unit shown in Figure 14 was built. It consists of several prototype measurement units, serial data collection interface unit and a laptop for data storing. The purpose of the development of the device was to expand the conventional two-wavelength technology to eight wavelengths.

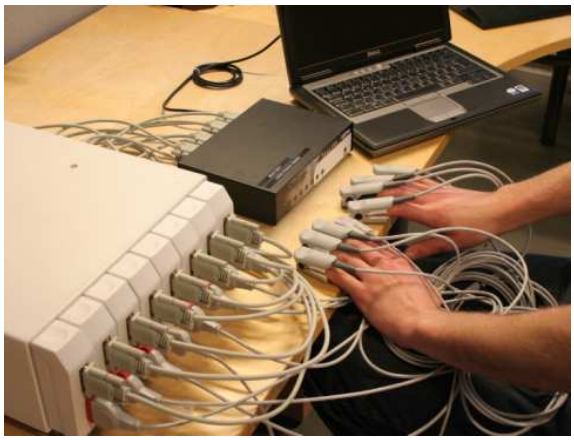

Figure 14: Data collection system of eight measurement modules and probes, serial data collection interface unit and a laptop for data storing.

To achieve the goal, the existing oximetry hardware and software were modified. The new sensor includes eight LEDs and an NTC resistor for temperature measurement. Figure 15 presents a high-level block diagram of the measurement module. The design is a copy of a conventional pulse oximeter design that is multiplied to eight wavelengths. The biggest difference is the LED switch that takes care of the multiplexing of control and demultiplexing of measurement signals. Other parts such as a microprocessor, a LED drive, a front end, analog-to-digital (A/D) converter, a module bus and a power block can be found from conventional oximeters. [59]

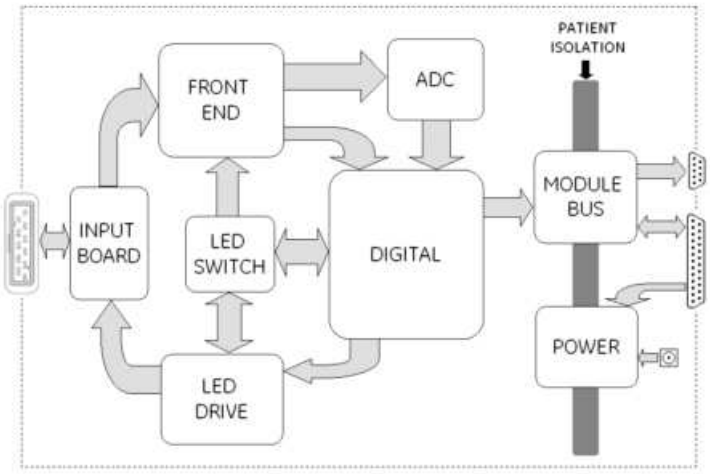

Figure 15: A block diagram of a measurement module

The optimization of wavelengths in sensor is difficult as several criteria must be taken into account. Wavelengths need to be selected from the tissue transmission window, which ranges from 600 to 1300 nm. At wavelengths shorter than 600 nm skin pigment and other tissue components have too high absorption and at longer wavelengths than 1300 nm the high absorption of water disturbs the measurement. Since LED emission is not exactly monochromatic and it changes as a function of temperature, wavelengths were selected from the regions were the spectrum is not changing fast to minimize the effect of the possible wavelength shifts. This means that the minimums and the maximums of absorption curve are good choices. Isobestic points were favored as they are good reference wavelengths. In addition, differential absorptions should be sensitive to changes in the hemoglobin fractions which means that there should be clear differences between extinction coefficients. [3, 47] To keep the costs low wavelengths should be selected from a range where silicon photodiode can be used as a detector. The selected LED center wavelengths (612 nm, 632 nm, 660 nm, 690 nm, 730 nm, 760 nm, 800 nm, and 890 nm) are shown as vertical lines in Figure 16 with hemoglobin extinction curves. [59]

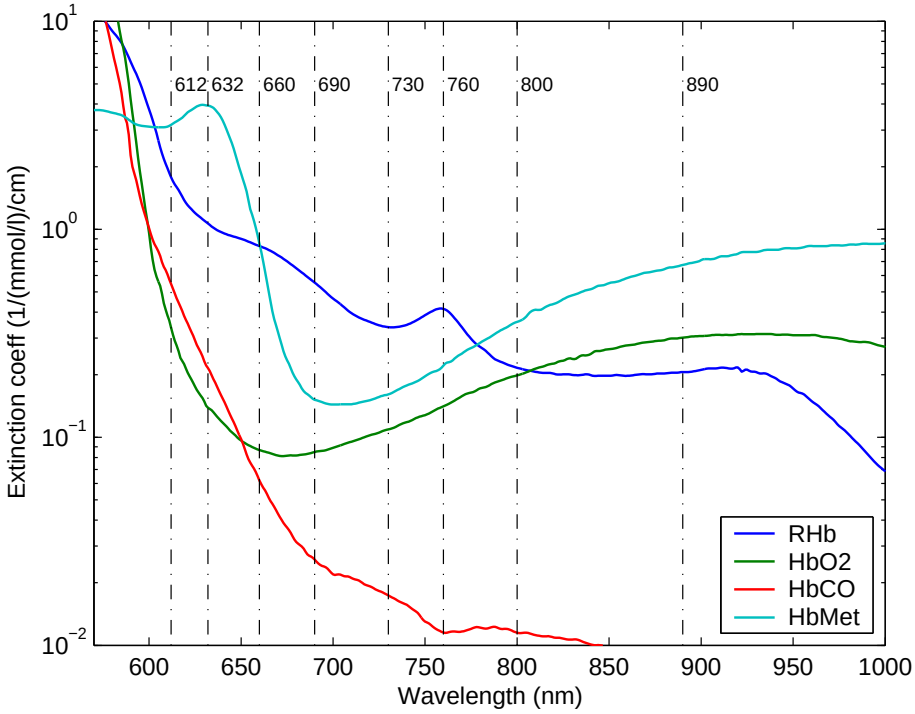

Figure 16: Extinction coefficients of hemoglobin species in the range of 570 nm to 1000 nm.

The prototype was tested against safety, regulatory compliance and technical specifications listed in Table 7. Performance testing including electromagnetic compatibility (EMC) test, electrical safety test, sensor surface temperature test and cross talk and noise measurements showed that the device is suitable for clinical tests and that the performance is comparable with standard pulse oximetry. [59]

Table 7: Prototype specifications [59]

Safety and compliance	**Description/Limit**
Patient isolation	1500 V (DC)
Maximum sensor temperature	41 °C
Max LED fault current	20 mA (continuous)
RoHS compliance	Compliant with appropriate standards
EMC compliance	Emissions shall be compliant with appropriate standards
Technical features	**Description/Limit**
Input voltage	15 V DC (from host monitor or power source)
Sampling rate	100 Hz
Signal performance	12 bits signal resolution (noise free bits)
Output data	8 channels of 19 bit plethysmographic waveform
Communication	Asynchronous RS232 serial communication Option for RS485 communication with host monitor
Wavelengths	600 – 1000 nm
Temperature measurement	Accuracy 0.1 °C, Range 20 – 50 °C
Adjustable LED currents	20 – 300 mA
Adjustable gain	At least two gain options. Common for all channels

Noise measurements were done with three different-sized test fingers. Noise free bits were calculated as a logarithm of two of the SNR. This tells the measurement resolution for the noiseless signal. Results presented in Figure 17 show that noise free bits decrease along the absorbance. With the thickest test finger (attenuation level 19) accuracy decreases to an insufficient level and some channels have very low performance. These problems arise mainly from the prototype's inability to control LED currents and channels gains to an optimized signal level for the AD converter. [59]

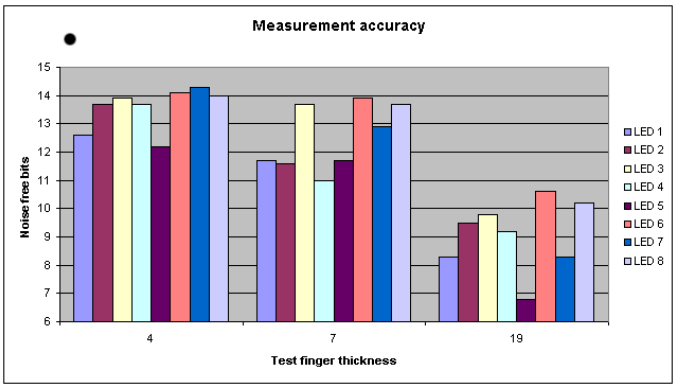

Figure 17: Noise measurement results expressed as noise free bits with different attenuation levels (low = 4, medium = 7 and high = 19) [59].

3.3 Clinical data collection

Clinical data collection was started after the prototype was accepted for use. Clinical studies were designed to cover wide enough parameter range for SpO_2, HbCO, and HbMet. Development data collection process is presented in Figure 18. Volunteer test subjects were recruited in the studies. Plethymosgraphic signals and reference blood data from CO-oximeters were stored for further off-line analysis with MATLAB®. This section explains in more detail when, where and how the data was collected. The clinical study protocols are described at the end.

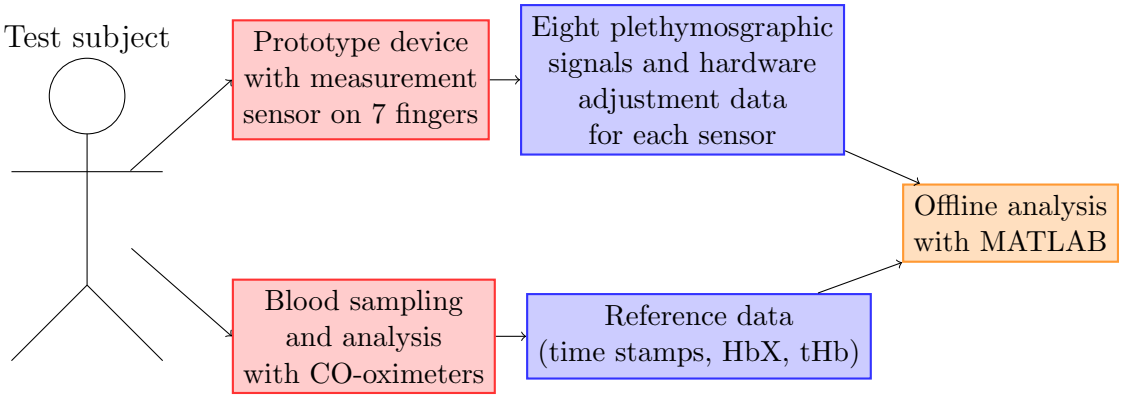

Figure 18: Data collection

The development studies for dyshemoglobin measurements included three separate studies. In the first study in April 2009, smoker volunteers were recruited. Normal dyshemoglobin study was conducted in January 2010 and elevated dyshemoglobin study in March 2010. The covered ranges in these three studies are shown in Figure 19. For HbCO and HbMet ranges of $0 - 20$ % were in target but due to ethical issues only range of $0 - 15$ % was achieved. SaO_2 range from 70 to 100 % was achieved in all studies. Altogether about 500 blood samples were drawn from the volunteer test subjects. Additional outcome from the normal dyshemoglobin study was preliminary data collection for tHb algorithm development. [60]

<table>
<tr><td></td><td></td><td colspan="3">HbCO</td></tr>
<tr><td></td><td></td><td>0-5 %</td><td>5-10 %</td><td>10-15 %</td></tr>
<tr><td rowspan="3">HbMet</td><td>0-2 %</td><td rowspan="2">3 subjects
7 devices
~20 blood samples
≈400 data points</td><td>10 subjects
7 devices
~13 blood samples
≈ 900 data points</td><td>11 subjects
7 devices
~16 blood samples
≈ 1200 data points</td><td></td></tr>
<tr><td>2-10 %</td><td colspan="3">6 subjects, 7 devices, ~20 blood samples ≈ 800 data points</td></tr>
</table>

Figure 19: Collected clinical data coverage

Smoker and normal dyshemoglobin studies were conducted in Clinimark laboratories and elevated dyshemoglobin study was conducted in the laboratory of

Department of anesthesia and perioperative care, University of California at San Francisco. Both laboratories use several CO-oximeters and multiple syringe runs to be able to reduce analytical errors. [27] Subjects that had deeply pigmented skin color, Body Mass Index (BMI) less than 15 or greater than 35, neurological disorder, diabetics, history of cardiac disease, and recent use of psycho-active medication were excluded. To cover different finger sizes and to study the effect of cushion color seven probes were used with each subject. Probes were attached to the fingers as listed in Table 8.

Table 8: Probe units attached to the fingers

Unit number	Cushion type	Finger
1	white	left middle
2	white	left ring
3	white	left pinky
4	white	left/right thumb
5	black/white*	right index
6	black	right middle
7	black	right ring

*unit type changed in January 2010 study

Eight plethymosgraphic signals from the seven prototypes, the hardware adjustment data and time were recorded using a PC. Blood samples were drawn from the subjects and they were analyzed with CO-oximeters. IL 682 CO-Oximeter and Radiometer OSM A hemoximeters were used in April 2009 and January 2010 studies. Radiometer ABL 800 FLEX and OSM hemoximeters were used in March 2010 study. Precisions reported by the manufacturers of these CO-oximeters are presented in Table 9. Reference data (fractional hemoglobins, tHb, and time of blood samples) were stored manually and electronically and delivered to the GE hemoglobin research group for further analysis. [60]

Table 9: Precision of CO-oximeters used in the clinical studies reported by manufacturers [61–63]

Manufacturer & Device	Abbreviation	Precision (±1 SD)		
		HbO_2	HbCO	HbMet
Radiometer OSM-3	OSM	0.4 - 0.7	0.5 - 0.6	0.4
Instrumentation Laboratory	IL	0.5	0.5	0.5 (0-10%)
682 CO-oximeter				1 (10-100%)
Radiometer ABL 830 FLEX	ABL	0.5	0.4 - 0.75	0.3 - 0.4

Smoker and normal dyshemoglobin studies followed a protocol that is depicted in Figure 20. At each stable level at least two arterial blood samples and one venous sample were drawn. First blood samples were taken in room air situation. Then blood volume in the finger was changed by lifting the hands above the heart. When

the hands were up no blood samples were drawn. After hands were returned back to the resting position, situation was stabilized and blood samples were drawn. In desaturation phase, arterial blood saturation was reduced gradually to two levels: $92-88$ % and $82-78$ %. In supersaturation phase, the saturation was raised with 100 % oxygen to a fully saturated blood level for 3–5 minutes. Last blood samples were taken after the subject was returned to the room air oxygenation level.

Figure 20: Protocol for data collection in smoker and normal dyshemoglobin studies.

Figure 21 presents a flow diagram of the protocol for elevated dyshemoglobin study that can be separated in two studies: carbon monoxide inhalation and nitride infusion study. In carbon monoxide inhalation study, carboxyhemoglobin level was altered by inhalation of CO/air mixture boluses until HbCO level reached 10 %. For safety reasons blood samples were drawn regularly at 2-3 minutes intervals. Before the desaturation phase subjects were interviewed to make sure that they feel well and want to continue to the desaturation phase similar to described above. After desaturation phase CO/air mixture inhalation was continued until HbCO level reached 15 %. Then subjects were recovered with 100 % oxygen mixture and followed up as long as HbCO level was less than 10 %.

In nitride infusion study, changing HbMet levels were achieved by infusion of sodium nitride ($NaNO_2$) using a calibrated commercial infusion pump. First infusion phase was continued until HbMet level reached 5 % and the second phase was ended when the level reached 10 %. Subjects were recovered with 50 % oxygen mixture and followed as long as HbMet level was less than 5 %. Otherwise the protocol was similar to the carbon monoxide inhalation study.

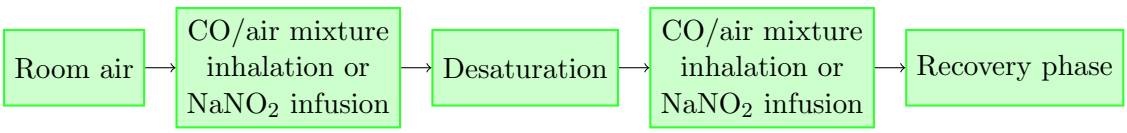

Figure 21: Protocol for data collection in elevated dyshemoglobin study.

3.4 Data analysis and algorithm development

The purpose of this thesis was to analyze the data that have been collected with the prototype device. Data analysis and algorithm development process can be divided in five steps as presented in Figure 22. Analysis was done off-line with MATLAB® environment for algorithm development. First reference CO-oximeter data is analyzed. Then plethymosgraphic data is preprocessed using signal processing methods of conventional pulse oximetry. After preprocessing the quality of the data is checked using statistical methods. In algorithm development statistical methods are used to find a regression model for fractional hemoglobins. Few different methods are used

and compared to each other. The best algorithm is validated using cross-validation techniques. In this section, the process is described in more detail.

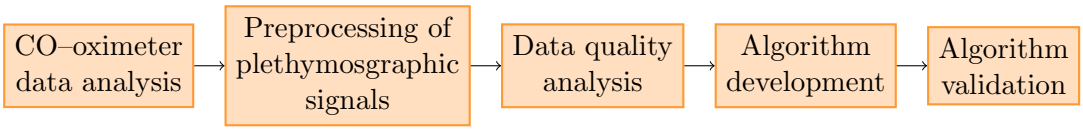

Figure 22: Data-analysis and algorithm development process.

3.4.1 CO-oximeter data analysis

CO-oximeter data points that were more than three standard deviations away from the mean were excluded. In addition, data accuracy was evaluated using Bland-Altman method. Bland and Altman method is a recommended analysis method for reporting and presenting CO-oximetry errors [28]. In Bland and Altman procedure, two methods of which neither can be stated to give the true value are compared. In Bland-Altman plot, difference between two measures is plotted against their average. From a data set mean and standard deviation of differences are calculated and marked in the plot as straight lines. [64] Bland-Altman plots are also used in evaluating pulse oximetry performance [26]. An example of Bland-Altman plot for conventional pulse oximetry data is shown on the left side of the Figure 23. On the right side the data set is pooled. Bias is marked with an asterix and SDs with whiskers.

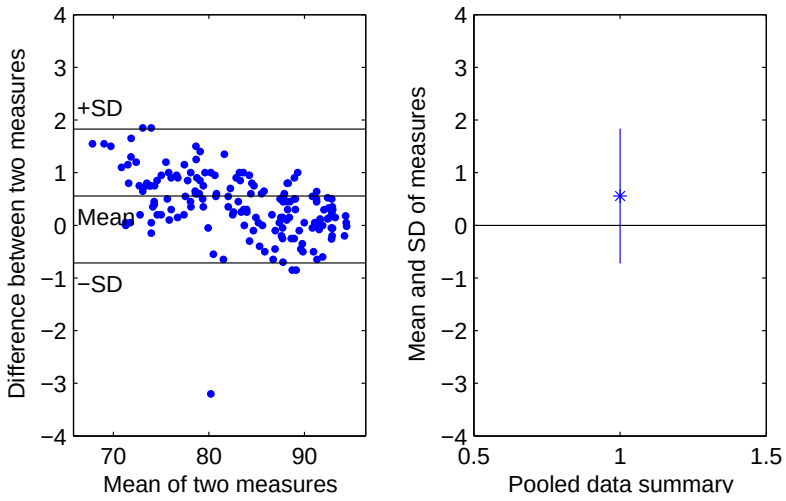

Figure 23: On the left: Bland-Altman plot of CO-oximetry data. On the right: Pooled data summary plot with mean and standard deviation.

3.4.2 Data preprocessing

This section describes how plethymosgraphic signal is processed and how different parameters such as ratio-of-ratios (Rs), DC component, and perfusion index (PI) are derived from plethymosgraphic signal. Block diagram of preprocessing steps is presented in Figure 24. Yellow circles represent quality parameters that are calculated from the signals and they are further discussed in the next section. Red circles are parameters derived from plethymosgraphic signal. Green rectangles represent processing steps and blue ellipses are signals used in pulse oximetry.

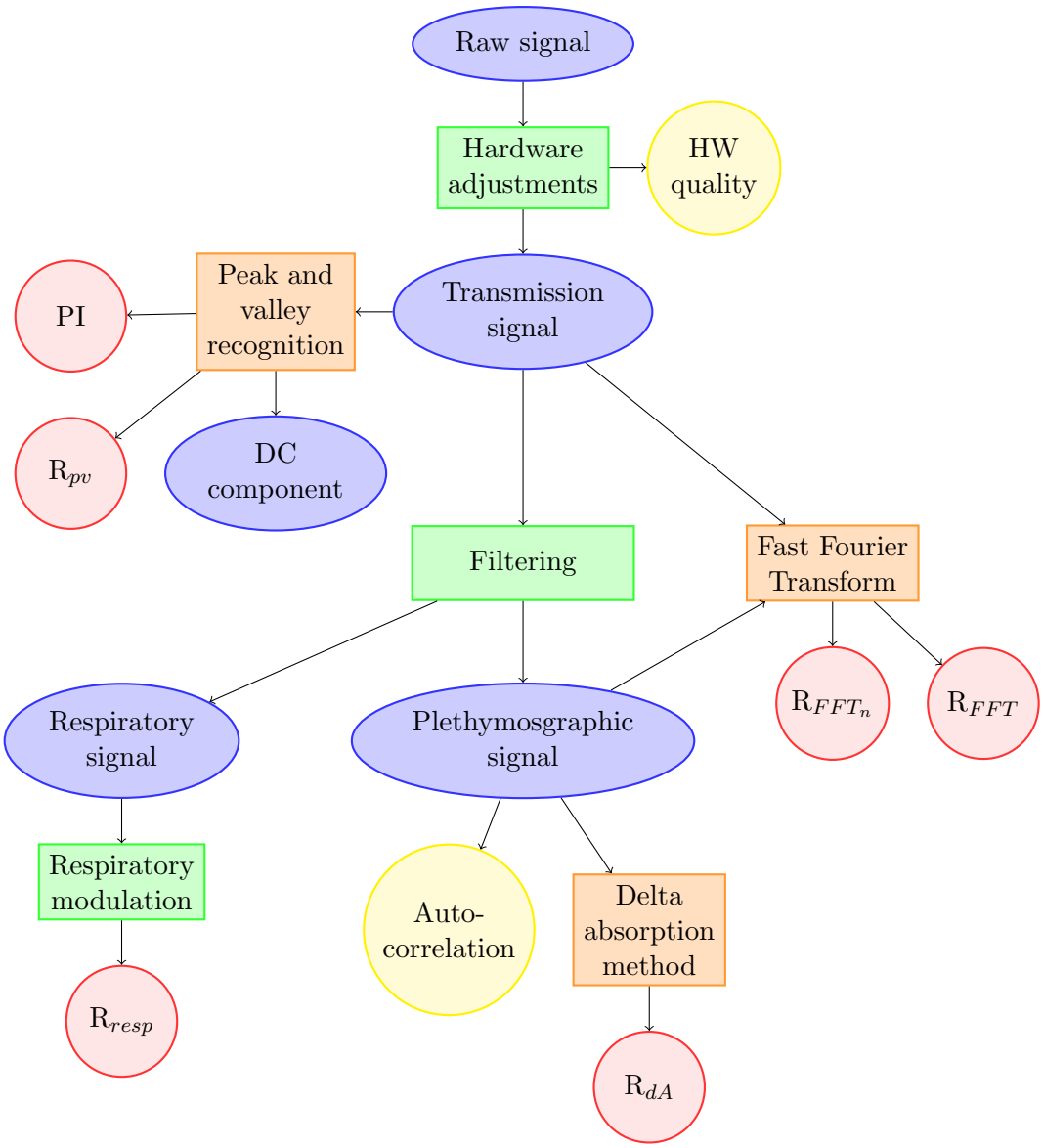

Figure 24: Block diagram of preprocessing steps

First raw data is adjusted with gain and LED drive current recorded from the hardware system to obtain transmission signals.

Peak and valley recognition is applied to the transmission signal. Peak values are stored as a DC component of the signal. Perfusion indexes are derived from the difference between peak and valley values. In addition, peak and valley method of ratio-of-ratios calculation is applied to the signal.

Transmission signals are filtered with generalized Butterworth filter that unifies the classical Butterworth filter and the maximally flat symmetric FIR (finite impulse response) filter. A high pass filter with cut-off frequency at 0.4 Hz produces the AC part of the signal. To reduce high frequency noise a low pass filter with cut-off frequency at 10 Hz is used. Respiratory signal is obtained with a band-pass filter from 0.1 Hz to 0.4 Hz. These digital filtering steps are all performed twice, forth and back, to eliminate group delays. Generalized Butterworth filters provide a good trade-off between performance and implementation complexity, which is important when the algorithm is applied to the final product. [65]

After filtering respiratory modulation ratios are calculated to obtain respiration-induced venous blood volume changes. Autocorrelation coefficients of the plethysmosgraphic signals are calculated to recognize signal artifacts. Delta absorption model and Fast Fourier transform (FFT) are used in ratio-of-ratios calculations that are further explained in the following section.

Methods of ratio-of-ratios calculations

Three different methods - peak and valley method, delta absorption model and the fast Fourier transform - were used in the thesis to calculate ratio-of-ratios, Rs (Eq. 8) for a multi-wavelength system.

Traditionally peak and valley method has been used. Peaks and valleys for each cardiac cycle are recognized from the transmission signal and the delta absorption (Eq. 7) is used to calculate ratio-of-ratios, R_{pv}, as shown in equation,

$$R_{pv} = \frac{dA_{\lambda 1}}{dA_{\lambda 2}} = \frac{AC_{\lambda 1}/DC_{\lambda 1}}{AC_{\lambda 2}/DC_{\lambda 2}}. \tag{19}$$

Figure 25 presents the transmission intensity as a function of time and the recognized peak and valley for R calculation using two different wavelengths (660 nm and 800 nm).

In delta absorption model, dA is calculated by dividing the intensity of two successive measurements by the average of the intensities for each wavelength as presented in equation,

$$dA_{\lambda} = \frac{I_i - I_{i-1}}{(I_i + I_{i-1})/2}, \tag{20}$$

where I_i and I_{i-1} are intensities of subsequent observations. Delta absorptions for two different wavelengths are plotted in xy scatter plot and a straight line is fitted to the data so that the sum of squares of perpendicular distances to the line is minimized. An example of a fit using the same data points as in peak and valley method, is shown in Figure 26. Ratio-of-ratios, R_{dA}, is the slope of the line and the constant can be used as a measure of the goodness of the regression. The constant

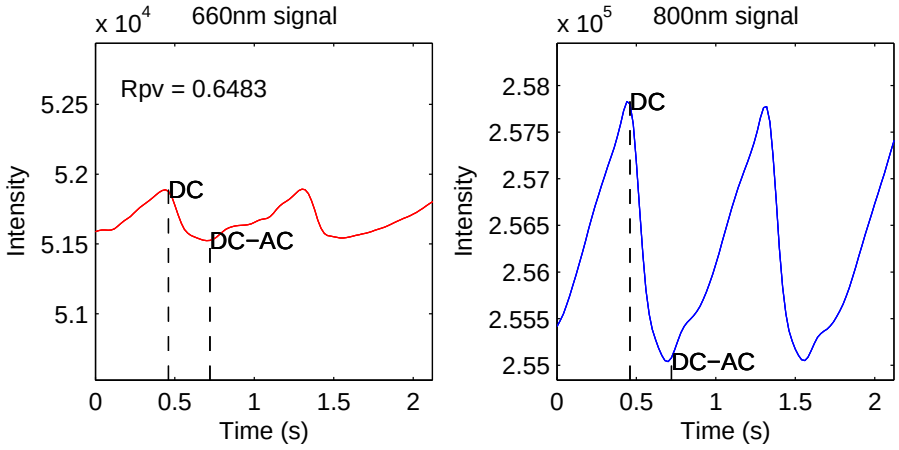

Figure 25: Peak and valley method

should be very near to zero, otherwise some kind of artifact is present in one of the signals. Also the sum of squares of perpendicular distances to the line can be used as a measure of the fit goodness. [66, p.288–292]

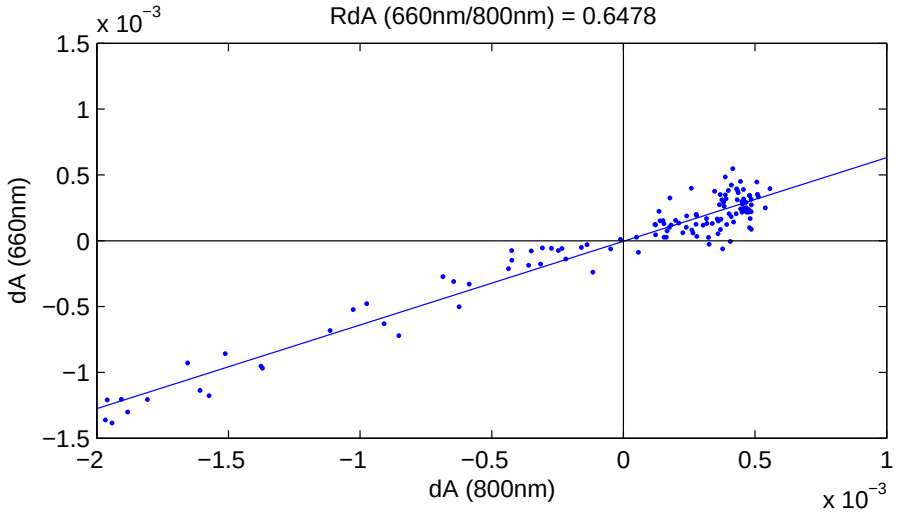

Figure 26: Delta absorption model

The fast Fourier transform (FFT) can be used to calculate ratios. FFT is an effective algorithm to compute discrete Fourier transform (DFT). Fourier transform is a mathematical operation that transforms the signal depending on time to a frequency domain. Since plethymosgraphic signal is periodic transforms using sinusoidal base functions should be good tools for analysis. The AC component is derived from FFT as the highest spectral line at the cardiac frequency ($1 - 2$ Hz) and DC component as the zero frequency component of the composite signal. After this R_{FFT} is obtained using Equation 7. To obtain the amplitude of the AC component of the plethymosgraphic signal accurately, the time interval should be at least one period as transform error reduces with longer time interval. [67] Figure 27 shows

a sample of FFT output excluding the large zero frequency component. Ratio-of-ratios R_{FFT_n} are also calculated with FFT directly from the differential absorption signal using a Hamming window to smoothen the boundaries.

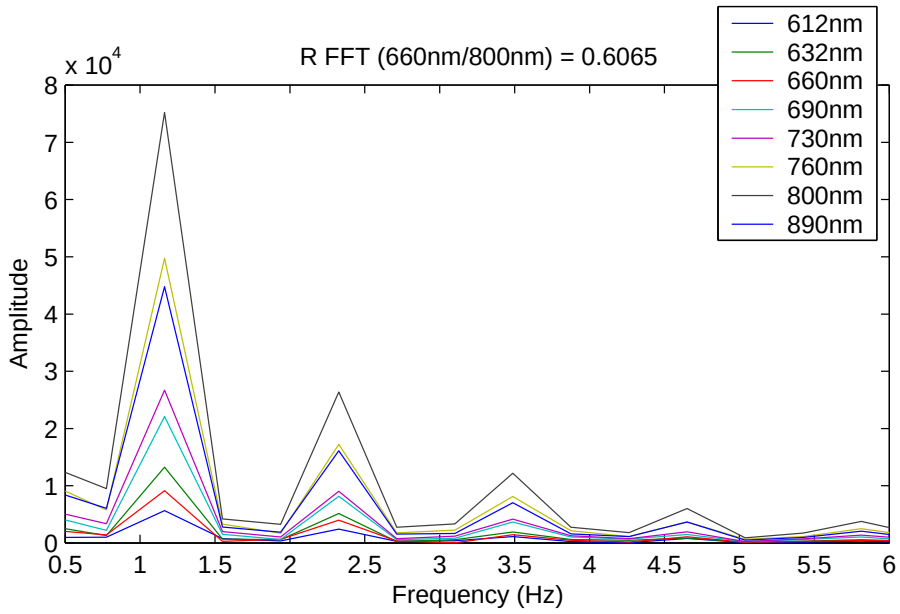

Figure 27: Output of a sample FFT from the transmission signal.

3.4.3 Data quality analysis

In this thesis, data that is too noisy to provide useful information was rejected. Correction algorithms were not used. Hardware adjustment and autocorrelation coefficient signals were used to track data quality.

Hardware adjustments, such as gain or LED drive current changes, that might cause artifacts in the signal for a short period of time, were stored. A common HW adjustment signal was formed to reject data in presence of hardware adjustments. Figure 28 shows an example a successful data rejection due to hardware adjustment.

Many signal artifacts created by movements or other external sources are present in all signals. As plethymosgraphic signal is periodic and should not have big changes in a short time period autocorrelation coefficient is used to recognize pulse to pulse variations. Autocorrelation coefficient signal is calculated with equation

$$acorr(t) = max_{\tau \in [0.3s \cdots 2s]} \left(\frac{\frac{1}{N} \sum_{n=t-2.5s}^{t+2.5s} x_\lambda(n) x_\lambda(n-\tau)}{\frac{1}{N} \sum_{n=t-2.5s}^{t+2.5s} x_\lambda^2(n)} \right), \tag{21}$$

where x_λ is the zero average plethymosgraphic signal, τ is the delay in time and N is the number of samples. Five second window is used in the calculation to make sure that at least three pulses fit in the window even with low heart rate. Autocorrelation coefficient signals are calculated with 1 second resolution. Rejection limit is set to 0.7 and signals are stored for all wavelengths. A total autocorrelation coefficient signal

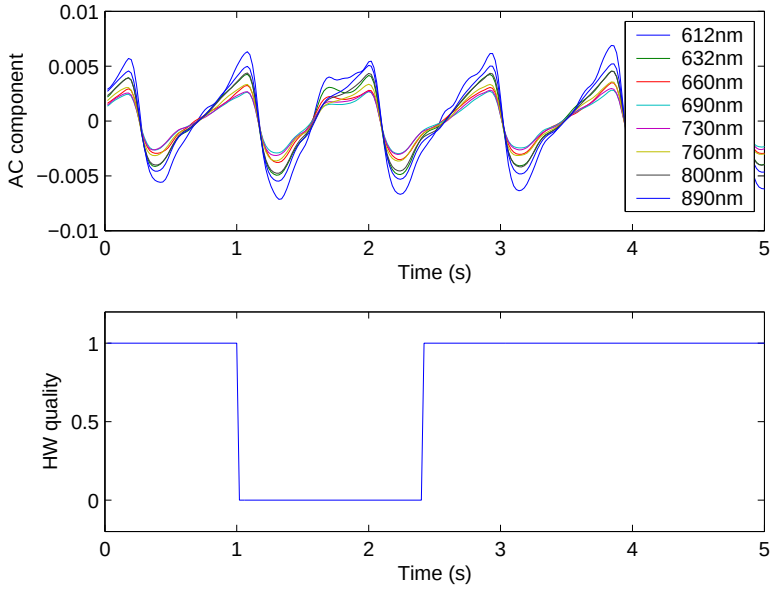

Figure 28: An example of successful data rejection due to hardware adjustment.

is created to indicate if the limit is violated with any of the wavelengths. Figure 29 presents a successful signal artifact recognition by autocorrelation coefficient signal while simultaneous hardware quality signal shows that artifact is not arising from hardware adjustments.

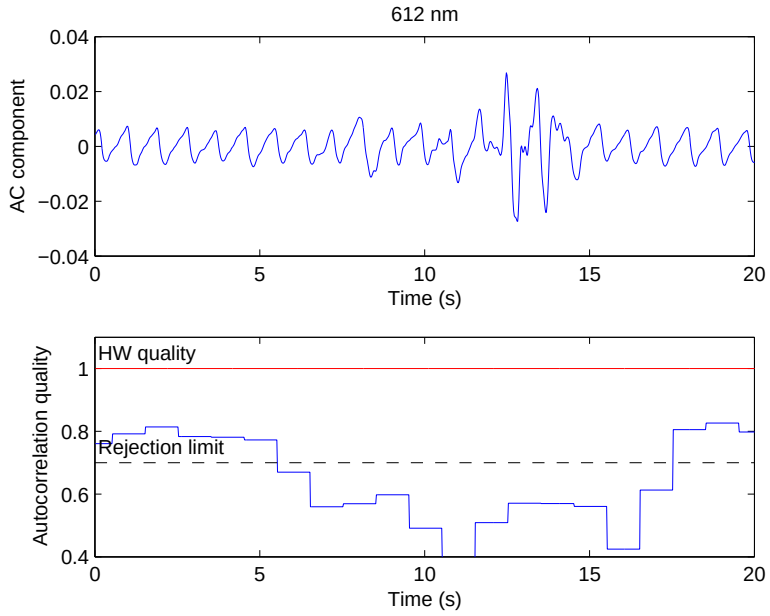

Figure 29: A successful rejection based on autocorrelation coefficient signal.

3.4.4 Development data selection

Development data was visually segmented around the blood samples to indicate good data quality. Only zero average plethymosgraphic signals are inspected using signal viewer SigView 3.11m (VTT Technical Research Center of Finland). Acceptance criteria for good signal are defined as repeating pattern in the signal without sudden big changes in the amplitude or in the period. If possible, segment is selected 15 seconds around the recorded time stamp. Selection of two shorter time periods is also accepted. Periods are required to be within 60 seconds around the sample. A snapshot of a good quality signal taken with SigView is presented in Figure 30. Plethymosgraphic signals of different wavelengths are shown in the upper panel. The lower panel shows the hardware quality signal. Vertical lines indicate the selected time interval and the blood sample time.

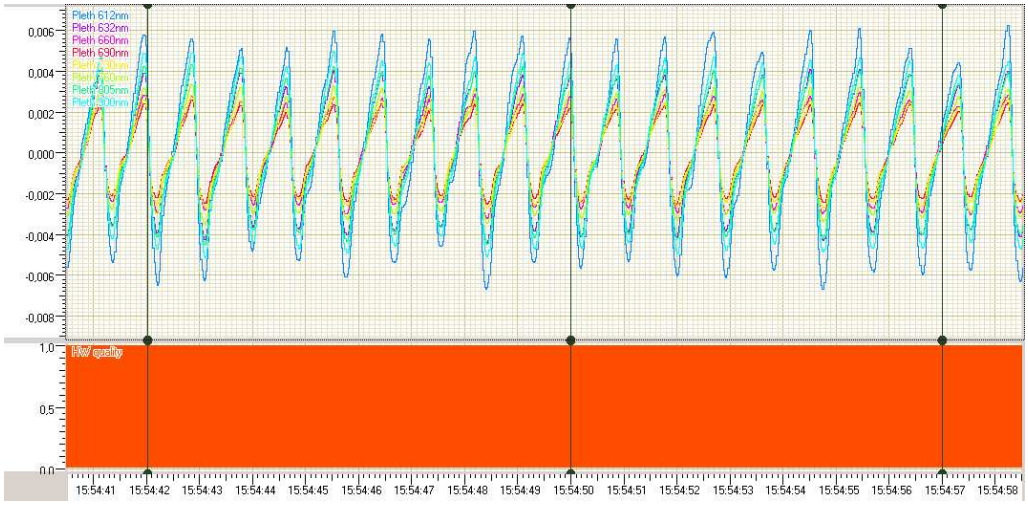

Figure 30: An example of a good data interval

Traditional SpO_2 values and noise of ratio-of-ratios are calculated from the visually segmented time intervals. Noise is calculated as the relative standard deviation defined in equation

$$\%RSD = 100\% \cdot \frac{R_{SD,\lambda}}{\bar{R}_\lambda}, \tag{22}$$

where $R_{SD,\lambda}$ is the standard deviation and $\bar{R}_\lambda$ is the mean of ratio-of-ratios in the evaluation period at wavelength λ.

The total noise in hemoglobin fractions can be estimated with equation

$$\Delta HbX = \sqrt{n_{COox}^2 + n_{instrumental}^2 + n_{physiological}^2}, \tag{23}$$

where n_{COox} is the error in CO-oximetry results, $n_{instrumental}$ is the noise in ratio-of-ratios calculations and $n_{physiological}$ is the subject-to-subject variability. The accepted noise in hemoglobin fractions is defined in Table 6. All data points, where the total noise exceeds the accuracy requirement, are rejected from the development data set to make sure that the development data quality is good.

3.4.5 Algorithm development

Fractional pulse oximetry (FrOx) algorithm presented in Figure 31 is developed to solve hemoglobin fractions (HbX) from set of equations presented in Equation 16. The equations are linearized by establishing the path-length transformation from the *in vivo* measured signals to the corresponding non-scatter signals in the Beer-Lambert model using parameters derived from the preprocessing phase. Also effective extinction coefficients are derived through extinction compensation. Then linear set of equations is solved to derive analyte concentrations.

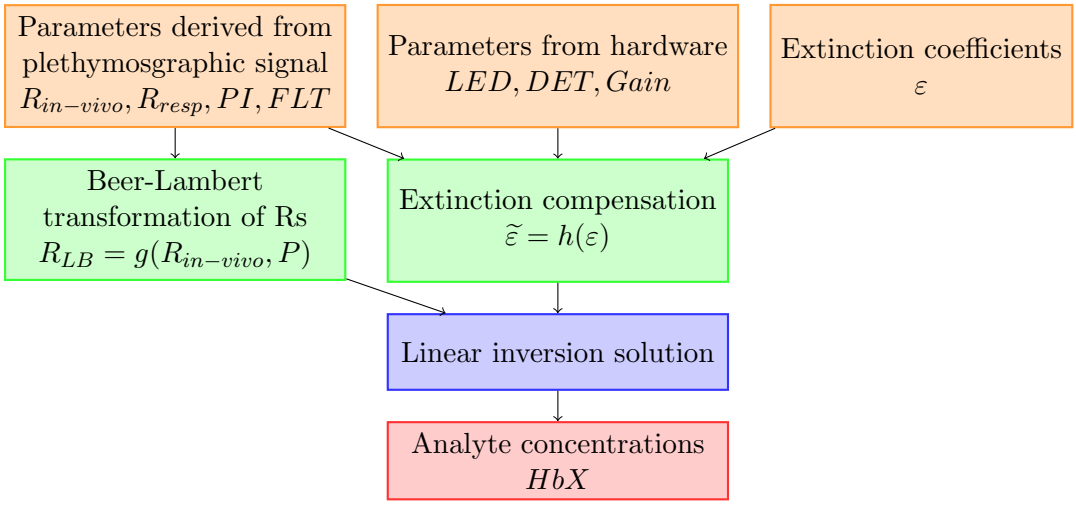

Figure 31: Steps included in fractional pulse oximetry algorithm

Extinction compensation

To address deviations from the theoretical model, extinction coefficients in Equation 6 need to be replaced with effective extinction coefficients defined in equation

$$\widetilde{\varepsilon}_{\lambda,HbX} = \frac{1}{W} \int LED_{\lambda,T} \cdot DET_{\lambda} \cdot \varepsilon_{\lambda,HbX} \cdot FLT_{\lambda} d\lambda, \tag{24}$$

where $LED_{\lambda,T}$ is the temperature(T)-dependent spectral intensity of the LED, DET_{λ} is the spectral photodetector sensitivity, $\varepsilon_{\lambda,HbX}$ is the Beer-Lambert extinction curve for hemoglobin species HbX and FLT_{λ}, functional light transmission, is wavelength-dependent transmission of the tissue and $W = \int LED \cdot DET \cdot FLT \cdot d\lambda$ is the normalization factor. [68]

First term takes into account deviations in the LEDs. LEDs are not monochromatic as their spectral bandwidth is typically in the range from 20 to 60 nm. The bandwidth increases with the wavelength, which can be seen from the Figure 32 that presents a typical LED emissions used in a multi-wavelength probe. [2]

In addition, the center wavelength of the LED shifts due to temperature changes. This can be corrected by measuring the temperature of the sensor and using correction function derived from the manufacturer. In addition, different drive currents of LEDs change the temperature of a particular LED. Especially with shorter

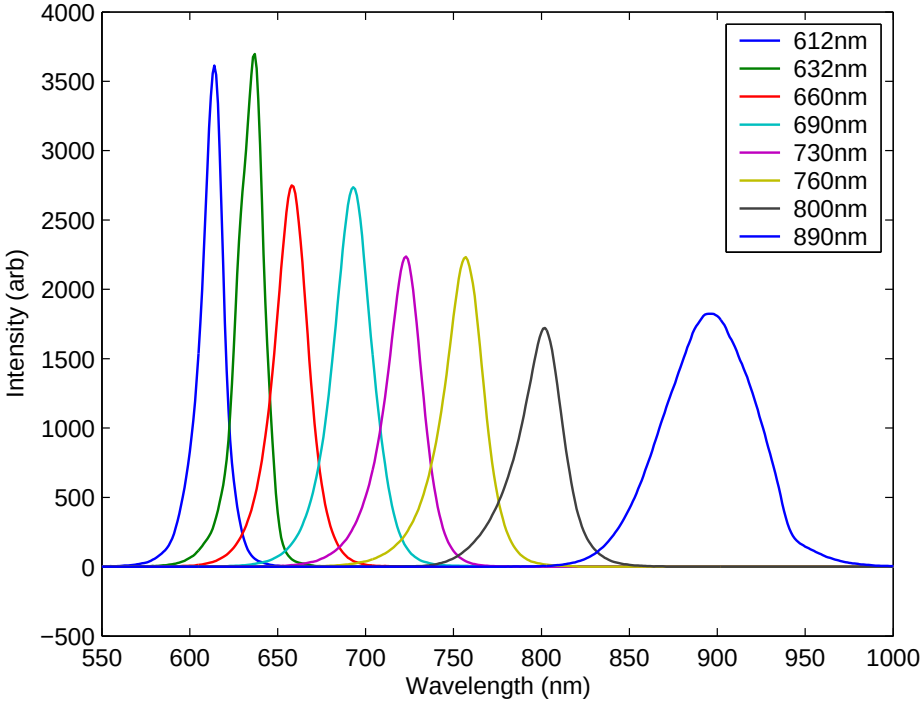

Figure 32: Typical spectrums of LEDs used in a probe

wavelengths than 660 nm the temperature change can be significant in this multi-wavelength system. Secondly the wavelength-dependent sensitivity of the photodetector is taken into account in the extinction compensation. [2, 68]

One part of extinction compensation is the calculation of tissue prefiltering effect. Functional light transmission (FLT_λ) at wavelength λ makes different DC values comparable to each other. FLT is defined according to equation

$$FLT_\lambda = \frac{fCTR_\lambda}{CTR_\lambda}, \tag{25}$$

where CTR is Current Transfer Ratio measured from the probe without tissue between the LEDs and the detector and fCTR is functional Current Transfer Ratio measured with finger in the probe. CTR is derived from DC light signal in absence of tissue that is normalized to correspond to an emitter current value of 1 mA. CTR is a measure of sensor characteristics such as the color and the geometry of the probe as it tells how efficiently light is transmitted from the LED to the detector. fCTR is a measure of tissue properties and can be determined from the DC light transmission signal after gain and current normalizations. FLT as ratio of fCTR and CTR describes light attenuation caused by the tissue as probe design characteristics are ruled out. Now spectral transmission can be estimated from the measured DC transmission values by interpolating the data. Values outside prototype wavelengths are estimated from previous spectrophotometric measurements. An example of tissue transmission derived this way is presented in Figure 33. [68]

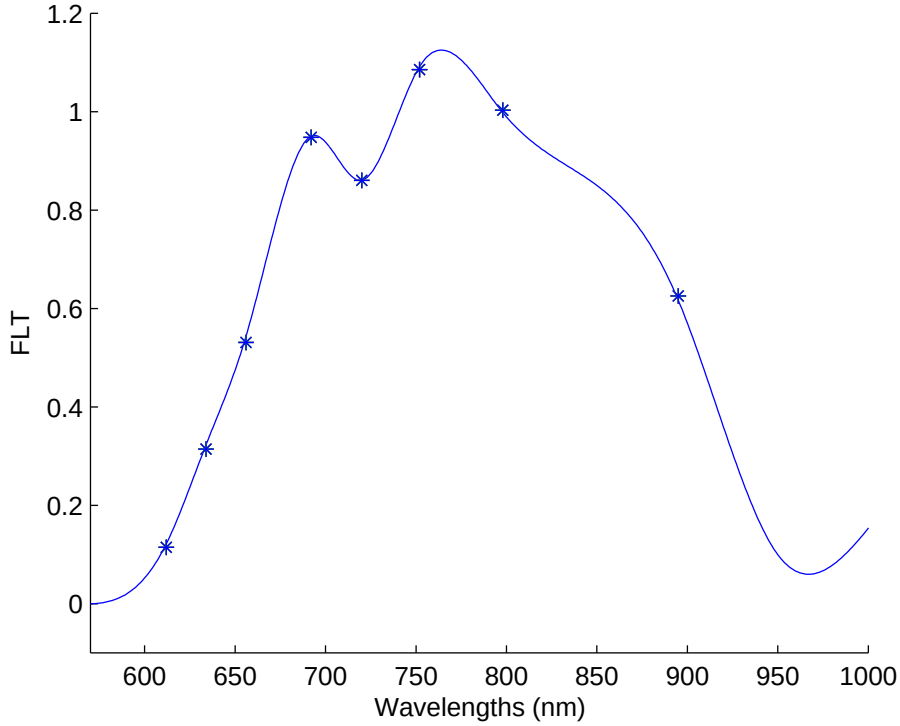

Figure 33: Functional light transmission derived through interpolation of measured DC light transmission values

Beer-Lambert transformations of ratio-of-ratios

In FrOx formalism, Beer-Lambert transformations represent the calibration of normal pulse oximeters by linearizing the set of equations so that they can be solved. Mathematically these transformations can be expressed as

$$R_{\lambda}^{LB} = g(R_{\lambda}^{in-vivo}, P_{\lambda}), \tag{26}$$

where R_{λ}^{LB} is the non-scatter Beer-Lambert ratio-of-ratio, $R_{\lambda}^{in-vivo}$ is the measured ratio-of-ratios, P_{λ} describe tissue properties affecting the path-lengths and g is the transformation function. In this thesis, the transformation, g, is established by regression of the Beer-Lambert ratio-of-ratios back-calculated from the measured blood sample hemoglobin concentrations to the corresponding measured *in-vivo* ratio-of-ratios calculated with delta absorption method described in previous section 3.4.2.

Regression of R_{λ}^{LB} is done with few regression methods. First parameters that most likely contain information of the tissue properties are selected to the model. List of selected parameters is presented in Table 10. Principal component analysis (PCA) and step-wise regression methods are used in the modeling of the transformations.

Principal component analysis converts a set of possibly correlating parameters into a set of uncorrelated parameters called principal components. In the transformation the first principal component represents the greatest amount of variability

Table 10: Parameters used in regression modeling

Parameter (P_λ)	Description
R_λ	Ratio-of-ratios at wavelength λ
FLT_λ	Functional light transmission at wavelength λ
PI_λ	Perfusion Index at wavelength λ
RR	Respiratory modulation depth

in the original data set. Determination of principal components is done using singular value decomposition. The number of principal components is calculated with different ways. First the number is required to account for 95 or 99 percent or of the variance. Then all principal components that account at least 0.5 percent of the variance are included. As comparative method scree plots are drawn to find a clear breakpoint after which variance is not decreasing significantly anymore. In scree plot, eigenvalues (representatives of the variance) are drawn as a function of ordered principal components. Sometimes 'an elbow' can be seen in the scree plot which gives an estimate how many principal components are significant. Examples of scree plots are presented in Figure 34. On the left side of the figure a clear elbow is seen as on the right side the curve is smooth. [69]

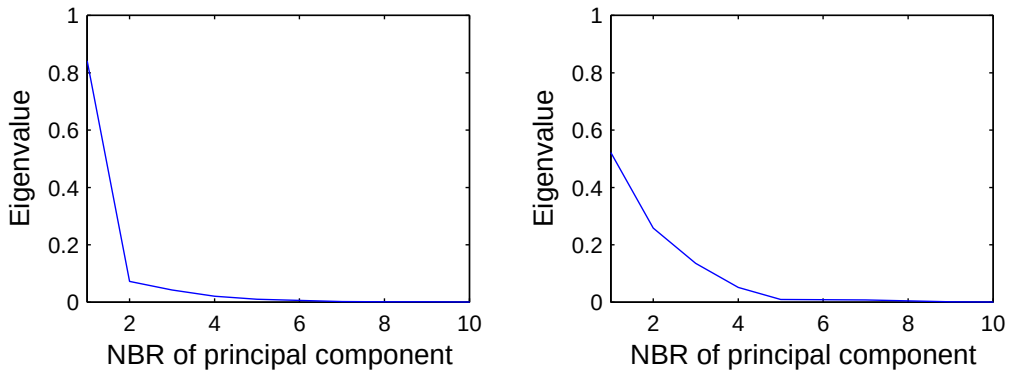

Figure 34: On the left: Scree plot with a clear elbow. On the right: A scree plot with smooth eigenvalue curve.

Forward selection method presented in Figure 35 is used in step-wise regression. Parameters are included in the model in the following order: linear terms, quadratic terms, third-order terms and cross-product terms. In forward selection method, parameters are included in the model one after another with criteria of the greatest decrease in the mean square error. In statistics, several methods for choosing the number of parameters in the model can be used. In this thesis, Schwarz Bayesian information criterion (SBIC) and F-tests are used. SBIC is an unbiased and efficient criterion in that sense that all accountable but none of the unnecessary terms are included in the model. SBIC is defined in equation

$$SBIC = \sigma_p^2 + 2p \cdot \frac{log(n)\sigma_p^2}{n}, \tag{27}$$

where $\sigma_p^2 = \frac{1}{n}\sum(g(R_\lambda^{in-vivo}, P_\lambda) - R_\lambda^{LB})^2$ is the error variance, p is the number of parameters and n is the number of data points. The best model minimizes the value of SBIC. [70]

F-test is used to test the equality of variances. Large F-values indicate that the null hypothesis, two normal populations have the same variance, is not true. Statistical significance of parameters is tested with 90 percent confidence level ($\alpha = 90$ %). If the included parameter is not statistically significant the model is ready. Hemoglobin fractions are solved with linear inversion solution for all stages. The fraction of values within specification, descriptive statistics and visual inspection of Bland-Altman plots are used to compare different models.

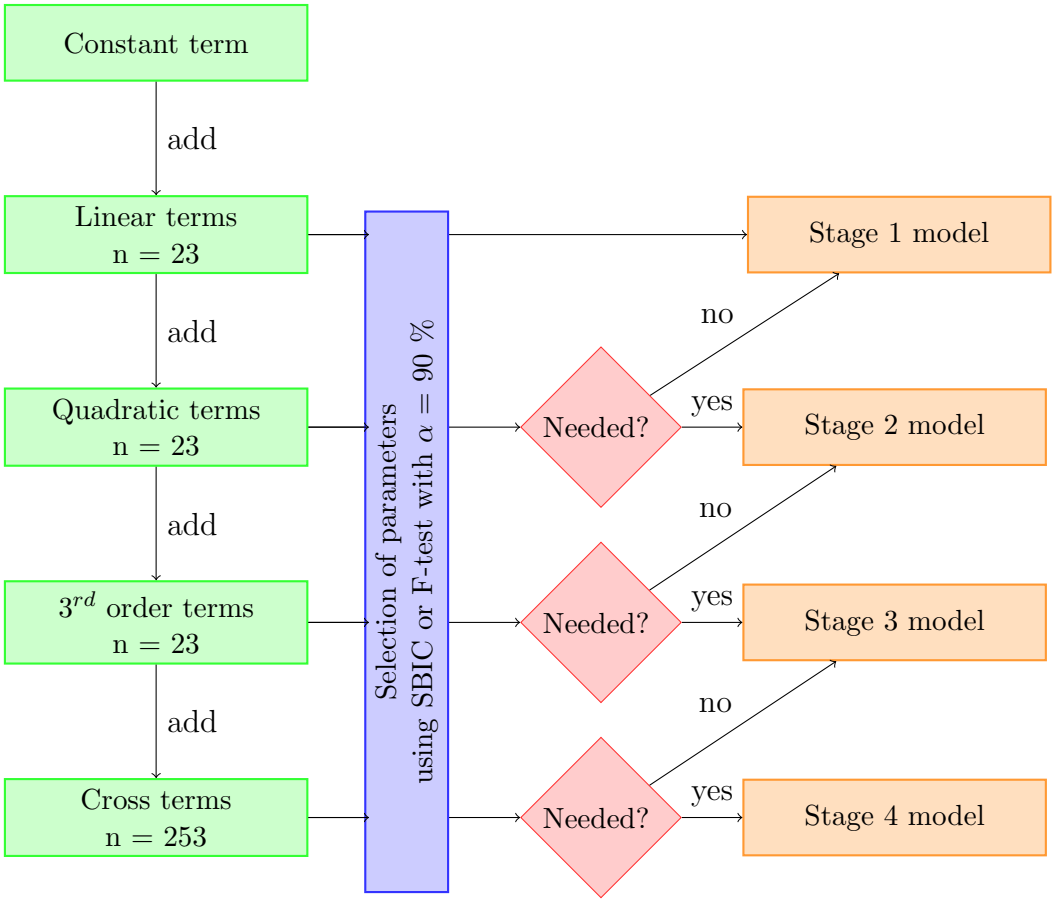

Figure 35: A flow diagram of the forward selection method for determining Beer-Lambert Rs. Green rectangles represent the included parameter. Then parameters are selected and hemoglobin fractions are solved to decide if the parameters are needed in the model.

Linear inversion solution

As the system is overdetermined (8 equations, 4 hemoglobin fractions) the method of least squares is used in the inversion. The method of least squares solves the set of equations in a way where the sum of square errors is minimized. Least squares solution for Equation 16 in Beer-Lambert situation can be expressed with equation

$$\underbrace{\mathbf{HbX_i}}_{4\times1} = \underbrace{(\mathbf{E^T E})^{-1}}_{4\times4}\underbrace{\mathbf{E^T}}_{4\times8}\underbrace{\mathbf{R_{LB}}}_{8\times1} = \underbrace{\mathbf{E^*}}_{4\times8} \cdot \underbrace{\mathbf{R_{LB}}}_{8\times1}, \tag{28}$$

where $\mathbf{E}$ is the extinction matrix, $\mathbf{E^*} = (\mathbf{E^T E})^{-1}\mathbf{E^T}$ and $\mathbf{R_{LB}}$ is the ratio-of-ratios vector derived from the Beer-Lambert transformation. Second row shows the sizes of the matrices.

When noise $\mathbf{n}$ is added to the system noisy estimate for a hemoglobin fraction will be

$$\mathbf{HbX_n} = \mathbf{E^* R_{LB}} + \mathbf{E^* n} = \mathbf{HbX_i} + \mathbf{\Delta HbX}. \tag{29}$$

The error in hemoglobin fractions $\mathbf{\Delta HbX}$ depends on the extinction coefficients and the actual noise. To evaluate how much noise is tolerated, robustness of the system is analyzed using a method presented in Figure 36. Beer-Lambert ratio-of-ratios are back calculated from the blood data and then noise is applied to see how the noise in ratio-of-ratios affects to the hemoglobin fractions. The noise is applied to one of the ratio-of-ratios or to all of them.

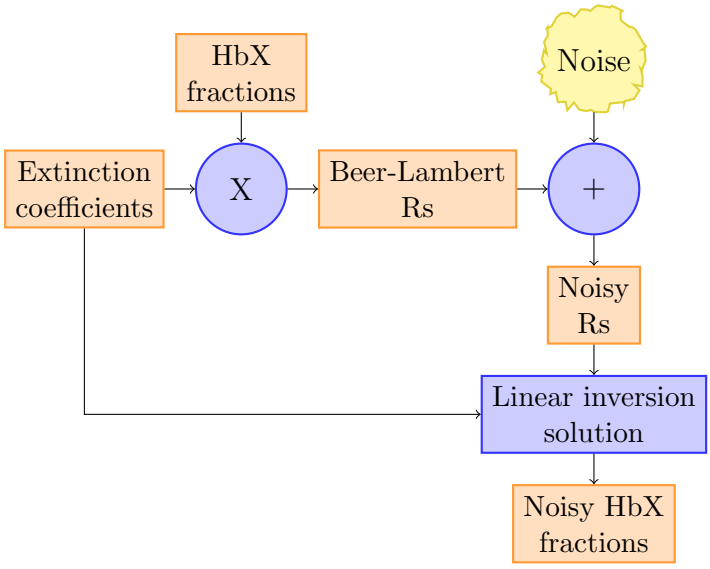

Figure 36: Robustness analysis of linear inversion solution. Beer-Lambert Rs are back calculated and noise is added to them. Then hemoglobin fractions are solved with the noisy Rs.

3.4.6 Algorithm evaluation and validation

In this thesis, several ways of evaluating the algorithm performance are used. Standard statistics, confusion matrix and k-fold validation methods are used to evaluate the algorithm performance. Direct modeling of hemoglobin fractions presented in section 2.3.2 is used as comparative method. Also Bland-Altman plots of the results are drawn.

Statistics

Bias (Eq. 13), precision (Eq. 14), and A_{RMS} (Eq. 15) are calculated for algorithm candidates. Another used method is to evaluate how many of the data points actually reach the accuracy presented in Table 6. If normal distribution of error and zero bias are assumed about 68 % of the values should be within the limits.

Confusion matrix

Confusion matrix presented in Figure 37 is a good tool for analyzing the performance of the algorithm in medical diagnostics. Confusion matrix shows the predicted and actual classifications based on the decided limits. [71] Dyshemoglobin limits that are relevant for clinical diagnosis were set to 2 % with elevated HbMet and to 6 % for elevated HbCO in the goal setting phase.

		Predicted	
		negative	positive
Actual	negative	TN	FP
	positive	FN	TP

Figure 37: Confusion matrix, T = true, F = false, N = negative, P = positive.

With the help of confusion matrix measures of accuracy, sensitivity and specificity can be defined:

- Accuracy = $\frac{TP+TN}{TP+TN+FP+FN}$
- Sensitivity = $\frac{TP}{TP+FN}$
- Specificity = $\frac{TN}{TN+FP}$

Accuracy describes how well the algorithm is measuring what is should measure. Sensitivity is a measure of how many of the values classified as positive really were positive and specificity how many of the values classified negative were correctly classified.

Cross-validation

Cross-validation methods are used in evaluating how well predictive models work in practice. They show how the results of the statistical models will generalize to an independent data set. Commonly used cross-validation methods include k-fold cross-validation and leave-one-out (LOO) cross-validation.

In this thesis, both were used to evaluate the algorithms. k-fold cross-validation process is presented Figure 38. In k-fold cross-validation, the original sample set is first divided randomly into k groups. Then k-1 groups are selected for development and the last one is left for validation. After development prediction errors are calculated with the data points in validation set. These steps are repeated k times and all groups are used once as a validation group. The whole k-fold cross-validation process is repeated for several times with different division of samples. LOO cross-validation is only a special case of k-fold cross-validation, where k is equal to the size of original data set.

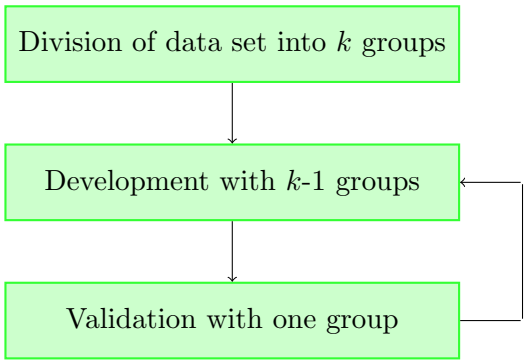

Figure 38: k-fold cross-validation process

The trade-off of changing k value is in the predictive power against how representative the result is for the larger population. The smaller the k the worse the result should be in a given small population. On the other hand large k might result in very good results within the small data set due to the fact that the validation population in itself is a bad representative of the larger population.

4 Results

Data processing was done with Matlab. This section presents all results from CO-oximeter data analysis to algorithm validation. First reference and development data are analyzed and the robustness of the linear inversion solution is studied. Then different algorithm candidates are developed and compared. At the end the best algorithm is validated.

4.1 CO-oximeter data analysis

Summary plots illustrating the CO-oximetry data accuracy are presented in Figure 39. The asterix represents the mean difference and the whiskers are plus minus one standard deviation for the difference. Values in y-axis are difference in CO-oximeter readings defined as OSM minus IL with smoker and normal dyshemoglobin studies and OSM minus ABL with elevated dyshemoglobin study. Positive difference means greater OSM values. Mean and standard deviation from smoker study are presented with blue, from normal dyshemoglobin study with red and from elevated dyshemoglobin study with black color. Results are consistent with the accuracies reported by CO-oximeter manufacturers listed in Table 9. Standard deviations deviations for HbCO and HbMet values are clearly in specifications. For HbO_2 and RHb greater deviations exist. Also offsets between devices are present.

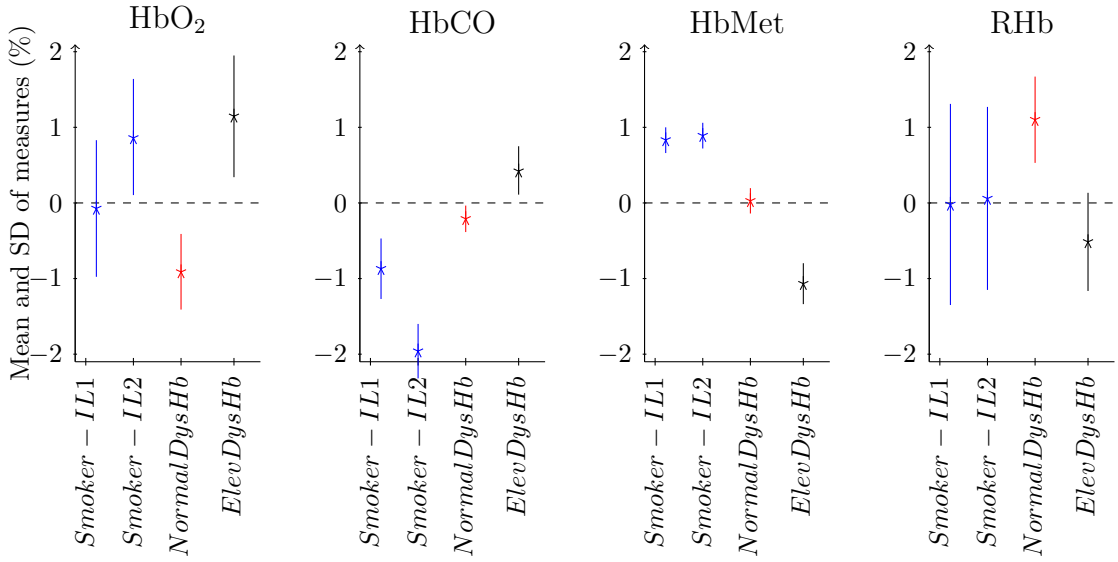

Figure 39: CO-oximeter accuracy analysis using summary plots. The asterix represents the mean difference and the whiskers are plus minus one standard deviation for the difference.

Statistical significance of the results above were tested using t-test, with null hypothesis of zero difference in CO-oximetry readings. p-value for each case is calculated and presented in Table 11. In most of the cases null hypothesis can be rejected with high probability.

Table 11: p-values of CO-oximeter analysis

	HbO2	HbCO	HbMet	RHb
Smoker-IL1	0.72	1.00	1.00	0.16
Smoker-IL2	1.00	1.00	1.00	0.47
NormalDysHb	1.00	1.00	0.94	1.00
ElevDysHb	1.00	1.00	1.00	1.00

CO-oximeter data outliers were removed with criteria more than three standard deviations away from the mean. Scatter plot of smoker study is presented in Figure 40. Outliers are marked with red asterixs. Altogether six samples were rejected from the smoker study, zero from the normal dyshemoglobin study and one from the elevated dyshemoglobin study.

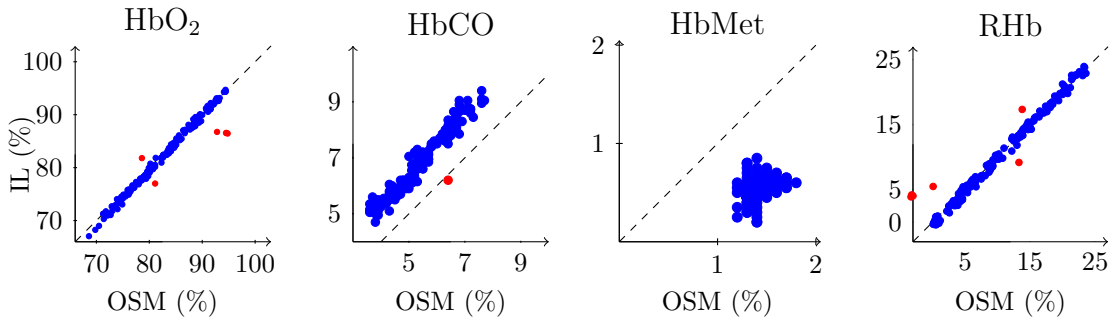

Figure 40: CO-oximeter scatter plots of hemoglobin fractions in smoker study.

According to literature analysis normal HbMet levels are about 0.5 %. In CO-oximetry,f RHb readings are calculated as 100 % minus HbO_2, HbCO, and HbMet. This means that errors in other fractions are accumulated in RHb readings. It is assumed that the mean of different devices is the best alternative to calculate hemoglobin fractions unless readings cannot be reasoned abnormal. In smoker study, mean of two IL runs is used. Standard deviations between IL devices are 0.70 % with HbO_2, 0.41 % with HbCO, 0.14 % with HbMet, and 0.59 % with RHb. OSM was rejected because of abnormally high minimum MetHb levels (range $1.2 - 1.8$ %, see Fig 40). From normal dyshemoglobin study mean of two readings with same IL device were used to be consistent with smoker study even though there was not any other reason to reject the OSM results. In these two studies, test laboratory was the same and even if there was nine month gap between the tests devices were the same. With elevated dyshemoglobin study OSM results were used and ABL results rejected because of too high minimum HbMet values (1.8 %).

When all data samples are pooled, standard deviation for HbO2 is 0.69 %, for HbCO 0.32 %, for HbMet 0.20 %, and for RHb 0.61 %. Bias is not taken into account in this evaluation as it should not affect the results. This is not entirely true in this case, as the difference in biases between studies introduces some error in the calibration phase. Standard deviations are used in evaluating the effects of CO-oximetry reading errors on final results.

4.2 Development data analysis

During the preprocessing phase the development raw data was analyzed. First plethymosgraphic data was visually inspected and quality was examined using the relative amount of hardware adjustments and autocorrelation coefficient signal. Since the focus was not to concentrate on rejection and handling of artifacts, data quality analysis was used to compare data from subject to subject and unit to unit. Then different methods for ratio-of-ratios calculations were compared and the effect of the reference wavelength was studied for the multi-wavelength system.

Development data quality analysis

During the visual segmentation some problems were inspected in the data. Sometimes signals include artifact at about 2 Hz. This artifact is presented in Figure 41. Most often it was visible with the thickest fingers, thumb and index. The reason for the artifact is unclear but it seems that it is present all the time but visible only when the transmission signal is weak.

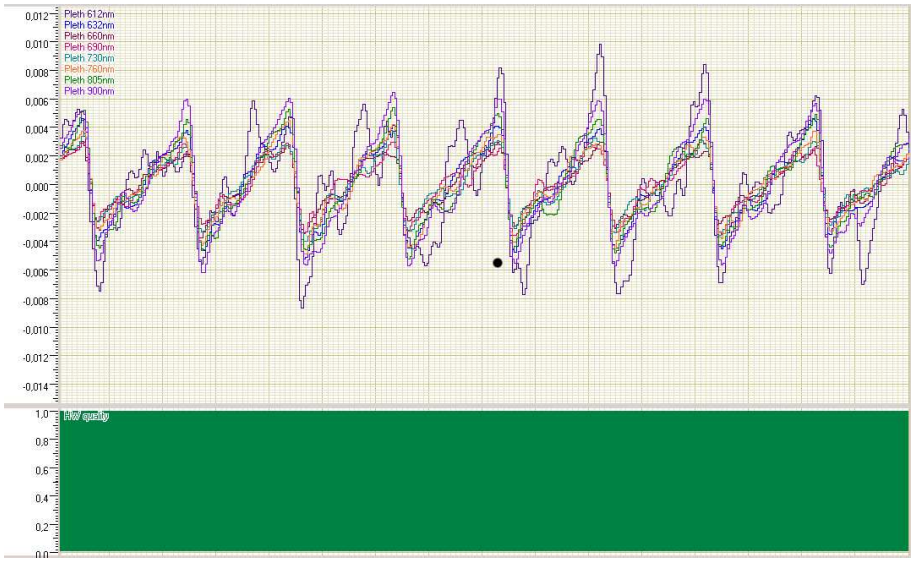

Figure 41: Higher frequency noise observed during the visual inspection.

Samples were rejected, when it was not possible to find a good interval around a blood sample. Subjectwise rejection percentages are listed in Table 12, if the subject had rejected samples. With subjects 25 and 30 the percentages are high. Good quality data sequences around the samples were difficult to find in elevated dyshemoglobin study.

Percentages of good quality data using hardware adjustment and autocorrelation coefficient signals were calculated for each subject and unit. Summary of these results is presented study-wise in Figure 42. Figure indicates that the amount of hardware adjustments is small and does not change from study to study. Autocorrelation quality is the only parameter that shows differences between studies indicating

Table 12: Subjectwise rejection percentages from manual data selection, when it was not possible to find a good interval around a blood sample. Only the subjects that violated the criteria are listed.

Study	Smoker	Normal DysHb	Elevated DysHb			
Subject	3	13	25	26	29	30
No data (%)	3	4	43	3	2	19

that the smoker study executed in April 2009 has the best quality data and that the quality deteriorates from study to study.

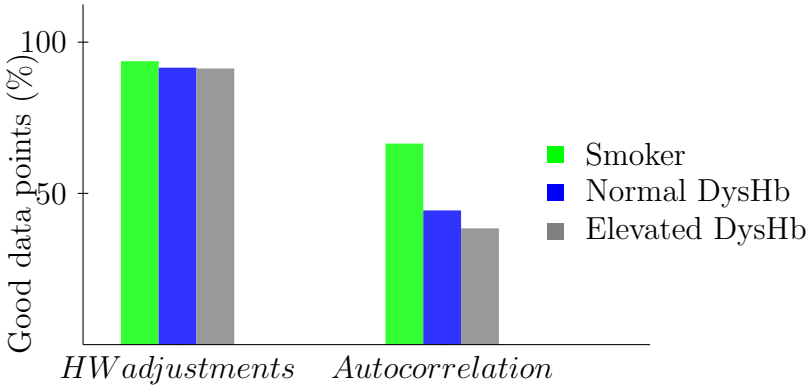

Figure 42: Percentages of good data points with different methods to calculate quality information.

As plethymosgraphic signal should have good autocorrelation between pulses autocorrelation coefficient signal was calculated to compare signal quality between different units. Sensor locations and cushion types of different units are presented in Table 8. Autocorrelation quality results are presented in Figure 43. Figure shows that units 3, 5, 6 and 7 show worse results than units 1, 2 and 4. Unitwise hardware quality analysis showed similar results. Black cushion units and units 3 (pinky) and 4 (thumb) are excluded from the following steps to make sure that good quality data is used in the development. Pinky showed equally worse results with black cushion units. Thumb was excluded since it quite different from the other finger and it is not used in standard pulse oximetry either. Further studies will use the thumb to discover if it can be used as well.

Ratio-of-ratios calculations

Conventional SpO_2 value was calculated using GE pulse oximeter calibration curve for $R_{660/900}$ to obtain accuracy information. From this information bias (Eq. 13) and precision (Eq. 14) were calculated. Because the calibration was not done for this particular prototype bias was negative with all methods. Results are presented in Figures 44 and 45. With peak and valley (PV) and delta absorption (dA) methods 2 seconds time window was used. Methods using Fast Fourier Transform, FFT and

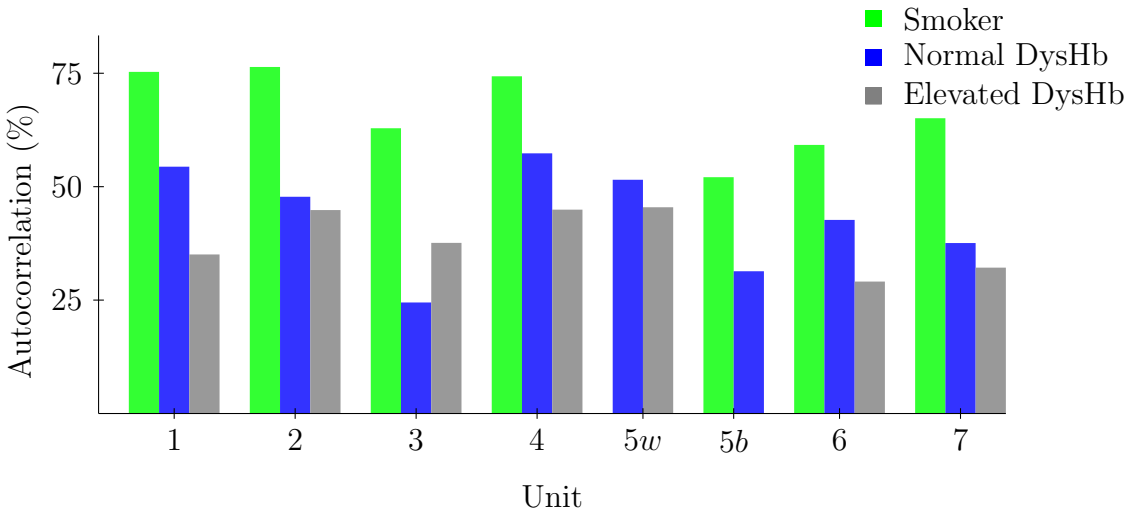

Figure 43: Good quality percentages using autocorrelation coefficient calculation for different units. Units 1-4 are white cushion units and units 6 and 7 are black cushion units. Unit 5 was changed to white cushion unit in normal dyshemoglobin study from subject 3 onwards.

FFT_n, were calculated with 128 points. In elevated dyshemoglobin study, standard deviation of SpO_2 is remarkably greater when ratio-of-ratios is calculated with PV method, which is reasonable as only few points from the data are used in the calculation. Also FFT showed poorer precision and large bias. Based on these results, dA and FFT_n methods were selected to further analysis.

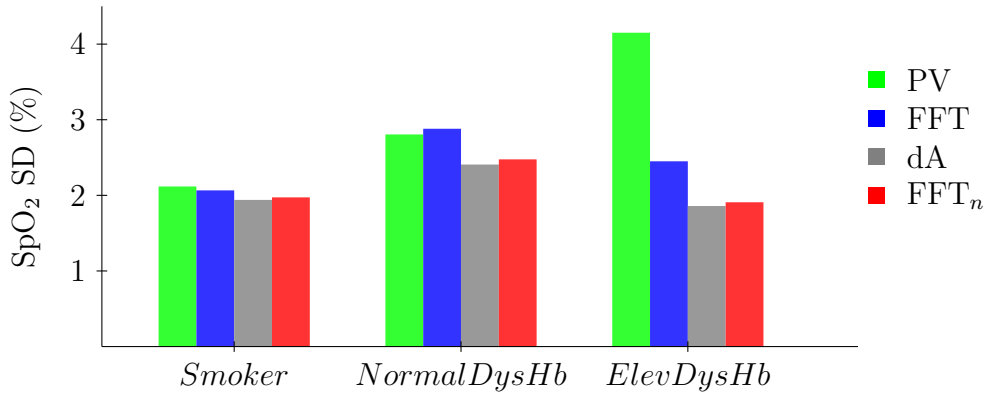

Figure 44: Precision in SpO_2 readings with different methods to calculate ratio-of ratios.

The length of the interval used in ratio-of-ratios calculations was selected to be the shortest possible, two seconds with dA method and 128-point FFT (2.56 s). The selection was confirmed by calculating the precision of SpO_2 with longer intervals. Five and ten seconds interval with dA method and 256- and 512-point FFTs were used. Results are presented in Table 13. With FFT the SpO_2 error due to transformation resolution should decrease as the length of the FFT increases. No significant

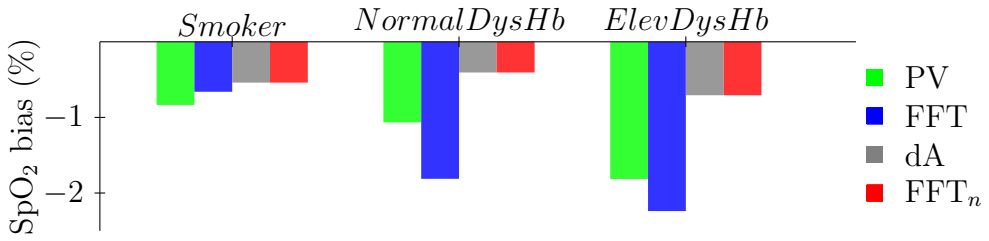

Figure 45: Bias in SpO_2 readings with different methods to calculate ratio-of-ratios.

differences arise in SpO_2 precision when the interval is lengthened. This confirmed that short intervals can be used.

Table 13: SpO_2 precision with different interval lengths

Interval length (s)	Smoker		Normal DysHb		Elevated DysHb	
	dA	FFT_n	dA	FFT_n	dA	FFT_n
2	1.977	1.991	3.443	3.445	2.052	2.191
5	1.973	1.993	3.435	3.459	2.058	2.199
10	1.967	1.975	3.431	3.437	2.053	2.156

Next the effects of different reference wavelengths were studied. Ratio-of-ratios were calculated against different reference wavelengths using dA method with two second window and 128-point FFT calculated from normalized ratios. Methods were compared by using visually defined good quality data sequences. RSDs of ratio-of ratios within these sequences for each reference wavelength were calculated. Mean of RSDs (Eq. 22) is presented in Figure 46. As dA method showed more stable Rs with all reference wavelengths it was selected to be used in ratio-of-ratios calculations. The analysis shows also that the noise is greater when 612 nm is used as a reference wavelength probably due to increased tissue effects with the 612 nm signal. Also signal balancing was not optimal with 612 nm signal according to the performance test results with the prototype.

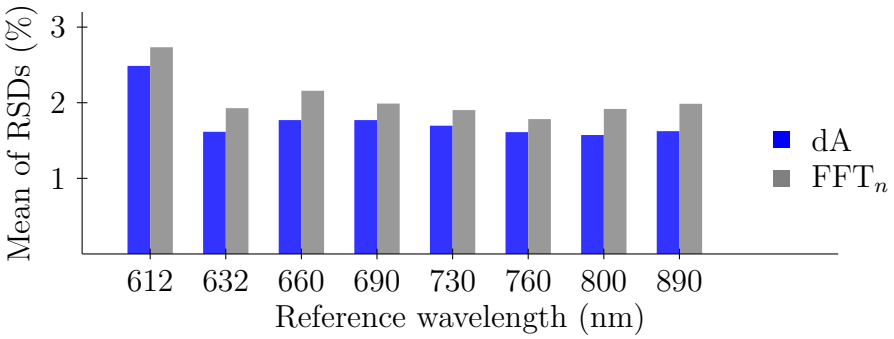

Figure 46: Mean of RSDs as function of reference wavelength. Ratio-of-ratios are calculated using dA and FFT_n methods.

Mean of RSDs with reference wavelengths 632 nm and 760 nm using dA method are presented in Figure 47. The mean of all RSDs was the lowest with these two wavelengths (Fig. 46). 760 nm (LED 8 in Fig. 17) showed good performance already in the prototype testing as 632 nm (LED 7 in Fig. 17) was one the worst. The RSDs are lower nearer the reference wavelengths, which indicates that the noise is correlated when plethymosgraphic wavelengths are close to each other. The noise is largest in $R_{612nm/ref}$.

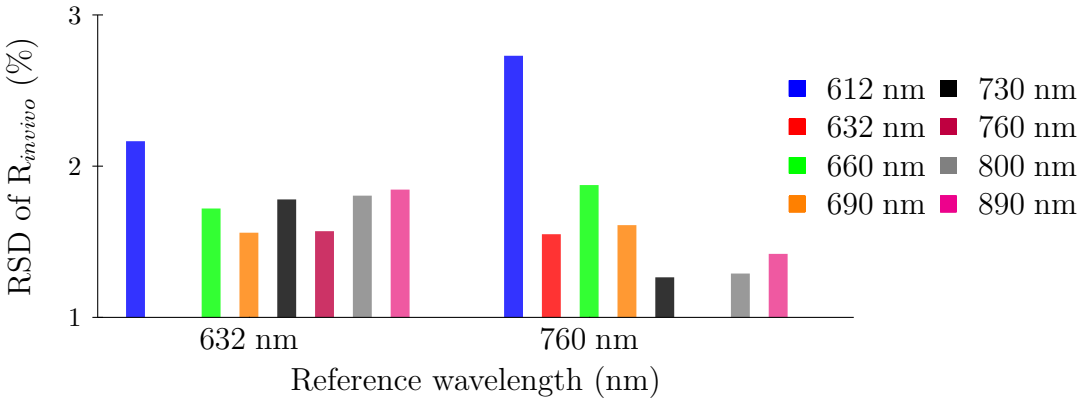

Figure 47: RSDs of R_{invivo}s when 632 nm and 760 nm signals are used as reference wavelengths.

A typical view of the plethymosgraphic signal from a subject in smoker study and the calculated ratio-of-ratios is shown in Figure 48. Plethymosgraphic signals of 612 nm (blue), 660 nm (turquoise), and 800 nm (orange) are presented in top of each other in the first panel. At the isobestic wavelength of HbO_2 and RHb, 800 nm, plethymosgraphic signal is stable regardless of the HbO_2 and RHb fractions. Both 612 nm and 660 nm signals increase, when the saturation falls, because the extinction coefficient of RHb is larger than the extinction coefficient of HbO_2 with 660 nm and 612 nm (Fig. 16). The change is larger with 660 nm signal. Supersaturation phase can be seen clearly from the 660 nm signal. Movement artifacts can be seen in the signals when hands are moved up or down. Ratio-of-ratios calculated with delta absorption method using 612 nm as reference wavelength are presented in the second panel and with 800 nmin the third panel. Figure shows that when 612 nm is used as a reference wavelength the noise is greater in $R_{660nm/ref}$ as expected. In both cases the noise seems to be random with constant variance. When the hands are moved the ratio-of-ratios do not change, because they are a measure of blood composition but after desaturation phase starts ratio-of-ratios become larger as the transmission with 660 nm signal increases. When 800 nm is used as a reference R changes from about 0.65 to 1.15. With 612 nm the change is from 0.45 to 0.65. Unnamed vertical lines in groups of three are blood sample times that are taken from stable plateaus. This can be seen from the $R_{660nm/800nm}$ signal during the desaturation phase. With $R_{660nm/612nm}$ plateaus are mixed with the noise. The lowest panel shows the hardware adjustment signal.

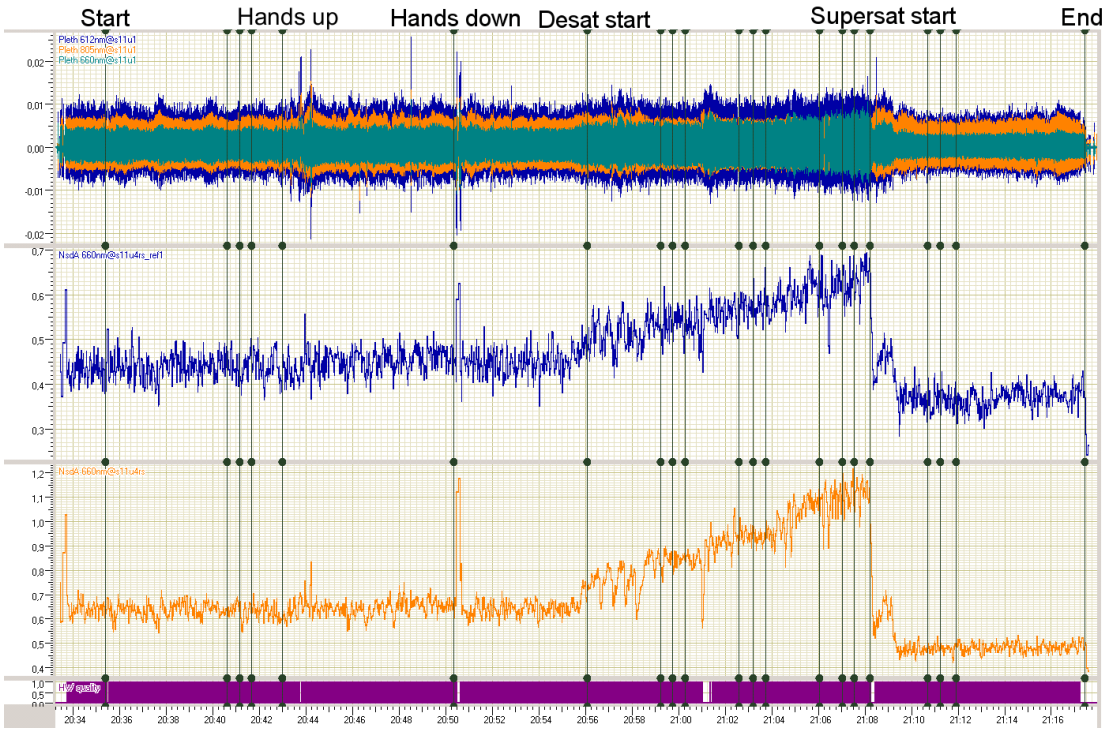

Figure 48: A typical view of the plethymosgraphic signals, 612 nm (blue), 660 nm (turquoise) and 800 nm (orange), and ratio-of-ratios signals, $R_{660nm/612nm}$ and $R_{660nm/800nm}$, from a test subject. Vertical lines represent time stamps for different phases in the test protocol and unnamed vertical lines in group of threes are blood sample times.

Development data selection

The amount of noise that the linear inversion solution can handle was studied using the method presented in Figure 36. First Gaussian RMS noise from zero to five percent was introduced to all R_{LB}s. Results are presented in Figure 49. Oxyhemoglobin, carboxyhemoglobin and reduced hemoglobin fraction specification targets are violated at noise levels of 2.7, 3.3 and 4.8 %, respectively. Methemoglobin and reduced hemoglobin accuracy requirements are not violated even with the largest amount of noise.

As CO-oximetry results are used in calibration of the multi-wavelength system, their accuracy affects to the results. The error (SD) in CO-oximetry readings is on average 0.69 % with HbO_2. Subject-to-subject variability is estimated to be about 1 % based on the conventional pulse oximetry accuracy. The maximum error caused by ratio-of-ratios is calculated with Equation 23 to be 1.6 % with oxyhemoglobin if the accuracy requirement of 2 % is used. This corresponds to about 1.9 % noise in R_{LB}s according to noise analysis presented in Figure 49.

Figure 48 showed that the noise in R_{invivo}s seems to be random. Averaging of random noise reduces the noise with a factor of $\sqrt{N}$, where N is the number of data points. When the noise in R_{invivo}s is assumed to transfer directly to the R_{LB}s and

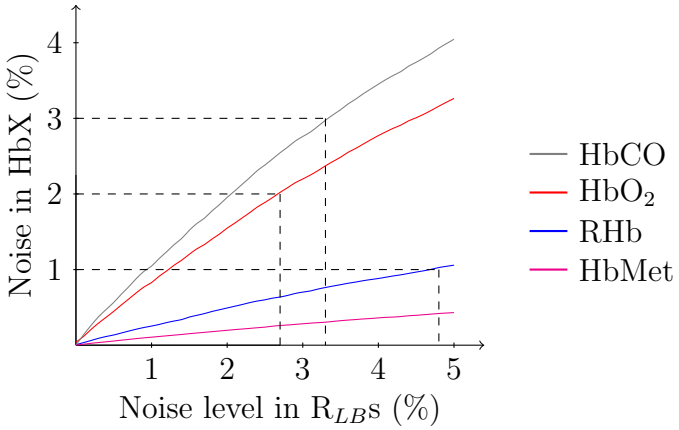

Figure 49: Effect of Gaussian RMS noise in R_{LB}s to hemoglobin fraction accuracy with linear inversion solution. Dashed lines represent hemoglobin fraction accuracy targets: HbO_2 and RHb 2%, HbCO 3%, and HbMet 1%.

it is calculated as RSD divided by $\sqrt{N}$ a limit for good data can be found. Based on this analysis data points where $RSD/\sqrt{N}$ of any of the Rs is greater than 1.9 % are rejected.

To find out which wavelength should be used as a reference, $RSD/\sqrt{N}$ of ratio-of-ratios were applied to the system to illustrate the noise. Precisions of hemoglobin fractions (Eq. 14) were calculated and they are presented in Figure 50. For solving HbO_2 and HbCO, 612 nm is the best reference wavelength although previous analysis showed that RSDs of Rs (Fig. 46) are greater when 612 nm is used as reference. With HbMet and RHb the best reference wavelengths were 632 nm and 612 nm, respectively. Based on these two analysis, 612 nm signal was selected to be used in further algorithm development, because it was the best reference for all other hemoglobin species except HbMet.

Rejection percentages using reference wavelength 612 nm are presented in Figure 51 for each subject. Some problems are present with the subject 11 in the smoker study and subject 21 in the normal dyshemoglobin study. Visual inspection reveals that the 2 Hz artifact is present with both of these subjects in the unit 1 (index finger) and probably affects even with the good intervals. Otherwise the data seems to be good. In elevated dyshemoglobin study, more than 20 percent of the data points are rejected with six of the nine subjects, even if the intervals were selected to be good with visual inspection.

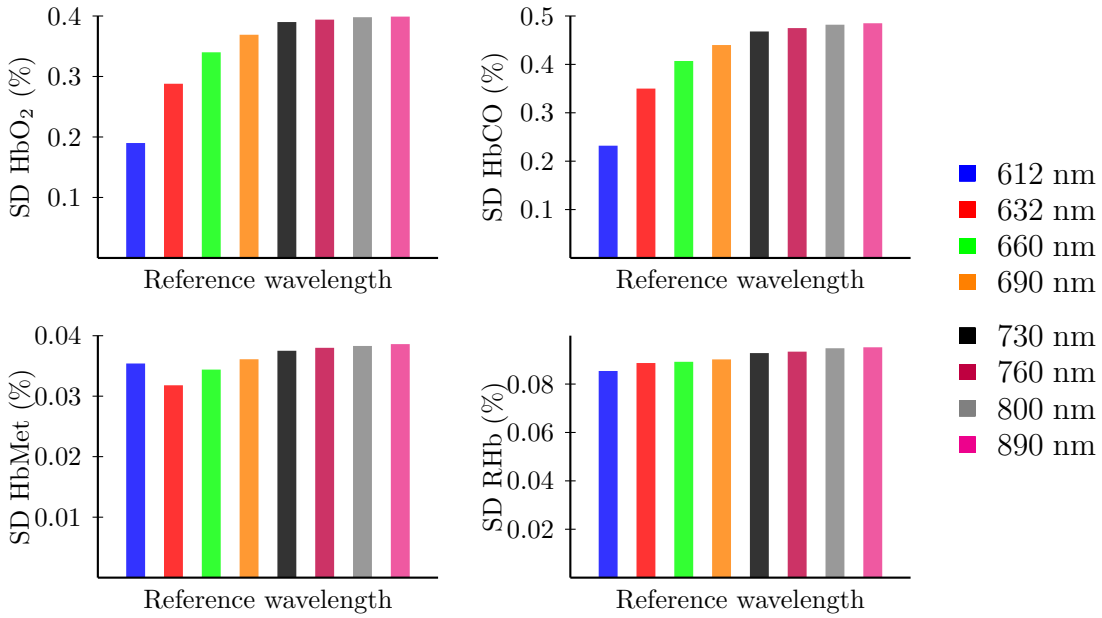

Figure 50: Standard deviations of hemoglobin fractions when RSDs of Rs are applied to the system with different reference wavelengths.

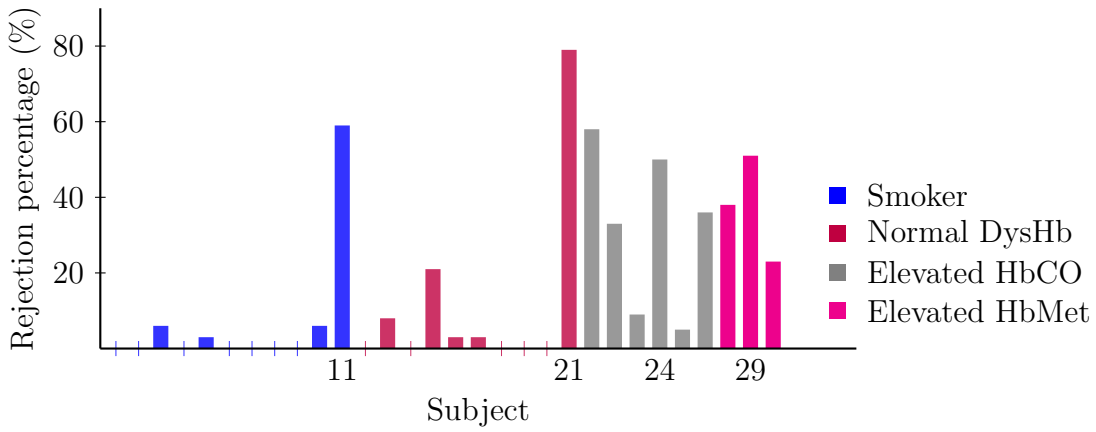

Figure 51: Rejection data percentage with different subjects.

4.3 Fractional pulse oximetry algorithm

In the algorithm development phase, direct modeling of hemoglobin species was used as a comparative method. Principal component analysis and forward selection methods were used to find a regression model for Beer-Lambert ratios. These methods are evaluated against specifications and with common descriptive statistics used in pulse oximetry. At the end the best algorithm is validated using k-fold cross-validation.

Forward selection method

Forward selection method was evaluated using F-test and SBIC. Rs were modeled in four stages with different parameters sets as shown in Figure 35. Table 14 presents the number of parameters selected in the model. Number of statistically significant parameters selected with F-test is low regardless from the parameter set. F-test is only valid is the residuals are normally distributed. Normality was tested with Kolmogorov-Smirnov test of normality and it revealed that this requirement is violated. Number of parameters determined through SBIC is remarkably larger.

Table 14: Number of parameters selected in the model using F-test and SBIC as selection criteria.

	Stage 1 model		Stage 2 model		Stage 3 model		Stage 4 model	
	F-test	SBIC	F-test	SBIC	F-test	SBIC	F-test	SBIC
632 nm	5	5	4	10	3	28	3	53
660 nm	0	6	0	6	0	23	0	28
690 nm	1	5	0	10	0	18	0	16
730 nm	1	4	1	17	0	22	0	28
760 nm	1	5	0	14	0	24	0	37
800 nm	2	5	2	11	0	33	0	50
890 nm	3	5	3	8	0	38	0	32

Figure 52 presents the mean square error (MSE) of the regression as a function of number of parameters included in the model for each ratio. A clear difference between models is not observable. The MSE for $R_{900nm/612nm}$ is the worst in all cases and the second worst is $R_{800nm/612nm}$. The number of parameters used in the forward selection method is selected with SBIC criteria.

Table 15 lists the first three parameters that were selected in different stages to the regression model using forward selection method and reference wavelength 612nm. Numbers indicate the wavelengths from the shorter to longer wavelengths: 1 equals 612nm and 8 equals 900nm. In Stage 1 model, R_2 and FLT_2 are common parameters. Same parameters or their quadratic or third order terms are often included in the following stages. This indicates that the shorter wavelengths are very important for solving the hemoglobin fractions. In Stage 4 model, R_8*FLT_2 is the first parameter for longer wavelength R_{LB}s and with shorter wavelength R_{LB}s only the $R^{in-vivo}$ is changed to the corresponding $R^{in-vivo}$. Because FLT_2 is often

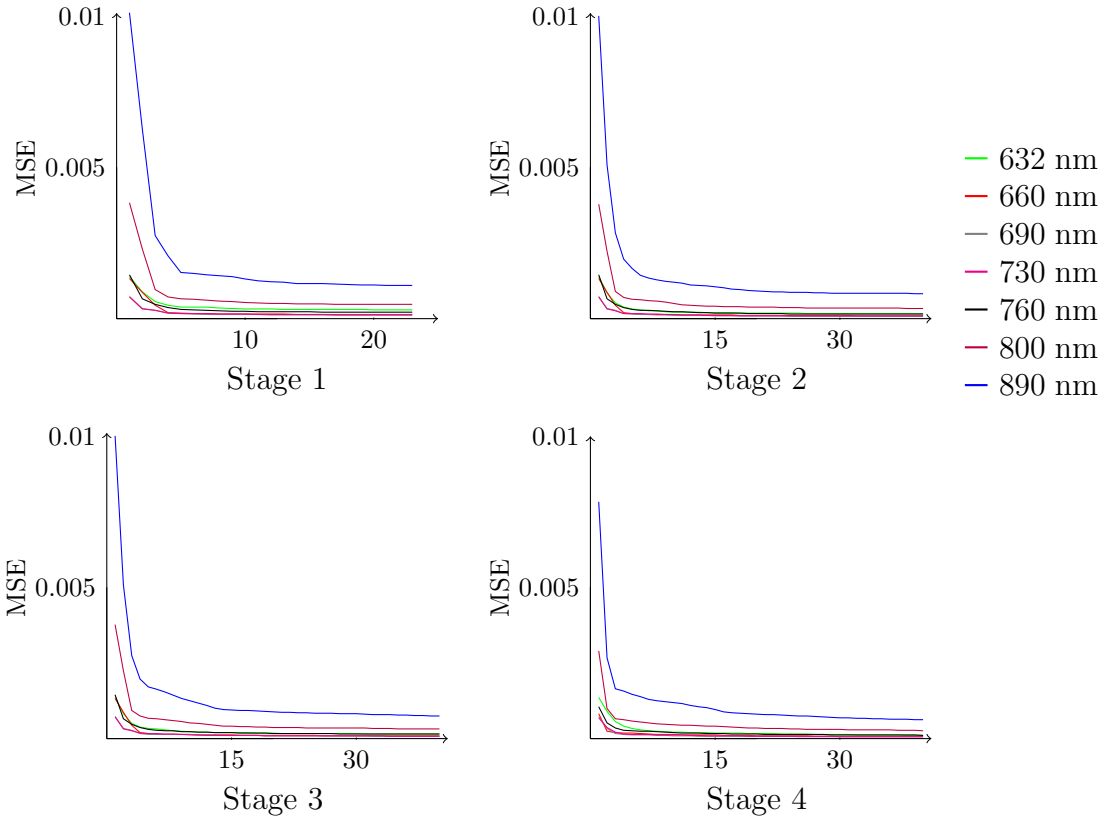

Figure 52: Mean square errors of the regression models from forward selection method as a function number of parameters.

included in the models, it might mean that the short wavelengths represent the tissue effects better than the longer wavelengths. In addition, it is beneficial to have the corresponding or neighbour $R^{in-vivo}$ in the model.

Table 15: Parameters selected in different stages to the regression model.

R^{LB}	Stage 1	Stage 2	Stage 3	Stage 4
2	R_2, FLT_2, R_4	R_2, FLT_2^2, R_4	R_2,FLT_2^3, R_4	R_2*FLT_2, R_2^2, FLT_3^2
3	R_3, FLT_2, FLT_3	R_3, FLT_2, FLT_3	R_3, FLT_2, FLT_3	R_3*FLT_2, R_5*FLT_3, FLT_3^2
4	FLT_2, FLT_3, R_3	FLT_2, FLT_3, R_3	FLT_2, FLT_3, R_3	R_4*FLT_2, R_4*FLT_3, R_2*R_7
5	FLT_2, FLT_4, R_1	FLT_2, FLT_4, R_2^2	FLT_2, FLT_4, R_2^3	R_8*FLT_2, R_8*FLT_3,R_2*R_8
6	FLT_2, FLT_6, R_2	FLT_2, FLT_6, R_2	FLT_2, FLT_6, R_2	R_8*FLT_2, R_7*FLT_4, R_2*R_8
7	R_2, R_6, FLT_2	R_2^2, FLT_2^2, R_6	R_2^3, FLT_2^3, R_6	R_8*FLT_2, R_2^2, FLT_2
8	R_2, R_6, FLT_2	R_3^2, R_4, FLT_2^2	R_3^2, R_4, FLT_2^3	R_8*FLT_2, R_3*FLT_7, R_2

Hemoglobin species were solved using Beer-Lamber Rs derived from the regression. From these results percentages that fulfill the requirements specified in Table 6, bias and precision of hemoglobin fractions were calculated. Comparison of the regression models is based on these figures.

Principal component analysis

In principal component analysis all terms were included in the regression. Number of principal components was determined so that 95 percent of the variance would be explained by the components. Also a scree plot of was drawn as a comparative method. Scree plot is presented on the left side of Figure 53. On the right side MSE of the Rs is presented as a function of the number of principal components used in the regression. Comparing MSEs to the MSEs from the forward selection method shows that they are worse with PCA. Again MSE for $R_{900nm/612nm}$ is the worst.

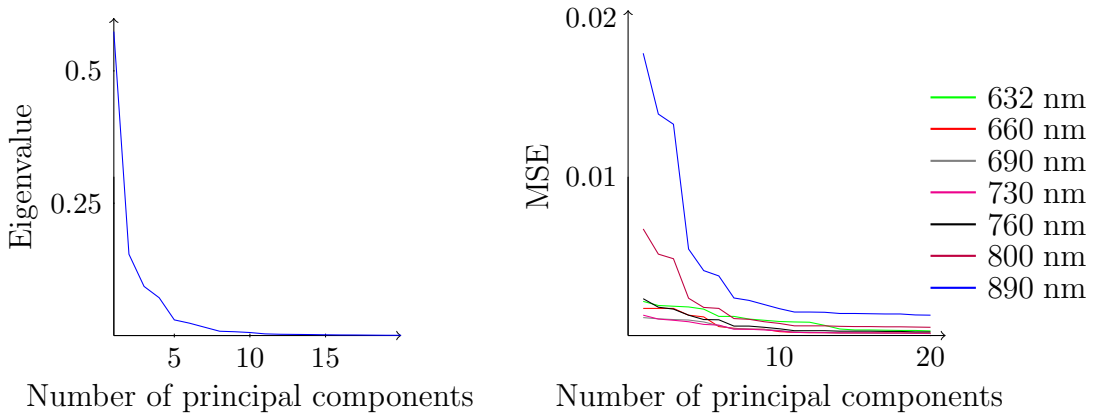

Figure 53: Scree plot of eigenvalues of principal component analysis using reference wavelength 612nm.

Number of principal components determined with different ways are listed in Table 16. With reference wavelength 612 nm six PCs accounted for 95 percent of the variance and nine PCs accounted for 99 percent of the variance. No clear elbow is seen in the scree plot, but smoother elbow is visible at five PCs. If each principal component is required to account at least for 0.5 percent of the variance then nineteen principal components should be used. It was decided to use six principal components with PCA method.

Table 16: Number of parameters with different order selection methods for PCA.

Method	Nbr of PCs
95 % of the variance	6
99 % of the variance	9
Scree plot	5
PC fraction of variance $> 0.5\%$	19

Algorithm candidate comparison

Few ways were used in evaluating the performance of the algorithms. If normal distribution of error is assumed, about 68 % of the hemoglobin values should be within the limits presented in Table 6. For normal distribution, 68 % of the values lie within one standard deviation (Eq. 14) of the mean. Results with different algortihms are presented in Figure 54. With all methods but PCA, RHb and HbMet are in specifications. HbO_2 and HbCO are under specifications. In direct modeling, second-order Taylor polynomes are used to estimate the Jarman's model for all hemoglobin fractions.

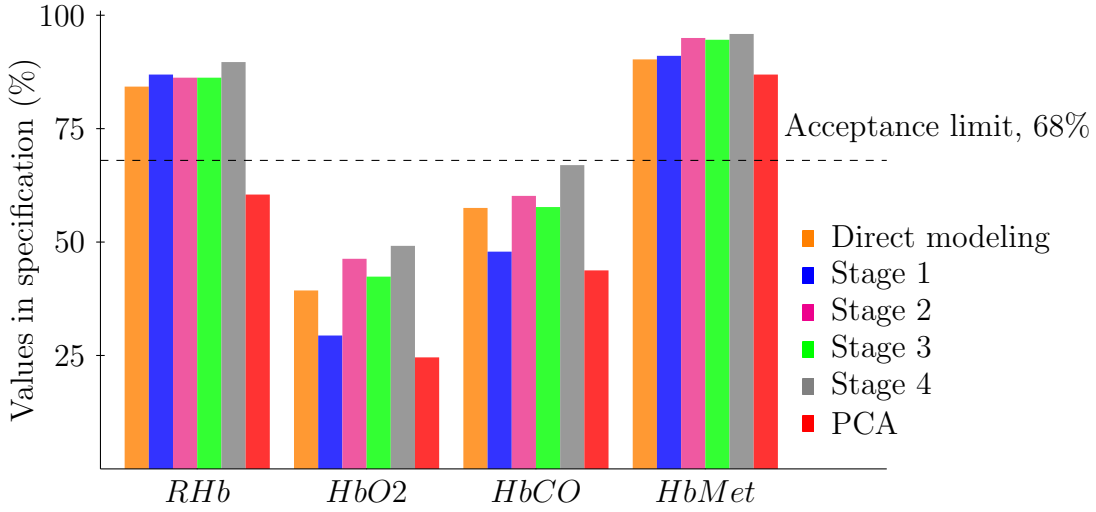

Figure 54: Percentage of hemoglobin concentration within specification using different modeling algorithms.

In addition, descriptive statistic, bias, precision, and A_{RMS} were calculated and the results are presented in Table 17. A_{RMS} statistics of SpO_2 are also calculated to be able to compare the algorithm to conventional pulse oximeters that have A_{RMS} smaller than two percent. A_{RMS} statistics of the algorithms show that they are close to the accuracy of conventional pulse oximeters. Together these results indicate that forward selection method with Stage 4 is the best algorithm. Stage 2 model shows the best results in terms of HbMet precision.

Above statistics do not tell the whole truth of the algorithm performance. Relatively small amount of elevated HbCO and HbMet data points were included the development data. Values within specifications were calculated separately for high and low HbCO and HbMet values. HbCO is defined as high if the fraction exceeds six percents and high HbMet limit is two percents. Figure 55 shows percentage of dyshemoglobin concentrations within specification using different modeling algorithms. Stage 4 model shows clearly the best results for low HbCO. Low HbMet levels are well recognized by all algorithms. Stage 4 model shows the best performance with high HbMet values but Stage 2 and 3 models are almost as good.

Table 17: Descriptive statistics of algorithm results

Statistics	Method	RHb	HbO_2	HbCO	HbMet	SpO_2
Mean bias (%)	Direct HbX	-0.04	-0.29	0.31	0.01	
	Stage 1 model	-0.15	-1.30	1.61	-0.16	
	Stage 2 model	-0.06	-0.59	0.69	-0.05	
	Stage 3 model	-0.16	-0.32	0.55	-0.07	
	Stage 4 model	-0.15	-0.17	0.39	-0.08	
	PCA	0.08	-0.96	1.12	-0.24	
Precision (%)	Direct HbX	1.61	4.00	4.43	0.84	
	Stage 1 model	1.60	6.12	6.67	0.93	
	Stage 2 model	1.71	4.81	5.11	0.62	
	Stage 3 model	1.73	4.23	4.68	0.71	
	Stage 4 model	1.39	3.42	3.87	0.72	
	PCA	3.72	7.60	7.58	1.71	
A_{RMS} (%)	Direct HbX	1.61	4.01	4.44	0.84	1.67
	Stage 1 model	1.61	6.25	6.85	0.94	1.66
	Stage 2 model	1.71	4.85	5.15	0.62	1.89
	Stage 3 model	1.73	4.24	4.71	0.71	1.83
	Stage 4 model	1.40	3.43	3.89	0.73	1.40
	PCA	3.72	7.66	7.66	1.72	4.48

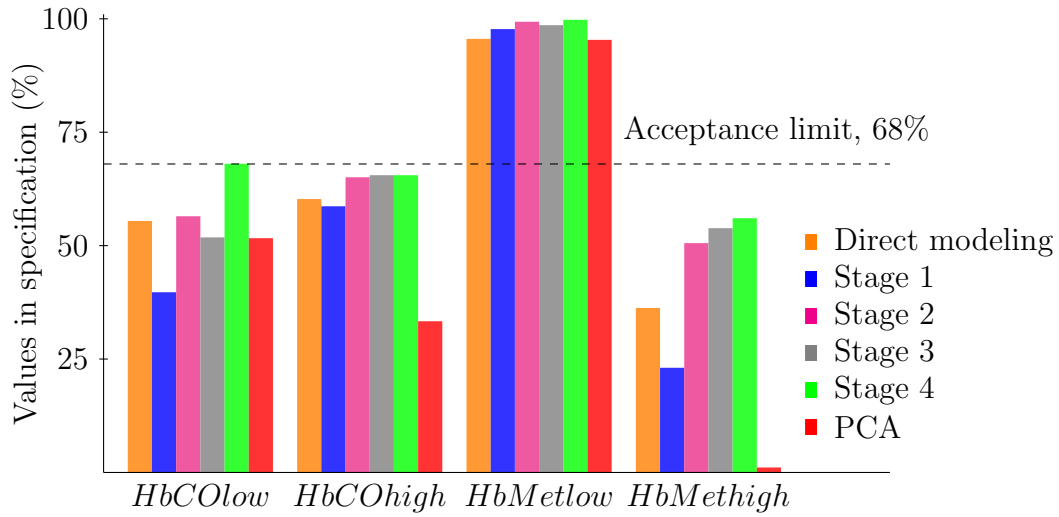

Figure 55: Percentage of dyshemoglobin concentrations within specification using different modeling algorithms.

Bland-Altman plots were drawn to see how the data points are scattered. Bland-Altman plot of Stage 4 model is presented in Figure 56. Differently colored data points in the figure indicate different subjects. Subjects having carboxyhemoglobin levels from four to ten percents due to smoking are colored with blue. Subjects having normal dyshemoglobin levels but changing total hemoglobin values are colored with red. Subjects that inhaled carbon monoxide are colored with green and subjects

with nitride infusion are colored black. With visual inspection Stage 4 model showed the best results in terms of a changing trend seen in HbCO. Carboxyhemoglobin plot shows that high false elevated carbon monoxide values near zero come mainly from nitride infusion subjects. Also higher carboxyhemoglobin values indicate falsely low oxyhemoglobin values as blue and green points are located mainly on the upper part of oxyhemoglobin plot.

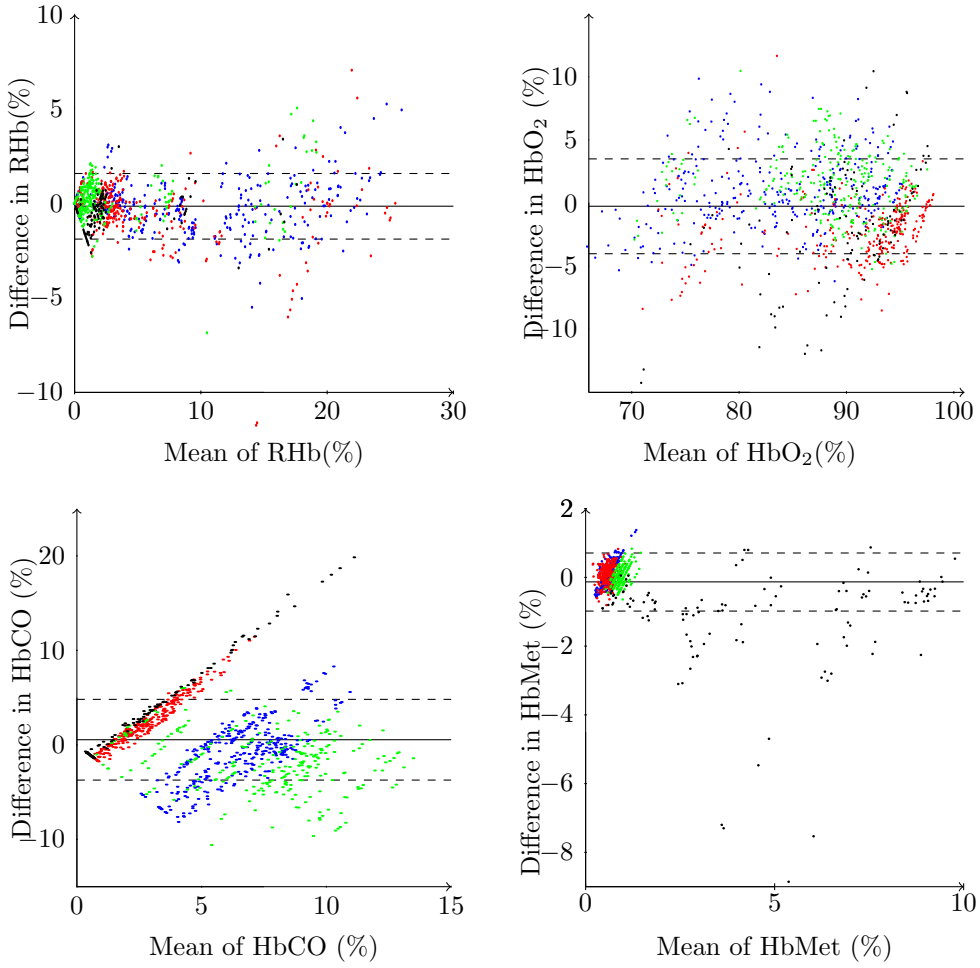

Figure 56: Bland-Altman plot of result with Stage 4 model. Differently colored data points indicate different type of subjects, blue points come from smokers, green from subjects with normal dyshemoglobin level, green from CO inhalation subjects and black from nitride infusion subjects. Vertical solid line is the mean bias and dashed lines describe precision of the measurements.

Screening tool performance

Statistics calculated in previous section do not describe the algorithm performance as a dyshemoglobin screening tool. For this purpose confusion matrix counts were calculated. Threshold for HbCO and HbMet were 6 % and 2 %, respectively. Counts for data points in each section and total numbers of data points in lower and upper ranges of confusion limits are listed in Table 18. Number of elevated HbCO data points is 438 and number of elevated HbMet data points is 91.

Table 18: Values for confusion matrix. FP = False positive, TP = True positive, TN = True negative and FN = false negative. HbCO threshold is 6% and 2% for HbMet.

	SaO2	FP	TP	TN	FN	N neg	N pos	N total
HbCO	70-100 %	165	290	414	148	579	438	1017
	70-90 %	45	83	62	47	107	130	237
	90-100 %	120	207	352	101	472	308	780
HbMet	70-100 %	1	70	925	21	926	91	1017
	70-90 %	0	2	231	4	231	6	237
	90-100 %	1	68	694	17	695	85	780

Figure 57 presents a scatter plot with limits used to recognize elevated HbCO and HbMet values. A clear trend is visible in methemoglobin but the values are biased downwards (bias = -0.08 %, precision 0.72 %). Because of the few elevated HbMet points statistics are highly impacted by lower values. If bias and precision are calculated from elevated HbMet range bias is -1.4 % and precision is 1.7 %. Comparing the elevated HbMet bias and precision with the newest study [58] from Masimo's SpMet accuracy (bias 0.16 % and precision 0.83 %), the FrOx algorithm performance is worse. For elevated HbCO bias is -1.9 % and precision 3.2 %. These values are as good as the values from latest study from Masimo's SpCO accuracy (bias 2.99 % and precision 3.27 %) [56].

Based on the values in Table 18 accuracy, sensitivity, and specificity of the algorithm was calculated. Results are presented in Table 19. Data points are also divided in low and high saturation ranges as literature analysis and previous experience suggest that the accuracy of pulse oximetry deteriorates as saturation falls. This is also true in this case. Part of this might be due to biased development data, there are three times more data points from the high saturation range.

Accuracy of the algorithm in predicting methemoglobin values is good. Elevated methemoglobin values are well recognized. Specificity of almost 100 % is reached which is important in medical care where no one wants to have false alarms. Sensitivity for HbMet at low saturation is only 33.3 %, but Table 18 shows that there are only six blood sample points from the low saturation range for elevated HbMet values. For carboxyhemoglobin figures are worse. Accuracy of about $60 - 70$ % means that three to four cases out of ten are falsely evaluated, which is much for an effective screening tool.

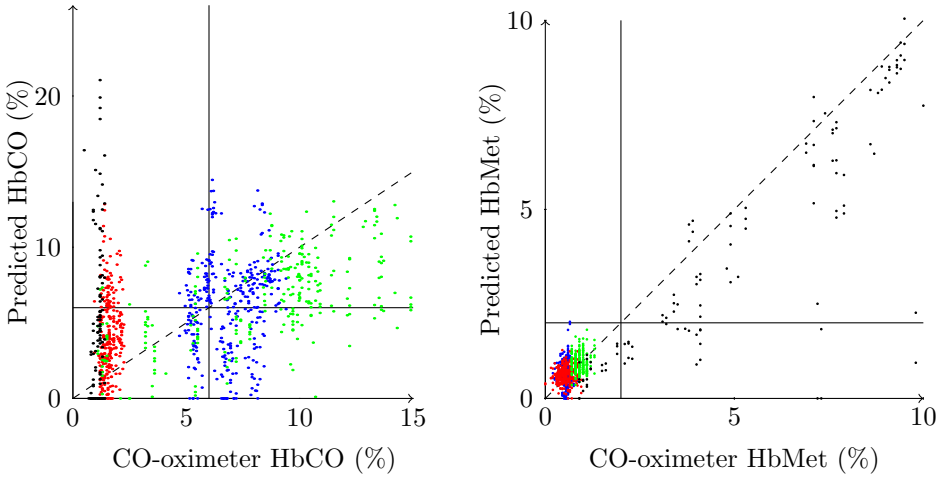

Figure 57: Scatter plot of dyshemoglobin concentrations using Stage 4 model. Vertical and horizontal lines describe threshold limits for elevated HbCO (6 %) and HbMet (2 %). Dashed line is the unity line.

Table 19: Predictive screening performance of algorithm for HbCO and HbMet with changing saturation range.

	SaO2 70-100% n = 1017		SaO2 90-100% n = 780		SaO2 70-90% n = 237	
	HbCO	HbMet	HbCO	HbMet	HbCO	HbMet
Accuracy	69.2	97.8	71.7	97.7	61.2	98.3
Sensitivity	66.2	76.9	67.2	80.0	63.8	33.3
Specificity	71.5	99.9	74.6	99.9	57.9	100.0

Since direct modeling is used as a comparative method, it was studied more closely. Figure 58 shows that direct modeling of hemoglobin concentrations does not recognize carboxyhemoglobin at all. Values are scattered around six percent regardless of the HbCO fraction in the blood. With elevated HbMet levels HbCO fraction elevates falsely in a similar way as with Stage 4 model. HbMet values are more evenly positioned on both sides of unity line even with elevated HbMet values (bias = -0.008 %) but the precision is 2.12 %. Since the amount of elevated MetHb values was relatively low and the quality in the elevated dyshemoglobin study was worse than with the other studies, it is possible that these problems can be solved by collecting more development data with better quality.

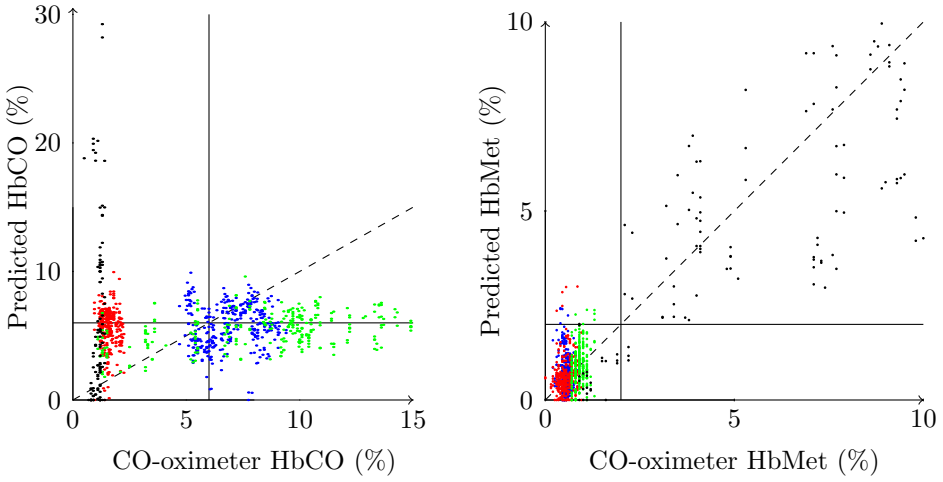

Figure 58: Scatter plot of dyshemoglobin concentrations using direct modeling of hemoglobin fractions. Vertical and horizontal lines describe threshold limits for elevated HbCO (6 %) and HbMet (2 %). Dashed line is the unity line.

The effect of noise in *in-vivo* measured ratio-of-ratios

As the noise was considered to be a problem in the development data, results were calculated with different amount of noise accepted in the measured *in-vivo* ratio-of-ratios. In one data set, all visually selected data points were used, in one data set RSD/$\sqrt{N}$ in any of the *in vivo* ratio-of-ratios was required to be less than 1.9 % and in one less than 1 %. Results were run using 5-fold cross-validation (RUN1) data division. When the noise level requirement is tightened, the amount of data points decreases from 1280 to 714 and the rejection percentages increase especially in the elevated dyshemoglobin study. The percentages of hemoglobin values within specification are presented in Figure 59. Results are better when the noise is reduced to 1.9 % but deteriotate a bit with HbMet and SpO_2 when the RSD/$\sqrt{N}$ requirement is set to 1 %.

Table 20 lists the available data points in elevated dyshemoglobin levels, when the noise requirement is changed. With the 1 % requirement only 43 elevated MetHb data points are left for the development, which makes the regression unreliable and the algorithm performance at high HbMet levels deteriotates.

Table 20: Number of datapoints with different amount of noise is accepted in *in-vivo* ratio-of-ratios.

Noise level	HbCO		HbMet		N
	low	high	low	high	total
All samples	730	547	1117	160	1277
1.9 %	579	438	926	91	1017
1.0 %	410	304	671	43	714

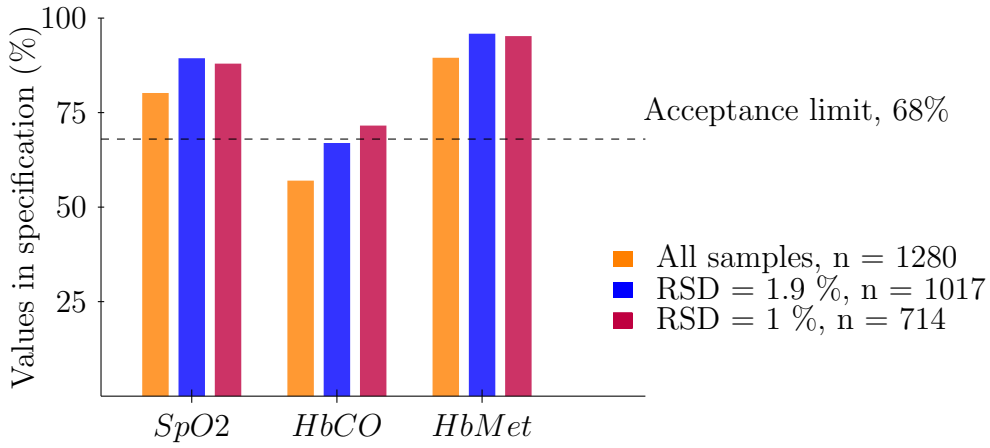

Figure 59: The effect of noise in R_{invivo}s to the accuracy of the FrOx algorithm.

Table 21 list the A_{RMS} values for SpO_2, HbCO, and HbMet using different noise levels. Noise reduction enhances the accuracy when 1.9 % criterion is used but when the noise is further reduced the enhancement is not obvious. With carboxyhemoglobin the error increases.

Table 21: A_{RMS} values for SpO_2, HbCO, HbMet with different noise levels.

Noise level	SpO_2 (%)	HbCO (%)	HbMet (%)
All samples	2.51	4.89	1.33
1.9 %	1.40	3.89	0.73
1.0 %	1.56	4.58	0.57

Figure 60 shows the scatter plot of HbCO fraction with different noise levels. The trend comes more visible when the noise is reduced but at the same time the amount of elevated HbCO data points reduces. Scatter plot shows that falsely elevated HbCO values near zero come mainly from elevated HbMet study.

If subjects with elevated HbMet levels are left out from the algorithm development, statistics for HbCO are presented in Table 22. A trend in the HbCO scatter plot, presented in Figure 61, becomes more visible. With this data set the performance of FrOx algorithm exceeds the performance of Masimo's SpCO measurement (bias 2.99 % and precision 3.27 %) in the latest study [56]. As a conclusion it seems that reducing the noise in *in vivo* ratio-of-ratios improves the algorithm performance.

Table 22: Statistics for HbCO with different noise levels.

Noise level	Bias (%)	Precision (%)	A_{RMS} (%)
All samples	0.26	3.54	3.55
1.9 %	0.04	3.12	3.12
1.0 %	0.01	3.14	3.14

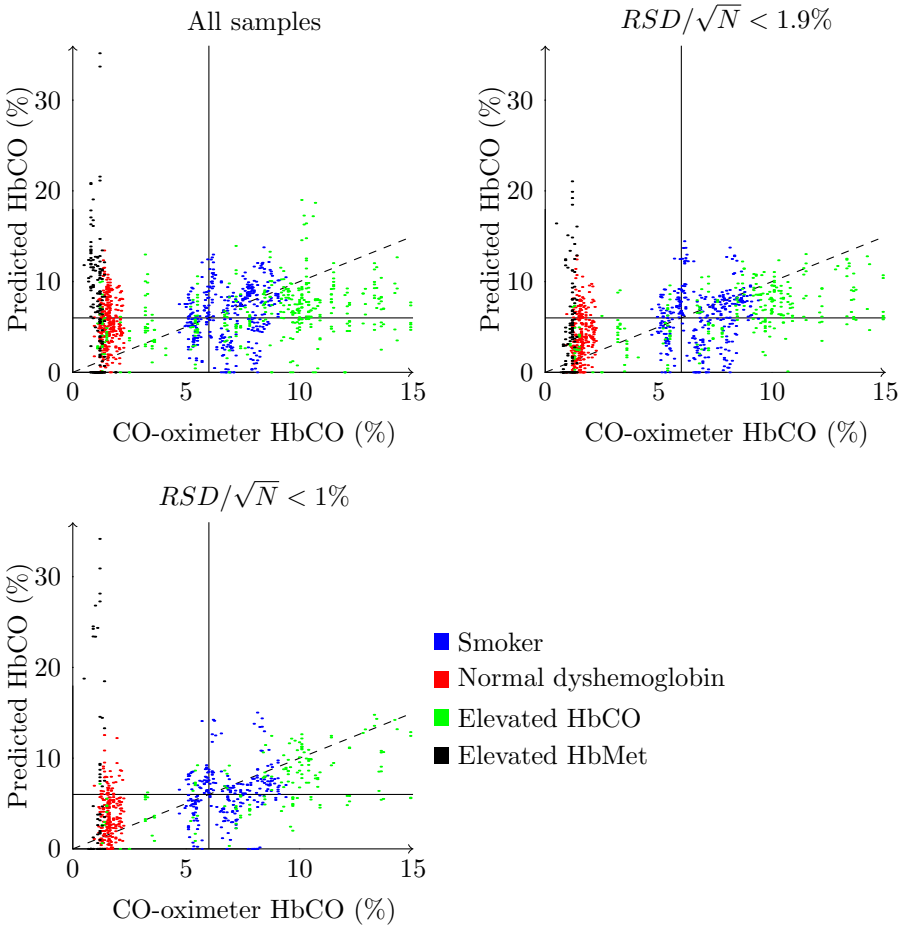

Figure 60: Scatter plot of carboxyhemoglobin fraction using three different noise levels. Dashed line is the unity line and solid vertical and horizontal lines represent the 6 % threshold for elevated HbCO level.

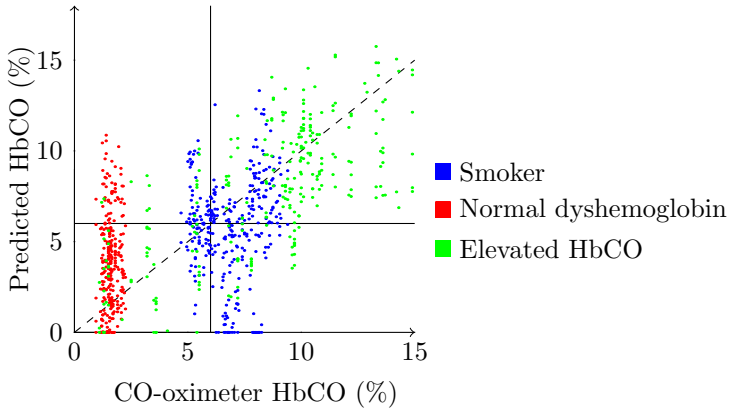

Figure 61: Scatter plot of carboxyhemoglobin fraction with 1.9 % rejection criterion when HbMet-subjects are left out from the algorithm development. Dashed line is the unity line and solid vertical and horizontal lines represent the 6 % threshold for elevated HbCO level.

Cross-validation

Until this point algorithms have been compared based on the results that they give. It seems that Stage 4 model from forward selection method gives the best algorithm. To get information from the algorithm reliability k-fold cross-validation is run.

Different criterias of division of development data sets can be used in k-fold cross-validation. Altogether data was collected from 30 subjects and seven units. As black cushion units and unit attached to left pinky were rejected the amount of units was reduced to three with 13 subjects and to four with 17 subjects. Data was partitioned subject-wise into k-fold groups because splitting of individual data files or unit-wise partitioning would not result in independent data points as development and validation data points would have come from the same subject.

5-fold, 10-fold, and 30-fold (LOO) cross-validation were calculated. To evaluate the robustness of the algorithm repeated 5-fold, 10-fold and LOO cross-validation were done. Since 5-fold cross-validation should show the most deviations it was run four times and 10-fold and LOO cross-validation were run once. Results are presented in Figure 62. Results indicate that the algorithm performs similarly regardless of the data point division. Bland-Altman plots were also drawn of each run and they were consistent with the one presented in previous section (Fig. 56), where results were calculated using the first division of 5-fold cross-validation.

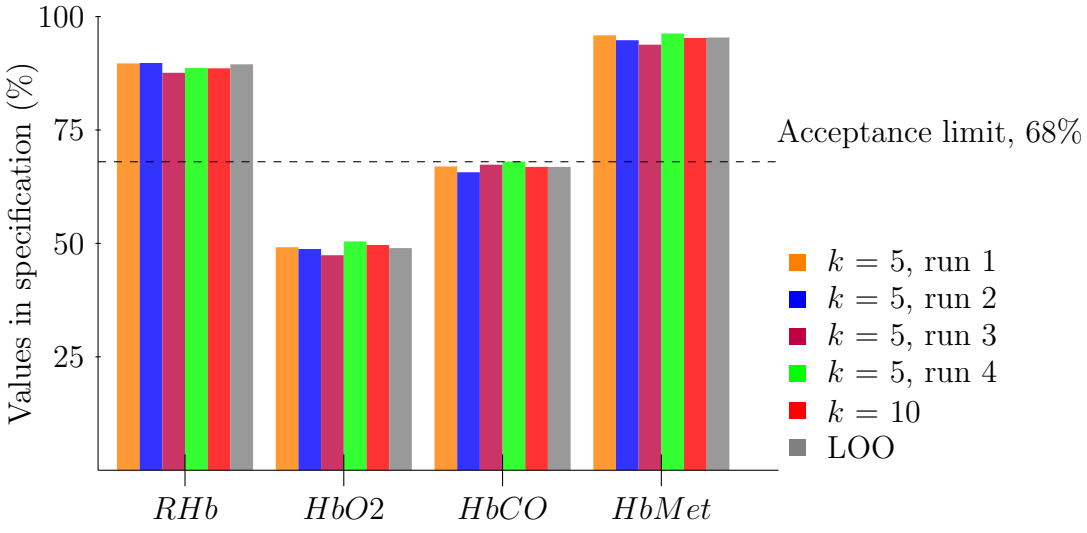

Figure 62: Percentage of hemoglobin concentrations within specification with different k-fold data divisions.

5 Conclusions

The development of the multi-wavelength fractional pulse oximetry algorithm proved to be challenging. Although the feasibility of the algorithm is not proven, positive signs were observed and a lot was learned during the research. As assumed, the measurement of carboxyhemoglobin turned out to be difficult. Methemoglobin measurement showed more promising results but the amount of development data was not sufficient for regression purposes.

One issue that occurred already in the analysis of the preprocessing results was that the development data quality was not as good as expected. The quality of the data from the elevated dyshemoglobin study that covered the elevated carboxyhemoglobin and methemoglobin levels, was significantly worse than in the previous two studies. Used methods to obtain information of the data quality proved to be good. Autocorrelation coefficient signal showed equal results with the impression of deteriorating data achieved during the visual inspection. These methods could be further studied and analyzed to find out how well they recognize abnormalities in plethymosgraphic signals. Autoregressive moving average models could be one possible way to reliably recognize abnormalities.

Despite the quality problems, the algorithm showed some promising signs; it almost reached the accuracy specification requirements. Compared to the commercially available fractional pulse oximetry device, the performance was equivalent or even better with carboxyhemoglobin and only a bit worse with methemoglobin measurement. Since the regression model uses linear, quadratic, third-order, and cross terms, it cannot be stated as either simple or robust, yet cross-validation showed that the results are consistent with different division of development data sets. In this thesis, part of the error in hemoglobin fractions might arise from the reference data as they were collected from three different studies and devices. A benefit from a single study would be that the whole data is developed with the same devices, and the possible offsets between devices do not disturb the regression modeling.

As there were only three subjects with elevated methemoglobin levels and the data rejection percentages from these subjects was relative high, the results are not reliable. A clear trend is seen with methemoglobin but the fraction is underestimated with the selected Stage 4 model. With direct modeling bias was negligible but the precision deteriorated. More data is needed to verify the algorithm performance as a methemoglobin measurement.

Changing the allowed noise level in *in-vivo* ratio-of-ratios enhanced the performance of the algorithm, which strengthens the hypothesis that with better quality data the feasibility can be proven. With less noisier data, carboxyhemoglobin showed a clear trend and it fulfilled the accuracy requirement. Even with greater noise levels, the algorithm reached the accuracy requirements if the subjects from the elevated methemoglobin study were excluded from the development. Still, it is difficult to say for sure how the algorithm would behave with better quality data, because reduction of the noise also reduced the amount of development data.

Noise level was the largest with 612 nm signal, but still it was the best reference wavelength to be used in the measurement. Also, parameters from the shorter

wavelengths were favored in the parameter selection. As the prototype development showed that the signal balancing system is not optimal, especially with shorter wavelengths, the first step in the future development would be to make improvements to the prototype device.

Analysis of the effect of reference wavelength showed that the noise level in *in vivo* measured ratio-of-ratios grows as the reference wavelength is further away from the other plethymosgraphic signal. This could be utilized in the algorithm development. The problem could be split in stages where reduced hemoglobin would be solved first with the longer wavelengths when carboxyhemoglobin hardly absorbs at all. Better regression model for the long wavelengths near the reference wavelength could be developed.

It seems that methemoglobin algorithm can be developed with a sufficient amount of data. If methemoglobin can be measured reliably, it can be used as an input to the second part of the algorithm, where rest of the hemoglobin fractions would be solved. This could solve the problem of many falsely elevated points near zero HbCO level where the values came simultaneously with elevated methemoglobin levels. Dividing the problem in parts makes the algorithm even more complex. An effective tool to determine which path to take is needed, if this approach is applied. Still, dividing the problem in parts is worth trying in future development of the algorithm.

Altogether the work conducted for this thesis succeeded well and a lot more is known of the requirements of fractional pulse oximetry measurement. An improved prototype needs to be developed using the information acquired during the development of the first prototype and this thesis. A single study including a sufficient amount of data from desired dyshemoglobin ranges needs to be collected to prove the feasibility of the algorithm. Also, the algorithm needs to be simplified and a lot more work is required before the technology can be commercialized and used as an effective tool in medical care.

References

[1] G. J. Tortora and S. R. Grabowski, *Principles of Anatomy and Physiology*. New York: John Wiley & Sons, Inc., 9th ed., 2000.

[2] J. G. Webster, *Design of Pulse Oximeters*. Bristol and Philadelphia: Institute of Physics Publishing, 1997.

[3] J. T. B. Moyle, *Pulse Oximetry*. London: BMJ Books, 2nd ed., 2002.

[4] Sigma-AldrichHomepage, *Hemoglobin, Heme Products & Erythrocytes*. Available in: http://www.sigmaaldrich.com/life-science/metabolomics/enzyme-explorer/learning-center/plasma-blood-protein/hemoglobin-heme-products.html, Accessed: Mar. 2011.

[5] R. M. Leach and D. F. Treacher, "Oxygen transport-2. Tissue hypoxia.," *BMJ (Clinical research ed.)*, vol. 317, pp. 1370–1373, Dec. 1998.

[6] A. Ernst and J. Zibrak, "Carbon monoxide poisoning," *New England journal of medicine*, vol. 339, no. 22, p. 1603, 1998.

[7] D. Bateman, "Carbon Monoxide," *Medicine*, vol. 31, pp. 41–42, Oct. 2003.

[8] M. King, "Unintentional Non-Fire-Related Carbon Monoxide Exposures - United States, 2001-2003," *Morbidity and Mortality Weekly Report*, vol. 56, no. 50, pp. 1309–1312, 2007.

[9] A. Harper and J. Croft-Baker, "Carbon monoxide poisoning: undetected by both patients and their doctors.," *Age and ageing*, vol. 33, pp. 105–109, Mar. 2004.

[10] J. Mott, M. Wolfe, C. Alverson, S. Macdonald, C. Bailey, L. Ball, J. Moorman, J. Somers, D. Mannino, and S. Redd, "National vehicle emissions policies and practices and declining US carbon monoxide-related mortality," *Jama*, vol. 288, no. 8, p. 988, 2002.

[11] N. B. Hampson and L. K. Weaver, "Carbon monoxide poisoning: a new incidence for an old disease.," *Undersea & hyperbaric medicine : journal of the Undersea and Hyperbaric Medical Society, Inc*, vol. 34, no. 3, pp. 163–168, 2007.

[12] W. A. D. and R. O. Wright, "Methemoglobinemia," in *Medical toxicology*, ch. 21, pp. 90–97, Philadelphia: Lippincott Williams & Wilkins, 3rd ed., 2004.

[13] H. Rehman, "Evidence-Based Case Review: Methemoglobinemia," *Western Journal of Medicine*, vol. 175, pp. 193–196, June 2001.

[14] S. J. Barker, R. Ash-Bernal, R. Moon, and G. Jay, "The Clinical Implications of Noninvasive and Continuous Carboxyhemoglobin and Methemoglobin with Masimo Rainbow SET Pulse CO-Oximetry," 2006.

[15] R. Ash-Bernal, R. Wise, and S. M. Wright, "Acquired methemoglobinemia: a retrospective series of 138 cases at 2 teaching hospitals.," *Medicine*, vol. 83, no. 5, pp. 265–273, 2004.

[16] G. C. Kane, S. M. Hoehn, T. R. Behrenbeck, and S. L. Mulvagh, "Benzocaine-induced methemoglobinemia based on the Mayo Clinic experience from 28 478 transesophageal echocardiograms: incidence, outcomes, and predisposing factors.," *Archives of internal medicine*, vol. 167, pp. 1977–1982, Oct. 2007.

[17] K. Ohashi, H. Yukioka, M. Hayashi, and A. Asada, "Elevated methemoglobin in patients with sepsis," *Acta Anaesthesiologica Scandinavica*, vol. 42, no. 6, pp. 713–716, 1998.

[18] T. J. Moore, C. S. Walsh, and M. R. Cohen, "Reported adverse event cases of methemoglobinemia associated with benzocaine products.," *Archives of internal medicine*, vol. 164, pp. 1192–1196, June 2004.

[19] J. Guay, "Methemoglobinemia related to local anesthetics: a summary of 242 episodes.," *Anesthesia and analgesia*, vol. 108, pp. 837–845, Mar. 2009.

[20] J. McMurdy, G. Jay, S. Suner, and G. Crawford, "Photonics-based In Vivo total hemoglobin monitoring and clinical relevance," *Journal of Biophotonics*, vol. 2, no. 5, pp. 277–287, 2009.

[21] J. W. McMurdy, G. D. Jay, S. Suner, and G. Crawford, "Noninvasive optical, electrical, and acoustic methods of total hemoglobin determination.," *Clinical chemistry*, vol. 54, pp. 264–272, Feb. 2008.

[22] M. Feissel, R. Kalakhy, J. Badie, G. Robles, J. Faller, and J. Teboul, "Plethysmography variability index: a new fluid responsiveness parameter," *Critical Care*, vol. 13, no. Suppl 1, p. P205, 2009.

[23] K. H. Shelley, "Photoplethysmography: beyond the calculation of arterial oxygen saturation and heart rate.," *Anesthesia and analgesia*, vol. 105, pp. S31–36, tables of contents, Dec. 2007.

[24] P. D. Mannheimer, "The light-tissue interaction of pulse oximetry.," *Anesthesia and analgesia*, vol. 105, pp. S10–17, Dec. 2007.

[25] J. Toffaletti and W. G. Zijlstra, "Misconceptions in reporting oxygen saturation.," *Anesthesia and analgesia*, vol. 105, pp. S5–9, Dec. 2007.

[26] N. Patel, "Draft Guidance for Industry and FDA Staff Pulse Oximeters - Premarket Notification Submissions [510 (k)s]," tech. rep., FDA, 2007.

[27] P. B. Batchelder and D. M. Raley, "Maximizing the laboratory setting for testing devices and understanding statistical output in pulse oximetry.," *Anesthesia and analgesia*, vol. 105, pp. S85–94, Dec. 2007.

[28] H. Gehring, L. Duembgen, M. Peterlein, S. Hagelberg, and L. Dibbelt, "Hemoximetry as the "gold standard"? Error assessment based on differences among identical blood gas analyzer devices of five manufacturers.," *Anesthesia and analgesia*, vol. 105, pp. S24–30, tables of contents, Dec. 2007.

[29] N. B. Hampson and K. L. Scott, "Use of a noninvasive pulse CO-oximeter to measure blood carboxyhemoglobin levels in bingo players.," *Respiratory care*, vol. 51, pp. 758–760, July 2006.

[30] J. E. Sinex, "Pulse oximetry: principles and limitations.," *The American journal of emergency medicine*, vol. 17, pp. 59–67, Jan. 1999.

[31] A. Jubran, "Pulse oximetry," *Critical Care*, vol. 3, pp. R11–17, 1999.

[32] S. Barker and K. Tremper, "The effect of carbon monoxide inhalation on pulse oximetry and transcutaneous PO2," *Anesthesiology*, vol. 66, no. 5, p. 677, 1987.

[33] M. Vegfors and C. Lennmarken, "Carboxyhaemoglobinaemia and pulse oximetry.," *British journal of anaesthesia*, vol. 66, pp. 625–626, May 1991.

[34] S. Barker, K. Tremper, and J. Hyatt, "Effects of methemoglobinemia on pulse oximetry and mixed venous oximetry," *Anesthesiology*, vol. 70, no. 1, p. 112, 1989.

[35] K. Reynolds, E. Palayiwa, and J. Moyle, "The effect of dyshemoglobins on pulse oximetry: Part I, Theoretical approach and Part II, Experimental results using an in vitro test system," *Journal Of Clinical Monitoring*, vol. 58, no. 3, pp. 81–90, 1993.

[36] J. Severinghaus and J. Kelleher, "Recent developments in pulse oximetry.," *Anesthesiology*, vol. 76, no. 6, p. 1018, 1992.

[37] J. R. Feiner, J. W. Severinghaus, and P. E. Bickler, "Dark skin decreases the accuracy of pulse oximeters at low oxygen saturation: the effects of oximeter probe type and gender.," *Anesthesia and analgesia*, vol. 105, pp. S18–23, tables of contents, Dec. 2007.

[38] M. Coulange, a. Barthelemy, F. Hug, a. L. Thierry, and L. De Haro, "Reliability of new pulse CO-oximeter in victims of carbon monoxide poisoning.," *Undersea & hyperbaric medicine : journal of the Undersea and Hyperbaric Medical Society, Inc*, vol. 35, no. 2, pp. 107–111, 2008.

[39] K. J. Chee, D. Nilson, R. Partridge, A. Hughes, S. Suner, A. Sucov, and G. Jay, "Finding needles in a haystack: a case series of carbon monoxide poisoning detected using new technology in the emergency department.," *Clinical toxicology (Philadelphia, Pa.)*, vol. 46, pp. 461–469, June 2008.

[40] S. Suner, R. Partridge, A. Sucov, J. Valente, K. Chee, A. Hughes, and G. Jay, "Non-invasive pulse CO-oximetry screening in the emergency department identifies occult carbon monoxide toxicity.," *The Journal of emergency medicine*, vol. 34, pp. 441–450, May 2008.

[41] D. Nilson, R. Partridge, S. Suner, and G. Jay, "Non-invasive carboxyhemoglobin monitoring: screening emergency medical services patients for carbon monoxide exposure.," *Prehospital and disaster medicine : the official journal of the National Association of EMS Physicians and the World Association for Emergency and Disaster Medicine in association with the Acute Care Foundation*, vol. 25, no. 3, pp. 253–256, 2010.

[42] M. Macknet, M. Allard, R. Applegate, and J. Rook, "The Accuracy of Noninvasive and Continuous Total Hemoglobin Measurement by Pulse CO-Oximetry in Human Subjects Undergoing Hemodilution," *Anesthesia & Analgesia*, vol. 111, no. 6, p. 1424, 2010.

[43] K. H. Jarman, *Method and apparatus for improved photoplethymosgraphic monitoring of oxyhemoglobin, deoxyhemoglobin, carboxyhemoglobin and methemoglobin.* US Patent 5,842,979, 1998.

[44] K. H. Jarman, *Two stage calibaration and analyte measurement scheme for spectrophotomeric analysis.* US Patent 5,891,024, Apr. 1999.

[45] T. Aoyagi, M. Fuse, N. Kobayashi, K. Machida, and K. Miyasaka, "Multiwavelength pulse oximetry: theory for the future.," *Anesthesia and analgesia*, vol. 105, pp. S53–58, tables of contents, Dec. 2007.

[46] T. Aoyagi, M. Fuse, C. Xie, and M. Kanemoto, *Apparatus for determining concentrations of light-absorbing materials in living tissue.* US Patent 6,230,035, May 2001.

[47] M. Huiku and K. Weckstrom, *Procedure, apparatus and detector for the determination of fractional oxygen saturation.* US Patent 6,104,938, Aug. 2000.

[48] R. Graaff, *Tissue optics applied to reflectance pulse oximetry.* Groningen: University of Groningen, 1993.

[49] Homepage, *Masimo Rad-57 Brochure.* Masimo Corporation. Available in: http://www.masimo.com/rad-57/index.htm, Accessed: Mar. 2011.

[50] C. Mottram, L. Hanson, and P. Scanlon, "Comparison of the Masimo Rad-57 Pulse Oximeter with SpCO Technology against a Laboratory CO-oximeter Using Arterial Blood [abstract]," *Respiratory Care*, vol. 50, no. 11, p. 1471, 2005.

[51] S. J. Barker, J. Curry, D. Redford, and S. Morgan, "Measurement of carboxyhemoglobin and methemoglobin by pulse oximetry: a human volunteer study.," *Anesthesiology*, vol. 105, pp. 892–897, Nov. 2006.

[52] T. Layne, C. Snyder, D. Brooks, and S. Enjeti, "Evaluation of a New Pulse CO-Oximeter: Noninvasive Measurement of Carboxyhemoglobin in the Outpatient Pulmonary Lab and Emergency Departments.," *Respiratory care*, vol. 51, no. 11, p. 1333, 2006.

[53] J. Kot, Z. Sicko, and P. Goralczyk, "Carbon monoxide pulse oximetry vs direct spectrometry for early detection of CO poisoning," *Anestezjologia Intensywna Terapia*, vol. 40, no. 2, pp. 75–78, 2008.

[54] A. Piatkowski, D. Ulrich, G. Grieb, and N. Pallua, "A new tool for the early diagnosis of carbon monoxide intoxication [abstract]," *Inhalation toxicology*, vol. 21, no. 13, pp. 1144–1147, 2009.

[55] M. Touger and A. Birnbaum, "In reply," *Annals of Emergency Medicine*, vol. 56, pp. 444–445, Oct. 2010.

[56] D. Roth, H. Herkner, W. Schreiber, N. Hubmann, G. Gamper, A. N. Laggner, and C. Havel, "Accuracy of Noninvasive Multiwave Pulse Oximetry Compared With Carboxyhemoglobin From Blood Gas Analysis in Unselected Emergency Department Patients.," *Annals of Emergency Medicine*, pp. 74–79, July 2011.

[57] J. R. Feiner, P. E. Bickler, and P. D. Mannheimer, "Accuracy of methemoglobin detection by pulse CO-oximetry during hypoxia.," *Anesthesia and analgesia*, vol. 111, pp. 143–148, July 2010.

[58] J. R. Feiner and P. E. Bickler, "Improved accuracy of methemoglobin detection by pulse CO-oximetry during hypoxia.," *Anesthesia and analgesia*, vol. 111, pp. 1160–1167, Nov. 2010.

[59] T. Tupala, *Development of Multi-Wavelength Oximeter Electronics for Hemoglobin Measurement*. Master of science thesis, Tampere University of Technology, 2009.

[60] M. Huiku, "Hemoglobin Technology Development Plan (GE internal document)," 2009.

[61] *OSM3 Hemoximeter User's Handbook*. Copenhagen: Radiometer.

[62] *682 CO-Oximeter System Operator's Manual Part No. 79682-01 Rev. 4*. Milan: Instrumentation Laboratory, 2003.

[63] *ABL 800 Flex Operator's Manual*. Copenhagen: Radiometer, 2005.

[64] D. G. Altman and J. M. Bland, "Measurement in Medicine: The Analysis of Method Comparison Studies," *The Statistician*, vol. 32, p. 307, Sept. 1983.

[65] I. Selesnick and C. Burrus, "Generalized digital Butterworth filter design," *IEEE Transactions on Signal Processing*, vol. 46, no. 6, pp. 1688–1694, 1998.

[66] J. Mandel, *The statistical analysis of experimental data.* New York: Dover Publications, 1984.

[67] T. L. Rusch, R. Sankar, and J. E. Scharf, "Signal processing methods for pulse oximetry.," *Computers in biology and medicine*, vol. 26, pp. 143–159, Mar. 1996.

[68] M. Huiku, *Compensation of human variability in pulse oximetry.* US Patent 6,882,874, Sept. 2005.

[69] J. Semmlow, *Biosignal and biomedical image processing.* Boca Raton: CRC, 2nd ed., 2009.

[70] I. Mellin, *Tilastolliset menetelmät.* Espoo: Helsinki University of Technology, Laboratory of mathematics, 2006.

[71] R. Kohavi and F. Provost, "Glossary of terms," *Machine Learning*, vol. 30, pp. 271–274, June 1998.